NORTHWESTERN UNIVERSITY

Biorefining Lignin into High-Value Products: Coupling a Microbial Electrolysis Cell to Lignin

Depolymerization

A DISSERTATION

SUBMITTED TO THE GRADUATE SCHOOL
IN PARTIAL FULFILLMENT OF THE REQUIREMENTS

for the degree

DOCTOR OF PHILOSOPHY

Field of Civil and Environmental Engineering

By

Natalia Obrzut

EVANSTON, ILLINOIS

September 2023

Abstract

Lignin is the largest store of renewable aromatic carbon. Due to its refractory nature, however, its chemical potential is not fully realized, rather, most lignin is treated as a waste, burned for low-value energy. Here, we propose a biorefinery where the treatment of wastewater by a microbial electrolysis cell (MEC) produces "clean" water and a caustic catholyte that can depolymerize lignin under mild conditions (i.e. ambient temperature and pressure) into two high value product streams. The specific goal of this research is to characterize the range of products that can be biorefined from lignin as a function of its source, method of extraction, and catholyte characteristics.

We determined the MEC operating conditions to produce a depolymerization solvent and characterize and quantify solution and colloidal phase products using an array of analytical techniques. We characterized bulk features such as soluble lignin, phenolic content and flavonoid content using UV vis spectroscopy. We found greater than 80% soluble lignin after an hour, and nearly complete solubilization over 7 days. We also determined bulk flavonoids at 20% and bulk phenolics at 50%. Using high resolution liquid chromatography and tandem mass spectrometry, we obtained and identified 11% of discrete aromatics (monomers and flavonoids). This contrasts with previous reports in the literature that obtain lower yields of low value products (BTX) with base catalyzed depolymerization. We closed mass balance by simultaneously producing lignin nanoparticles. We characterized the lignin nanoparticles through nanoparticle tracking analysis and dynamic light scattering for size, concentration, and polydispersity, zetasizer for zeta potential (surface charge that indicates colloidal stability), and scanning electron microscopy to verify the shape and size. In part, our higher product yield is due to selective repolymerization to form flavonoids and nanoparticles.

Furthermore, we explored the efficacy of depolymerization in the conditions of our biorefinery when we change the lignin source. The biomass source (i.e. herbaceous, softwood, and hardwood) influences the amount of lignin available, as well as the ratio of monomers (S/G) and content of breakable bonds (β-O-4 linkages). The structure, specifically the number of β-O-4 linkages, is further affected by the extraction method (i.e. Milled Wood (mild), Organosolv (medium), and Klason (harsh)). We found that herbaceous lignin extracted via the Organosolv process is best suited for depolymerization in our biorefinery. Herbaceous Organosolv lignin, solubilizes to the greatest extent (~100% over 7 days), produces the greatest amount of phenolics and flavonoids, and has the most and smallest lignin nanoparticles. Additionally, this depolymerized mixture has the highest antioxidant capacity. Only the harsh, Klason method successful extracts lignin from all three sources, but the herbaceous and hardwood sources are depolymerized to a lesser extent than the Organosolv method. With low density of labile bonds, softwood lignin cannot be depolymerized under the conditions of our biorefinery. Milled Wood lignin does not efficiently extract lignin from any of the biomass, and the extracted lignin is low purity, which does not allow it to be processed in our biorefinery.

Finally, we explored the extent to which we can tune the lignin nanoparticles. We varied the salt concentration, salt type, and pH and monitored the concentration, size, and shape of the nanoparticles, as well as the antioxidant capacity of the mixture. We found that the pH can be used to produce a higher concentration of lignin nanoparticles quickly, albeit at a larger size. We also found that the salt type influences the shape of the lignin nanoparticles – ranging from spherical (phosphate), rod-like (nitrate and chloride), and flower-like (carbonate). Additionally, the shape and the size influence the antioxidant capacity due to changes in the surface area to volume ratio. The flower-like nanoparticles have a high surface area to volume ratio and the highest antioxidant

capacity, the same antioxidant capacity to the industrial antioxidant Trolox. The antioxidant capacity of both discrete products and nanoparticles illustrates their high potential value in the pharmaceutical, nutraceutical, personal care, and agricultural industries.

Acknowledgments

First, and foremost, I would like to thank my advisor, Dr. Kimberly Gray. She has shown me unconditional support, patience, and guidance throughout the last five years and none of this would have been possible without her. I appreciate her ideas, feedback, and intellectual curiosity that has really moved this project forward.

I would like to thank the members of my committee: Dr. Neal Blair, Dr. Benjamin Owens, and Dr. George Wells for their support and insightful comments. I also thank everyone that trained me on various instruments in our departments as well as at shared facilities including: Yingqian (Chan) Xiong, Arsen Gaisin, Nathaniel Kabat, Alexandra Kolot, and Tirzah Abbot.

I am thankful to current and past members of the Gray Group. I would specifically like to thank Dr. Patricio Carnelli for helping me at the beginning of my Ph.D and teaching me basic and advance lab techniques, as well as supporting me as I learned how to be a researcher. I would like to thank Rob Hickmott and Lily Shure, who helped with experimentation. I am eternally thankful for my lab-mates and friends, Haley Lewis and Han Fu. They not only tangibly helped support my research but also made coming into work a lot of fun and something I looked forward to.

I also thank my grandfather-in-law, Kenneth Lancor, for kindly donating over 20 different species of wood. My parents-in-law, Michelle and Troy Lancor, for providing me with corn stover, and my dad, for helping me turn it all into dust with his power saw.

Finally, I am so thankful for my husband – Kyle Lancor, my parents – Malgorzata and Rafal Obrzut, my brother – Patrick Obrzut, and my friends - specifically Dr. Rylee Venn, Hanna Sutton, and Amanda Fiebelkorn. It really takes a village to get a Ph.D and I wouldn't have gotten here without the support and encouragement from everyone in my life.

Table of Contents

Table of Figures

List of Tables

Chapter 1 : Introduction

1.1 Research Motivation and Significance

Excessive exploitation of petrochemical resources and fossil fuels are causing severe environmental impacts – including climate change, air, water, and land pollution, as well as environmental justice infractions [5]. The Intergovernmental Panel on Climate Change (IPCC) reports that anthropogenic activities have caused approximately 1.1 °C of global average warming above pre-industrial levels and if emissions continues to increase at this rate, we will reach 1.5 °C of global warming between 2030 and 2052 [6]. Global temperature increases are already having detrimental environmental effects such as: increased intensity of precipitation and drought events, loss of biodiversity and ecosystems, as well as effects to humans such as, risks to health, livelihood, food security, water supply and human security [6]. Rapid decarbonization is essential strategy to hold the global temperature to 1.5-2.0 °C by reducing the amount of CO_2 emissions.

Biomass is an attractive substitute for fossil fuels and petroleum-based products. Biomass is the only source of renewable carbon. Lignin makes up 15-40% of biomass and is responsible for structural stability as well as water transport in plants [7]. Lignin is a highly amorphous 3D polymer that is the only renewable source of aromatic carbon but is difficult to convert to useful products – leaving it to be burned for low-grade fuel instead of unlocking its chemical value. Lignin for energy is not a viable valorization route as it is low value and there are other more efficient alternatives for green energy [8]. Converting lignin to chemicals rather than fuels can be ten times more profitable [9]. Lignin has the potential to serve as an alternative starting material to produce functionalized aromatics instead of petroleum derived benzene, toluene, and xylene

[10]. Lignin is also an excellent source of natural antioxidants, which act as reducing agents and protect materials from oxidation. Artificial antioxidants are obtained through chemical synthesis of fossil resources [11, 12]. Biomass conversion is key to creating circular bio-economies, which will contribute to decarbonization and ideally reduce the dependence on fossil fuels [13].

Although the bioavailability and aromatic content make lignin an attractive potential chemical feedstock, conversion into valuable monomers has historically been difficult [14]. Most of the research on valorizing lignin does so through depolymerization. Conditions like those used in the petroleum industry (hydrocracking) are often used for depolymerization and require high temperature and pressure, expensive catalysts, or harmful solvents, and result in low yields [9, 15, 16]. Lignin is typically depolymerized through gasification for energy or through hydrolysis or oxidation for aromatics. Obtaining products in a chemically mild way is important in reducing input costs and preserving aromatic structure and thus, obtaining higher value aromatic products or materials.

The goal of the proposed work is to investigate the conversion of lignin to high value products in an integrated biorefinery based on the processing of wastewater rich in volatile fatty acids in a microbial electrolysis cell (MEC). Our biorefinery is novel in several ways: 1) it is the only approach to focus on four product streams simultaneously – two (clean water and caustic catholyte) from the MEC and two (aromatics and nanoparticles) from the biomass – closing mass balance on lignin, 2) it is the only approach coupled with the waste stream from an MEC under ambient conditions (without introducing heat or pressure), and 3) it is the only approach that creates repolymerization reactions for higher molecular weight products.

1.2 Hypothesis and Objectives

Although long studied, methods to depolymerize lignin often employ harsh conditions, which do not preserve the aromaticity of the lignin derivatives [9, 10]. We propose a gentle depolymerization of lignin, which not only preserves the aromaticity but also promotes the formation of oligomers. The depolymerization also produces nanoparticles at basic and neutral pH. These two products close mass balance and are produced at ambient temperature and pressure using waste streams as inputs. We hypothesize that **lignin can be processed in an integrated biorefinery to efficiently create high value products in the form of low molecular weight aromatic chemicals and carbon-based nanoparticles**. Based on the value of the products, as well as the yield, the process may be optimized to favor one product stream over another.

There are three objectives that test this hypothesis:

1. Identify, characterize, and quantify the products from treating lignin with MEC effluent under set conditions through a combination of analytical techniques including chromatography, spectroscopy, and light scattering.

2. Determine how other sources of lignin and extraction methods behave in this biorefining process, determine how the products change in yield and properties. Determine the relationships between lignin source and extraction and products.

3. Explore the effects of pH, salt type, and salt concentration on product yields and properties, with special focus on LNP characteristics including, size, shape, stability, polydispersity and antioxidant capacity.

1.3 Dissertation Organization

The organization of this thesis follows the order of the objectives. In Chapter 2, we take a deep dive into the background of lignin. We begin with the structure of lignin in general and follow up with a discussion on the sources of lignin as well as the extraction. Chapter 2 wraps up with a discussion on what has been shown in the literature about the discrete aromatic products and Lignin Nanoparticles (LNPs) that can be created from lignin and their potential applications. Chapter 3 covers the first objective of our hypothesis – that lignin can be depolymerized with the use of MEC effluent to produce products. The results in this chapter provide a proof of concept for biorefining lignin to products and qualitatively and quantitatively characterized products. Chapter 4 reports the effects that lignin source (herbaceous, softwood, and hardwood) and extraction (MWL, Organosolv, and Klason) have under the conditions of our biorefinery on depolymerization products and their properties. We also discuss the relationships between the initial structure of lignin and its products, as well as the relationship products have to each other. In Chapter 5, we explore how changing the salt type (buffers: phosphate and carbonate; simple sodium salts of chloride and nitrate), concentration, and pH change the product composition and properties. We finally summarize the findings of this research and conclude with next steps in Chapter 6.

Chapter 2 : Background[1]

2.1 Introduction

The climate emergency requires that we rapidly and deeply decarbonize our economy and these efforts must extend beyond replacing fossil fuels in the energy sector to include the petrochemical industry as well. Decarbonization also requires the creation of circular economies, where waste materials are used as inputs in resource recovery and material reuse cycles [17]. Biomass is an attractive alternative for fossil fuels in petroleum-based chemical products. Biomass is the only source of renewable carbon and lignin, which is responsible for the structural stability as well as water transport in plants, makes up 15-40% of biomass [7]. Lignin is a highly amorphous 3D polymer that is the only source of renewable aromatic carbon but is difficult to convert to useful products – rendering it, in many cases, a low-grade combustion fuel. As a valorization route, the use of lignin for energy is not generally competitive as it has low value and there are other more efficient alternatives for green energy [8]. Converting lignin to chemicals rather than fuels has the potential to be ten times more profitable [9]. Lignin could potentially serve as an alternative feed stock material to produce functionalized aromatics reducing use of petroleum-derived benzene, toluene, and xylene [10]. Lignin is also an excellent source of natural antioxidants, which act as preservatives in food and have other applications in the cosmetic industry, as well as in the pharmaceutical sector. Lignin derived antioxidants could replace artificial antioxidants that are typically obtained through chemical synthesis of fossil resources such as butylated hydroxytoluene (BHT) [11, 12].

---

[1] This chapter has been published. Obrzut, N. and K. Gray, *Chapter 17: Biorefining renewable aromatic carbon: unlocking lignin's potential to produce high-value products*, in *Photosynthesis*, H. Hou, Editor. 2023: Elsevier.

Although the supply (2×10^{11} tons/year of lignocellulosic residue) and aromatic content make lignin an attractive potential feedstock, conversion into valuable chemicals has historically been difficult [14]. Most of the research on valorizing lignin focuses on depolymerization. Some depolymerization routes employ conditions similar to hydrocracking in the petroleum industry which require high temperature and pressure, expensive catalysts, or hazardous solvents, and result in low yields [9, 15, 16]. Most often lignin depolymerization is achieved in gasification via syngas ($CO + H_2$) for energy or through hydrolysis or oxidation for aromatics. Obtaining products under chemically mild conditions is challenging but may be advantageous in reducing input costs and obtaining higher value aromatic products or materials.

The goal of this chapter is to explore various depolymerization routes to unlock the potential value of lignin. This chapter is divided into five major sections. The first section discusses the structure of lignin and the effects of extraction on both its structure and the efficiency of downstream processing. The second section describes the biorefinery approach to lignin valorization, highlighting our own research which investigates the efficacy of using a microbial electrolysis cell to process an organic wastewater stream coupled to lignin depolymerization [18]. The third section explores various depolymerization methods, with a special focus on low temperature and pressure conditions. The fourth section focuses on a potentially high value depolymerization product, lignin nanoparticles – their properties, synthesis, and tunability. Finally, the fifth section provides examples of potential applications of these products in a variety of industries.

2.2 Lignin: A Store of Aromatics

2.2.1 The Structure of Lignin

Biomass, of which cell walls comprise 70%, is the largest store of renewable carbon [19]. The cell walls of plants are made up of two polysaccharides – cellulose and hemicellulose – plus lignin, an aromatic polymer of phenyl-propanois subunits. Cellulose, the main component (comprising up to 50% of the cell wall), has a stable and insoluble structure of β-(1-4) linked D-glucoses. Lignin is the second most abundant component of the cell wall, comprising up to 40%, and is responsible for the rigid structure of plant cells as well as water transport [20]. Related structurally to cellulose and functionally to lignin, hemicellulose is composed of units of different hexoses and pentoses that readily dissolves in water [21]. Hemicellulose is a minor component and sometimes makes up less than 10% of the cell wall.

p-coumaryl alcohol   Coniferyl alcohol   Sinapyl alcohol

4-hydroxyphenyl (H) group   Guiacyl (G) group   Syringyl (S) group
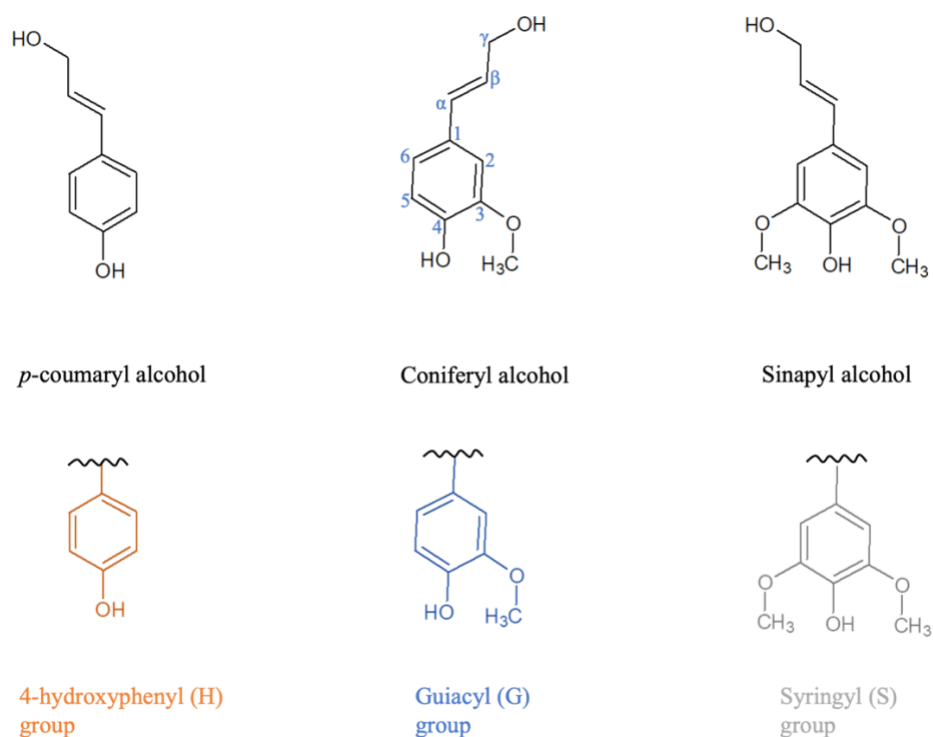
Figure 2.1 The three monolignols and their polymerization units in lignin. Adapted from Ganewatta [22].

Lignin is an amorphous, 3D polymer composed of three monomeric units (monolignols): p-coumaryl alcohol (H, 4-hydroxyphenyl group), coniferyl alcohol (G, guiacyl group), and sinapyl

alcohol (S, syringyl group) as shown in **Figure** 2.1 [21, 23]. The ratio of monolignols varies with plant species and is summarized in **Table** 2.1. Generally, angiosperm (hardwood) lignin, such as birch and poplar, are composed primarily of S and G monolignols, whereas gymnosperm (softwood) lignin, such as pine and spruce, are composed mostly of G monomers. Herbaceous lignin, like switchgrass and corn stover, typically contain all three monolignols, but the H content is low (below 5%) [23, 24].

Table 2.1. Properties of different sources of plants.

Source	Examples	% lignin	S/G ratio	% β-O-4
Hardwood	Oak, birch, poplar	18-25%[23]	1.01-3.60 [25, 26]	60-62%[10]
Softwood	Pine, spruce, cedar	21-35%[21, 23]	0.021-0.050 [23, 25, 27]	45-50%[10]
Herbaceous	Switch grass, corn stover	11-24% [21, 23]	0.32-0.64 [28]	74-84%[10]
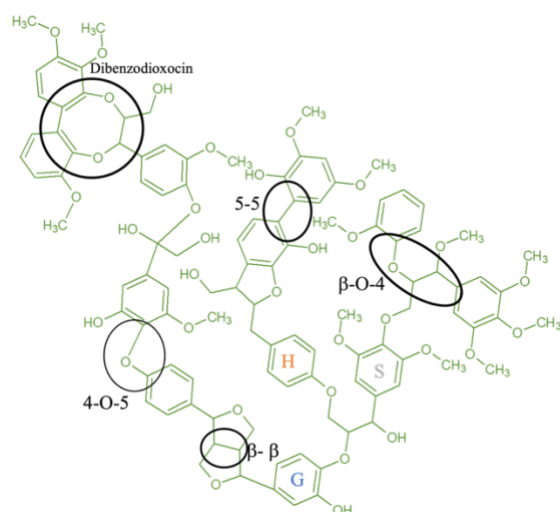
Figure 2.2 A potential structure of the lignin polymer, highlighting common bonds.

Monolignol bio-synthesis begins in the cytosol and lignification occurs in the cell wall [23]. The process of lignification is a radical process induced by peroxidases and lactases. The process is greatly influenced by physical conditions such as light, temperature, salinity, and pH [10], such that the resulting lignin structure is random and cannot be determined beyond the ratio of monolignols and types of linkages. The amount of lignin varies between 10 and 35% depending on the plant species with softwood typically containing the highest percentage of lignin and herbaceous containing the lowest percentage of lignin (**Table** 2.1) [21, 23]. There are 14 unique linkages that weave monolignols into a lignin structure, some of these are highlighted in **Figure 2.2** [29]. The most

common linkages are β-ethers which, depending on the plant type, comprise 50-80% of the total linkages. The most common of these linkages is the β-O-4 linkage, which constitutes 60-62% of linkages in hardwood, 45-50% in softwood, and 74-84% in herbaceous lignin [10]. The bond dissociation energy (BDE) of the β-O-4 linkage is between 221 and 295 kJ/mol making it easier to break than the 5-5 (carbon-carbon) bond which has a BDE of 471-483 kJ/mol [9, 10]. The abundance of the β-O-4 bond, as well as the relatively lower BDE, makes this bond a common target of depolymerization processes.

2.2.2 Lignin Extraction

Lignin extraction or fractionation from biomass has a significant effect on the structure of lignin. Extracted lignin is often referred to as technical lignin. Lignin extraction falls into two broad categories: delignification, which liberates lignin from the biomass matrix and preserves the carbohydrates in a pulp, and carbohydrate conversion, which targets and solubilizes the carbohydrate fraction, leaving the lignin as a solid [23]. Within each category, there are a variety of specific extraction methods that preserve the native structure of lignin and others that modify it greatly. The extraction of milled-wood lignin (Bjorkman process), ionic liquid lignin and cellulolytic enzyme lignin tends to conserve its natural (native) structure [9, 23]. **Table** 2.2 summarizes the type of extraction, conditions, and resulting lignin. The most common industrial method of lignin extraction without severe structural modification is the Organosolv method, which is used to separate cellulose for bioethanol production and produces the second largest lignin stream [30].

The Kraft process is used in paper production to convert wood into wood pulp or almost pure cellulose fibers and creates the largest commercial lignin stream, comprising 85% of the total

technical lignin produced globally [31, 32]. The Kraft process does not preserve the β-O-4 linkages, resulting in lignin that varies immensely from its native structure, is highly condensed, is difficult to use as feedstock for subsequent processing, and is typically regarded as a waste stream that may be burned for energy in paper making. Similarly, high temperatures and alkaline reagents are used to produce lignosulfonate and soda lignin, which also have little resemblance to the native structure [23]. Klason lignin utilizes high temperature and concentrated acid to dissolve all the carbohydrates – this method is often used to quantify the amount of lignin in a sample, but the isolated lignin is highly degraded.

There is a link between the extraction of lignin from biomass, the resulting structure of the lignin, and its valorization. The target of valorization tends to be monomers and in order to liberate monomers, β-O-4 linkages need to be preserved in extraction since these are the easiest bonds to cleave. It is more difficult to depolymerize the highly condensed structure of certain technical lignin (i.e. Kraft, Klason etc.) into monomers, because there are no more β-O-4 linkages to cleave and 5-5 bonds, require twice as much energy to break [9, 10]. In order to avoid the difficulties present with most technical lignin streams, most biorefinery research focuses on lignin first fractionation to preserve the labile bonds in lignin [33]. Research in this area focuses on: 1) genetic modification to allow easier separation/more structural preservation of lignin [34, 35], 2) stabilizing the low molecular weight lignin to avoid repolymerization [36], and 3) determining fractionation methods to better conserve the structure of native lignin [37-44].

Table 2.2. A summary of the conditions and characteristics of resulting lignin structure from various extraction techniques [23].

Type of extraction	General Conditions	Name of Lignin/Process	Reaction Conditions (temperature, reagents)	Resulting lignin
Delignification	Alkaline	Kraft lignin	140-170 °C, H_2O, NaOH, Na_2S	Highly degraded oligomers, 3% sulfur
		Lignosulfonate	140-170 °C, H_2O, Na, NH_4, Mg or Ca salts of SO_3^{2-} or HSO_3^-	Highly degraded oligomers, 8% sulfur
		Soda lignin	160-170 °C, H_2O, NaOH, anthraquinone	Highly degraded oligomers
	Acidic	Organosolv lignin	100-210 °C, organic solvent (methanol, ethanol, glycerol, dioxane, formic acid, acetic acid etc.) H_2O, mineral acid	Degraded oligomers, alpha Alkoxy groups, ester groups
	Other	Ionosolv lignin	90-170 °C, Ionic Liquid	Oligomers, partial preservation of β-O-4, possible sulfur incorporation
		Milled Wood lignin	Room temperature, ball milling	Resembles native lignin
Carbohydrate conversion	Acidic	Klason lignin	20-25 °C, concentrated acid (H_2SO_4)

170-300 °C. dilute acid | Highly degraded oligomers |
| | | γ-valerolactone (GVL)-extracted lignin | 120-170 °C, H_2O, γ-valerolactone (GVL), H_2SO_4 | Oligomers, effective preservation of β-O-4 |
| | Enzymatic | Cellulolytic enzyme lignin (CEL) | 40-60 °C, H_2O, pH 4-5 buffer, cellulolytic enzymes, ball-milled biomass | Resembles native lignin |
| | | Enzymatic mild acidolysis lignin (EMAL) | Step 1: cellulolytic enzymes, ball-milled biomass

Step 2: Dioxane/H_2O, HCl, 80-90 °C | Resembles native lignin |
| | Thermal | Pyrolytic lignin | 400-600 °C, absence of oxygen, acidic zeolite (catalyst) | Highly degraded small oligomers C8-units |

Genetic modification includes designing plants to contain more lignin, lignin with more β-O-4 linkages, or lignin with more specific residues that promote certain commercial properties. Yamamoto et al. found that increases in the coniferyl aldehyde content in lignin significantly improves the plant's ability to be used for feed, pulping, and biorefinery without affecting plant growth in a major way. There is a genetic pathway that regulates the amount and position of the coniferyl aldehyde residue in lignin and therefore can be controlled with cellular regulation [35]. As lignin is extracted, reactive monomers and low molecular weight lignin risk undergoing immediate repolymerization. To combat this process, Subbotina et al. studied the use of zeolites as catalysts to stabilize reactive monomers during Organosolv extraction and inhibit repolymerization [36].

The lignin extraction method has a stunning effect on its properties. Using corn stover, an herbaceous source of lignin, we compared the β-O-4 content as a function of three extraction techniques (Milled Wood lignin, Organosolv, and Klason) relative to untreated biomass, In Figure 2.3 the FTIR peak area ratio for ethers to aromatic carbon-hydrogen illustrates that lignin extracted via the Milled Wood lignin process contained 80% of β-O-4 linkages of the
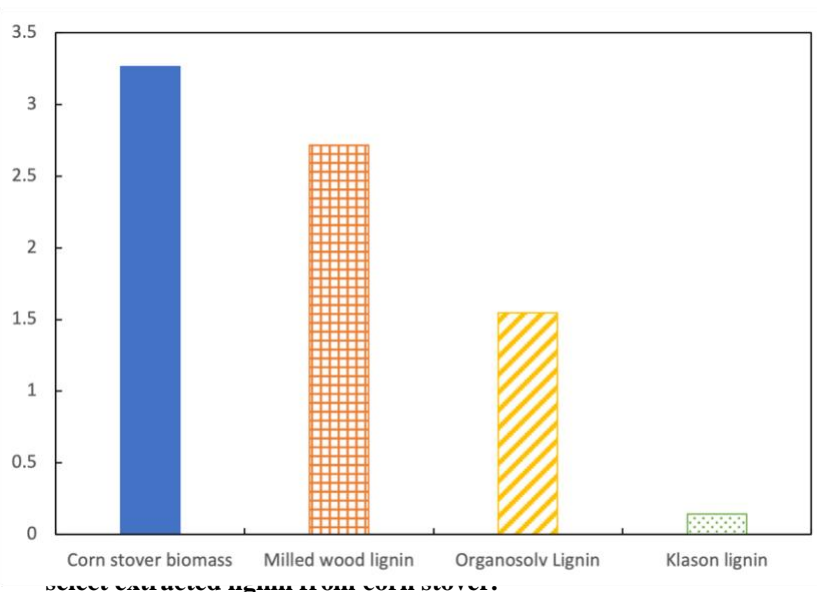
select extracted lignin from corn stover.

native biomass. Organosolv lignin contained half as many β-O-4 linkages as Milled Wood and Klason contained only 5% of the β-O-4 linkages as Milled Wood [45]. By using extraction methods that preserve the native structure of lignin, we can facilitate the ease of downstream depolymerization and valorization.

2.3 Biorefineries

Biorefining is well defined for cellulose and hemicellulose to produce paper (cellulose) and alcohols (cellulose and hemicellulose). Integrating cost-effective lignin bioprocessing into the larger biomass biorefinery could contribute to greater economic and environmental sustainability [46]. Research on lignin biorefining falls into one of three areas: 1) extracting/fractioning lignin from biomass, 2) depolymerizing lignin into simpler molecules, and 3) upgrading the lignin products into valuable chemicals [46].

According to the International Energy Agency, (IEA), a biorefinery is defined as " a sustainable processing of biomass into a spectrum of marketable products and energy" [47]. Moncada goes further to describe a biorefinery as "a network of facilities that integrates biomass conversion processes and equipment to produce biofuels, energy, and chemicals from biomass" [48]. Similar to oil refineries, a biorefinery converts biomass through thermal/physical, chemical or biological processes and separates the products into various product streams. **Table** 2.3 summarizes various feedstocks, conversion methods, and products obtained from a biorefinery and illustrates that lignin is an example of a second-generation feedstock.

Table 2.3. A summary of examples of feedstocks, conversion methods, and products for different biorefineries [33, 46, 48-51].

Feedstock		Conversion		Products	
Sources	Examples	Type	Example	Classification	Example
Edible Crops (1st Gen)	Sugar cane, rice, wheat	Thermochemical	Pyrolysis, gasification, combustion	Biofuels	Bioethanol, Biodiesel
Residues (2nd Gen)	Waste cooking oil, saw dust, crop residuals (lignin)	Biological	Anaerobic digestion	Food Products	Sugar, protein
Algae (3rd Gen)	Micro algal biomass	Chemical	Hydrolysis, Solvent extraction	Bioenergy	Steam, Electricity, heat
Non edibles (4th gen)	Castor bean, CO_2	Physical	Distillation, Mechanical Extraction	Biomaterials	Paper, Bioplastic, Activated Carbon
				Biochemicals	Glycerol, Fertilizers, Pharmaceuticals, Vanillin

An example of a biorefinery is Alpena in Michigan (DOE) [52]. This biorefinery converts the woodchip waste stream from a neighboring board manufacturing mill into bioethanol and de-icing chemicals. The U.S Department of Energy describes the input capacity of this project as 23 dry tons of woodchip waste per day to produce 800 thousand gallons of cellulosic ethanol annually. The process is defined by three steps: 1) evaporation and hydrolysis, 2) fermentation, and 3) distillation. In addition to biofuel, this biorefinery is able to convert recovered acetic acid from the evaporation and hydrolysis stage of the process into 790 thousand gallons of potassium acetate

which may be used to de-ice airport runways. This process is summarized in **Figure 2.4**
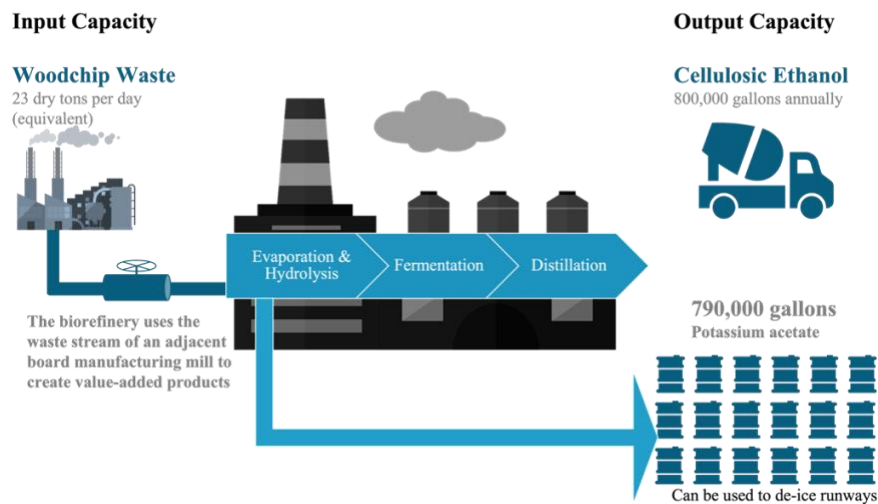
Figure 2.4. The Alpena Biorefinery. A schematic of the biochemical conversion of industrial wood waste from the DOE. Redrawn from https://www.energy.gov/eere/bioenergy/alpena-biorefinery
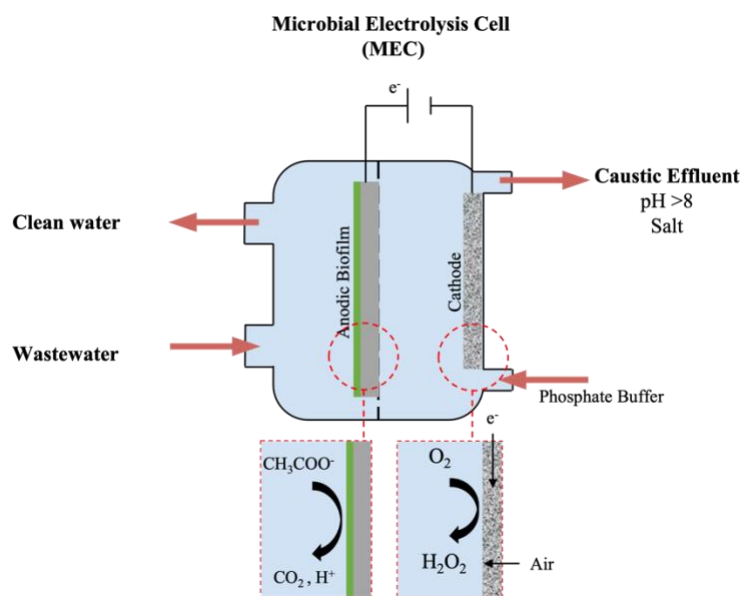
Figure 2.5. A schematic of the microbial electrolysis cell used by Griffin et al. [4]

An emerging technology that can be used in biorefineries is a microbial fuel cell or microbial electrolysis cell [53]. Traditionally wastewater, especially from the food industry, contains dissolved organics that require a considerable amount of energy to biodegrade through aeration. A microbial fuel cell (MFC) is a method of degrading organics from water while producing electricity, rather than consuming it [54]. Alternatively, microbial electrolysis cells (MEC) require the application of an electrode potential but can produce products such as methane, hydrogen peroxide, caustic, acetate, or ethanol, rather than electric

current [55]. **Figure 2.5** shows a schematic of an MEC adapted from Griffin et al [4]. At the anode, there is an electrochemically active microbial biofilm of exoelectrogens composed mainly of bacteria in the genus *Geobacter* capable of transferring electrons extracellularly [54]. These electrons are produced by the microbial metabolism of fatty acids in the wastewater to oxidize the BOD/COD $(2H_2O + CH_3COO^- \rightarrow 2CO_2 + 7H^+ + 8e^-)$. At the cathode, oxygen is reduced to water (or hydrogen peroxide), by consuming protons, which allows electrons to flow between the anode and the cathode $(4e^- + 4H^+ + O_2 \rightarrow 2 H_2O)$ and producing a high pH, high salt effluent [4]. This cathode effluent has had success in lignin depolymerization as discussed in 2.5.1 A New Types of Base Catalyzed Depolymerization. Previous research showed that a biomass pyrolysis-MEC process simultaneously produced bio-oil from the oil phase of pyrolysis products and used the aqueous phase organic carbon as a substrate in an MEC to produce renewable hydrogen [56].   An MEC fed the hydrolysate from the hydrothermal treatment of wheat straw produced hydrogen and phenols, yielding 22 g of hydrogen and 9 g polyphenolics from 1 kg of wheat straw [57].

2.4 Producing Chemicals from Lignin

2.4.1 Types of Lignin Depolymerization

Lignin depolymerization is an essential step in an efficient lignocellulosic biorefinery. There are countless methods of depolymerization, each with their own advantages and disadvantages. Some of the methods discussed below are reductive, oxidative, thermal, hydrothermal, photocatalytic, biocatalytic, electrocatalytic, and base-catalyzed depolymerization [46, 51]. **Figure 2.6** locates each depolymerization process as a function of their operational temperature and resulting degree of functionalization, product and product value.
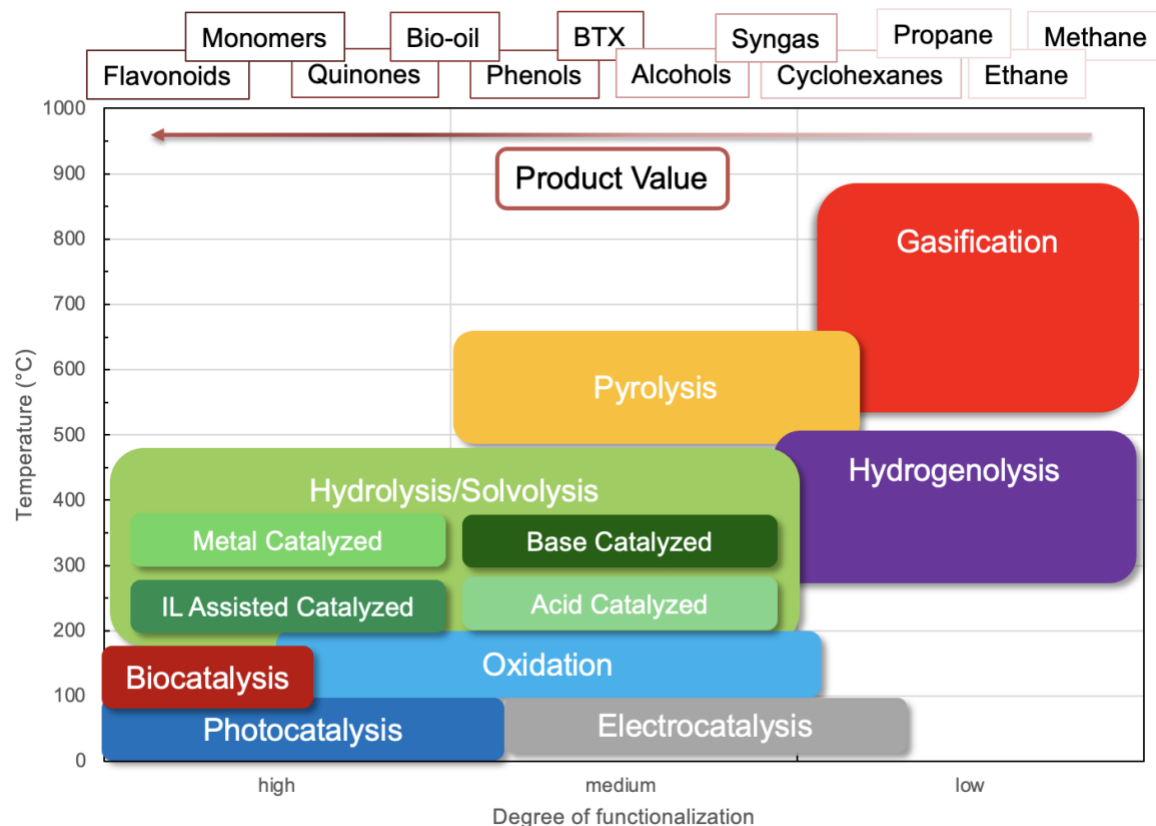
Figure 2.6. A graph showing different depolymerization methods along with temperature and product value/degree of functionalization. Adapted from Rößiger [2].

Reductive depolymerization or hydrogenolysis is highly selective for cleaving C-O and C-C bonds and typically uses a precious metal catalyst like palladium [46]. Reductive depolymerization produces aromatic monomers or more reduced products such as cycloalkanes and arenes. Bio-oil (a complex mixture of organics) produced via this method has great potential as a biofuel due to the high hydrogen to carbon ratio [58-61]. On the other hand, oxidative depolymerization shows promise because of its ability to preserve the functional groups on the aromatic rings. However, most research is done on lignin model compounds which display high conversion rates to products that are not predictive of product yields when applied to whole lignin [62-65].

The most common thermal methods of depolymerization are pyrolysis and gasification. Pyrolysis is carried out at moderate to high temperatures (400-800 °C) in the absence of oxidizing agents to produce bio-oil and bio-char. Pyrolysis has low product selectivity and the complicated product mixtures are difficult to separate [46]. Gasification is performed at high temperature (> 800 °C) in the presence of oxygen to produce syngas ($CO + H_2$). The co-production of coke and tar poses an issue [46].
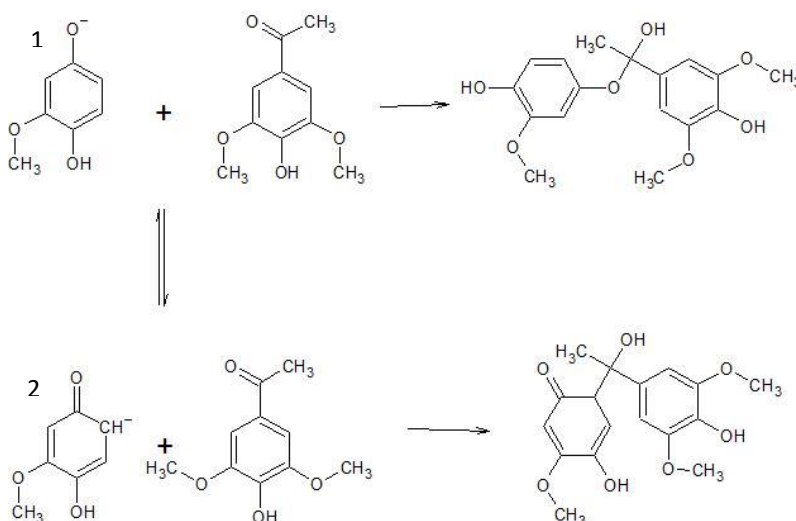
Figure 2.7. The resonance of the phenolate (1) with the carbanion (2) and the repolymerization reactions that ensue. A carbon-carbon bond as seen in the bottom right is much harder to break than the ether bond in the molecule in the top right. Adapted from Erdocia et al [3]

Hydrothermal liquefaction uses water as the solvent at moderate temperatures (< 350 °C) and high pressures (up to 25 MPa). It is a more favored alternative to pyrolysis because the bio-oil produced from this process has lower oxygen content and the process can be used on wet biomass [46, 50].

Photocatalytic depolymerization relies on the principle that lignin is produced via photosynthesis and subsequently can be depolymerized photochemically. This concept works at room temperature and atmospheric pressure – conserving energy and minimizing its environmental impact [46]. Homogenous catalysts (Ru, Rh, phosphines etc.) as well as heterogeneous catalysts (metal oxides such as TiO_2, carbon-based nanomaterials) can catalyze these light-driven reaction [66]. Electrocatalysis comes in the form of electro-oxidation – transforming lignin into oxidized products, electroreduction – transforming lignin into reduced products, and a hybrid redox – transforming lignin to reduced and oxidized products. It is a low cost, reagent free,

environmentally friendly process, although it has the risks of unfavorable side reactions, low selectivity, and overoxidation [67-69]. Bio-catalysis entails the enzymatic conversion of lignin to aromatic products. This process has the potential of being very selectiv;, however, when this process is applied to native lignin rather than model compounds, the conversion fails to produce aromatic oligomers [70, 71].

Base catalyzed depolymerization (BCD) typically uses concentrated base under high temperature and high-pressure conditions to produce monomers. Identified monomers include: phenol, cresols, guaiacol, catechol, 4-methylcatechol, syringol, acetovanillone, syringaldehyde, acetophenones, and vanillin [72, 73]. BCD typically obtains a low concentration of monomers. Most methods report yields of bio-oil under 20% and identified monomers are even less, often under 4% of the initial lignin mass [3, 29, 72, 73]. The yield depends on the lignin source, as well as the extraction method. Harsh extraction, such as Kraft, causes condensation of lignin, which makes depolymerization difficult as the number of readily breakable bonds decreases. In one study, the yield of monomers varied between 2.4 and 3.6% depending on whether olive tree pruning lignin was extracted using acetosolv, formosolv, or acetoformosolv [3]. There are two reasons that explain the low monomer yield. The first reason is that to free one monomer, two β-O-4 linkages must be broken [25]. For this reason, the S/G ratio is very important in predicting monomer yield. Since, the sinapyl monomer has a methoxy group at the C5 position, which prevents a 5-5 linkage from forming, a higher S/G ratio has more labile bonds [25]. The second reason is the phenomenon of repolymerization as illustrated in **Figure 2.7.** The mechanism of repolymerization involves a hydrogen abstracted from the hydroxyl group of a phenolic compound to form a phenolate (**Figure 2.7.1**), which can react with a ketone to re-create another ether bond, or the phenolate can rearrange to a carbanion (**Figure 2.7.2**). The carbanion reacts with a ketone to form a carbon-carbon bond,

which has a higher BDE than the original ether bond, making it more difficult to break [3]. In fact, running the depolymerization reaction a second time on the residual lignin, which is thought to be a mixture of repolymerized lignin and native lignin, does not increase the bio-oil yield by more than 2% [29].

There is research on reducing the degree of repolymerization. Methods focusing on scavenging carbanions, for example, by introducing formaldehyde in the extraction process, have had positive effects [9]. The addition of boric acid to the depolymerization experiments has also shown successful results. At pHs below 4 or above 12 boric acid caps phenolic hydroxyl groups with a boric ester, doubling the yield of monomers [29]. Historically, research favors strategies to maximize the yield and stability of monomers, rather than looking at potential applications for the oligomers [5, 11, 12, 74-77].

2.5 Analysis of Products from Base Catalyzed Depolymerization

2.5.1 A New Types of Base Catalyzed Depolymerization

BCD was discussed in detail in the section above. Traditional methods of BCD have a considerable number of downsides including low yields, complicated mixtures, repolymerization, and harsh reaction conditions. We detail a novel method of BCD that runs under ambient conditions using the effluent from an MEC to produce discrete aromatics in comparable yields to previous literature reports and that encourages repolymerization to produce flavonoids. Figure 8 illustrates the biorefinery schematic used in our research. Error! Reference source not found..**a** illustrates the MEC previously detailed in **.**

2.3 Biorefineries. In addition to "clean" water, the MEC produces a catholyte that is high in salt and has a pH above 8 – typically around pH 11. This catholyte is combined with lignin (Error!

Reference source not found..**b)** and produces two product streams: Low molecular weight aromatics and lignin nanoparticles.
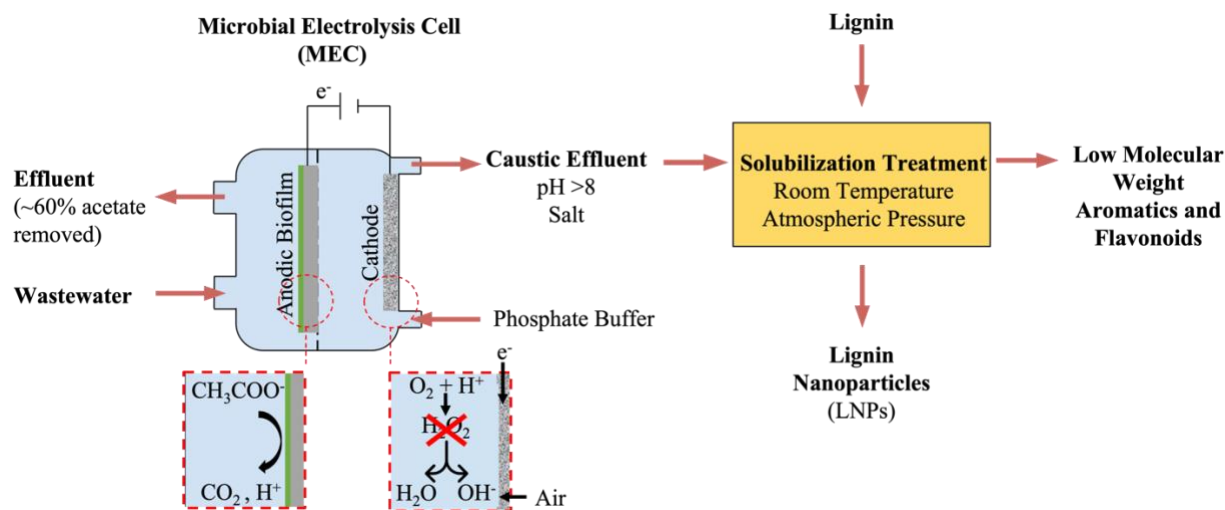
Figure 2.8. A schematic of the biorefinery used by Carnelli and Obrzut [18]. a) the MEC described by Griffin et al [4]; b) the lignin depolymerization process to produce 2 product streams.

We have quantified a total yield for identified, discreet aromatics between 7-12%. Most of these compounds (6-9%) are oligomers and flavonoids and the remaining 0.7-2.5% are fine monomers (monomers that have commercial value, ex. vanillin) [78]. In the literature, researchers using BCD albeit at high temperature and pressure, have reported 0.1-5.8% of their identified compounds to be BTEX and the remaining 0.02-2.80% to be fine monomers [3, 29, 72].

2.5.2 Techniques for Identifying Products

There are a variety of techniques that can be used to identify depolymerization products which are summarized in **Table** 2.4**.** UV-vis spectroscopy is useful as a bulk measurement. A calibration curve can be created by dissolving a specified lignin mass completely at pH 13 and measuring its absorbance at 280 nm and then used to determine the amount of solubilized lignin

due to a depolymerization method [79]. UV-vis spectroscopy can also be used to determine the total concentration of phenols and flavonoids. The Folin-Ciolcalteu method is used for the bulk quantification of phenols and combines 100 µL of the solubilized mixture with 2 mL of a 2 % sodium carbonate solution [80, 81]. After incubating at room temperature for five minutes, 100 µL of the Folin-Ciolcalteu reagent are added. Then, absorbance is measured at 750 nm after incubating at room temperature for another 30 minutes. A calibration is performed with a solution of gallic acid (3, 4,5-trihydroxybenzoic acid). The Zhishen method quantifies the total flavonoid content by combining 300 µL of solubilized lignin, 3.4 mL of a 30 % methanol solution, 150 µL of a 0.5 mmol·L-1 sodium nitrate solution and 150 µL of a 0.3 mmol·L-1 aluminum chloride hexahydrate solution at room temperature [81, 82]. After 5 minutes, 1 mL of 1 mol·L^{-1} sodium hydroxide solution is added, and an absorbance value is obtained at 510 nm. The calibration curve is made using the flavonoid rutin.

High Performance Liquid Chromatography (HPLC) is a useful tool in separating compounds in complex mixtures. By varying the solvents, similar compounds can be separated and analyzed. HPLC can be coupled with a UV-vis detector so that the spectra of each compound is available as well; this can aid us in making preliminary identifications of compounds by comparing the spectra to online databases or to purchased standards. Liquid chromatography mass spectroscopy (LCMS) and tandem mass spectroscopy (LCMSn) are an additional tools useful for identifying individual compounds. High resolution LCMS separates aromatic compounds and each peak provides an accurate molecular weight, double bond equivalence, and a potential molecular formula. MSn provides fragmentation patterns of characteristic molecular ions. By combining this information, potential structures can be proposed [83-88] and by comparing the spectral

information to standards, chemical structures are confirmed. NMR can also complement MSn to help confirm the presence of functional groups.

Table 2.4. A summary of techniques used to identify and quantify discrete aromatics products from BCD of lignin.

Technique	Result
UV-vis Spectroscopy	Bulk properties such as, dissolved concentration, aromaticity, phenolic content , and flavonoid content [79-82].
High Performance Liquid Chromatography (HPLC)	Separation of aromatic compounds, both monomeric and larger (typically between 100 and 1000 Da). UV- vis spectra of separated compounds [83-88].
High Resolution Mass Spectroscopy (MS)	Molecular weight, double bond equivalence, molecular formula [83-88].
Tandem MS	Fragmentation pattern providing insight to structure [83-88].
Nuclear Magnetic Resonance (NMR)	Functional groups via proton, C^{13}, or P^{31} NMR, as well as the position of the functional groups [89-94].

2.5.3 BCD Products

Generally, there are three classes of discrete aromatics produced from BCD: oil by-products, fine chemicals, and flavonoids. Oil by-products are compounds such as BTEX and do not offer much value because they are produced at high volume through a variety of routes such as catalytic reforming, steam cracking, and coal processing of fossil fuels. For example, benzene is produced from petroleum and coal via catalytic reforming, steam cracking, and coal processing and in 2019, benzene production reached more than 61 million metric tons [95]. These products are typically low yield through BCD, reaching a maximum around 5% of the initial lignin, meaning

this is not a commercially competitive product to target. Fine chemicals are more substituted aromatic chemicals such as flavorings like vanilla. Natural vanilla from the vanilla bean in Madagascar is responsible for less than 1% of the global production of vanilla. Vanilla beans contain only 2% of extractable vanilla flavor, meaning that pure vanilla reached a high of $11,000 per kilogram. 85% of global vanilla comes from the petrochemical industry with the remaining 15% coming from lignin via the Borregaard process [96]. Vanilla from lignin is possible through the oxidation of guiacyl units, yielding up to 7% vanilla from the initial lignin [97]. The Borregaard process uses lignosulfonate as the starting material and oxidizes it with copper sulfate and sodium hydroxide at high temperature (160-170 ℃) and high pressure (10-15 bar) [98]. The resulting sodium vanillate is acidified with sulfur dioxide to produce vanillin. BCD usually yields 0.007% [3]. Although our BCD yields up to 0.5% vanillin, it is still not commercially competitive with the petrochemical industry or the Borregarrd process.

The third BCD product stream is flavonoids. These products have not been a target of depolymerization historically, as their value has not been well understood. Typically depolymerization has targeted smaller compounds that could be up-cycled. Flavonoids have properties that make them of high value in the food and pharmaceutical industries as antioxidants and nutritional supplements. Typical sources of flavonoids are plants, such as fruits, vegetables, and teas (USDA). Flavonoids are already sold over the counter as mixtures in supplements eliminating the need for separating the mixture into low yield pure flavonoid components.

2.5.4 Yield and mechanism off flavonoid formation by BCD

Although flavonoids may be a very valuable product, the literature contains few reports that discuss optimizing lignin depolymerization conditions to yield flavonoids. Flavonoids

produced via our BCD method were identified by MSn – using the exact molecular weight, double bond equivalence, and fragmentation pattern - and then quantified with a Tricin standard calibration curve. Through this methodology we identified approximately 3% of Tricin, 1% of Antiarone-F, and 1.5% of 7-[(9-hydroxynonyl)oxy]-3-[4-(9-hydroxynonyl)phenyl]-4H-1-benzopyran-4-one, totaling a quantified flavonoid yield greater than 5% of the initial lignin mass. As described in 2.5.2 Techniques for Identifying Products, the Zhishen method was employed for bulk quantification of flavonoids and determined the percent flavonoids in our BCD experiments ranges between 10-17%. This suggests that there are flavonoids in our mixture that we have not identified via MSn. Results from the Zhishen method have not been reported in other lignin depolymerized research in the literature. The Zhishen method, however, has been applied to a plant, red clover, which is commercially available over the counter as an herbal supplement due to the activity of isoflavones. The flavonoid content of red clover was measured in the range of 0.6-2.7%[81]. This suggests that our biorefining of lignin is potentially commercially competitive with other plant sources.

There is little research into the mechanism of flavonoid formation from lignin. Only recently has it been postulated that flavonoids play a role as authentic monomers of lignin [99]. We propose that flavonoids are repolymerization products of BCD. To test this mechanism we used the Zhishen method to measure the flavonoid content in two experiments. In the first experiment we combined monomeric phenols (m-hydroxybenzaldehyde, vanillin, p-coumaric acid, and ferulic acid) with MEC effluent to determine if the MEC effluent causes repolymerization of monomers to flavonoids to occur. In the second experiment we combined lignin extracted with water, to see if there were any free flavonoids in the extracted lignin . We found 2.6% flavonoids in the treated monomeric phenols mixture compared to 0% in the water, indicating that

repolymerization of BCD products likely plays a role in producing flavonoids and that there are not free flavonoids present in extracted lignin.

Our current research explores the relationship between lignin structure and flavonoid yield. Here we compare three different extraction methods of a herbaceous lignin (milled, Organosolv, and Klason) as described in 2.2.2 Lignin Extraction. The ratio of β-O-4 linkages to aromatic carbon-hydrogen in these samples decreased from 2.3 (Milled Wood lignin - least harsh) to 1.0 (Organosolv) to 0.14 (Klason - most harsh). After processing the three lignins with our BCD treatment, we measured the concentration of the flavonoid,
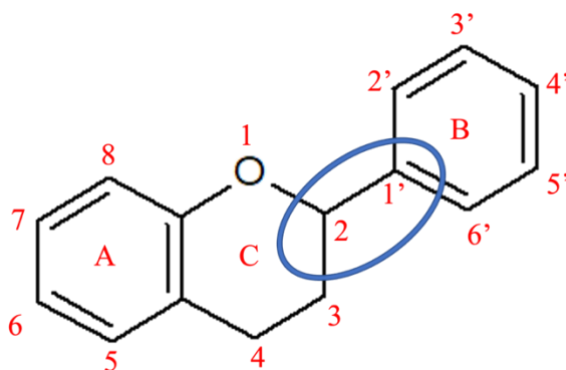
Figure 2.9. The labeled diphenylpropane skeleton of flavonoids. Adapted from Kumar et al.

tricin, by LCMS to find that the concentration of tricin increases with decreasing ether linkages. We see that Klason lignin contains 8.4% of tricin, compared to 2.4% for Organosolv, and 1.2% for Milled Wood lignin. This may also be true for other flavonoids. This finding suggests increased condensation in the starting lignin favors the production of flavonoids. This could be due to the 2-1' condensed bond that is present in the diphenylpropane skeleton of the flavonoid structure as shown in **Figure 2.9.**

As shown in **Table** 2.1**,** lignin source controls its structure and the most notable differences among herbaceous, softwood, and hardwood lignin are the S/G ratio and varying proportions in β-O-4 linkages. Hence, we expect that lignin source may influence flavonoid yield under our biorefining conditions.

2.6. Lignin Nanoparticles

2.6.1 Characteristics of Lignin Nanoparticles

Nanoparticles are ubiquitous in consumer products and serve to improve performance, durability, and enhance certain properties [100-102]. Recent research reveals that lignin may be a source of carbon-based nanoparticles [103-105] and the synthesis and characterization of lignin nanoparticles (LNPs) has grown exponentially over the last decade [104, 106]. For example, lignin nanoparticles under 200 nm have properties that make them attractive for drug delivery such as prolonged circulation time in blood, excellent stability with dilution, enhanced permeability, and retention [107]. Nanoparticles can be high yield, high value products that can be synthesized simultaneously with low yield, high value aromatics [108].

Lignin nanoparticles are characterized by size and shape and are typically spherical ranging from 2 nm (carbon quantum dots) to the micrometer scale, depending on solvent type, rate of addition, and pH [104, 109-112]. Stability is analyzed by observing how the diameter of the LNPs changes with pH, time, and salt concentration. Most LNPs are stable for at least 30 days, dissolve at high pH and aggregate at high salt concentration [104, 109, 111]. There is also aggregation at low pH (around 2) due to protonation of lignin moieties, which makes the charge on the lignin neutral [111].

2.6.2 Mechanisms of Formation of Lignin Nanoparticles

Generally, the formation of LNPs relies first on dissolving lignin [5, 104, 109-114]. This is where the similarities among reports end. The starting lignin material ranges from hardwood lignin to softwood, from Kraft to Organosolv, and from unmodified to acetylated lignin. The lignin

can be dissolved generally in two ways: 1) high pH or 2) an organic solvent. High pH is not a very common way of dissolving lignin for LNP production and most researchers opt for organic solvents, such as, ethylene glycol, ethanol, tetrahydrofuran (THF), dimethylsulfoxide (DMSO), acetone or castor oil. The second step is to then decrease the solubility of lignin. Regardless if the lignin was dissolved in high pH or in an organic solvent, solubility can be decreased through the addition of acid (HCl, HNO_3, or H_2SO_4). LNP formation is initiated by the molecular weight dependent precipitation of the dissolved subunits of lignin, where large molecules precipitate first and form a critical nuclei (40-70 nm) [115]. This is followed by the collision-driven particle growth and adsorption. This mechanism can be seen below in **Figure** 2.10**.**
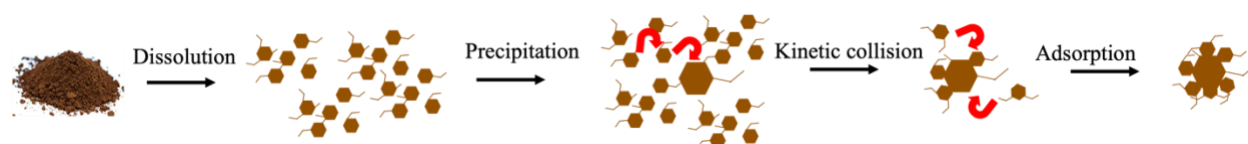
Figure 2.10. A potential mechanism of LNP formation involving precipitation to a critical nuclei and kinetic growth [104, 111, 116, 117].

The solubility of lignin dissolved in an organic solvent is diminished by the addition of an antisolvent. An anti-solvent is a solvent in which lignin does not dissolve, for instance a polar solvent, such as water. This mechanism has been postulated to be the same as in **Figure** 2.10 by some researchers [116, 117]. The number of LNPs is determined as the pH drops, based on the number of critical nuclei formed, and with time, the size of the nanoparticles increases as smaller dissolved subunits adsorb to the surface of the critical nuclei. The initial concentration of LNPs should not increase with time since no new nuclei are produced after the solubility is decreased and critical nuclei have formed. This mechanism is controlled by the initial lignin concentration, the strength of the acid or anti-solvent added, and the rate of addition of acid or antisolvent [111].

The size of the LNPs can be controlled by stopping the growth reaction by diluting the solution with water.
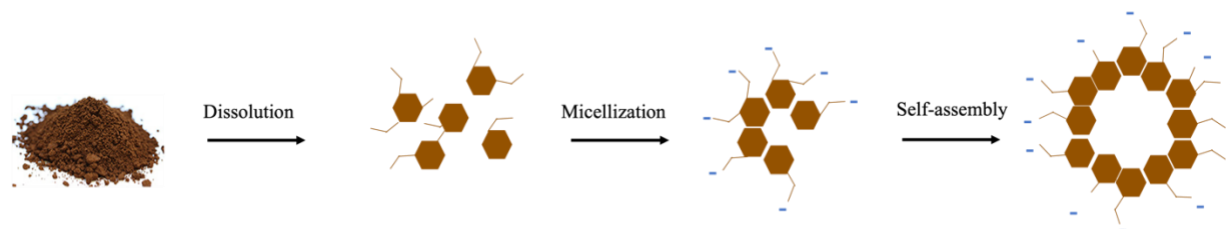
Figure 2.11. Another potential mechanism of LNP formation involving micellization [114, 118, 119].

Other researchers have proposed that the mechanism of LNP formation is micellization (**Figure** 2.11) [114, 119, 120]. Micellization involves alignment of the hydrophobic and hydrophilic parts of the lignin depending on the solvent characteristics [116]. First, lignin depolymerizes in an organic solvent followed by the addition of a water phase. The subunits aggregate in the water phase to form a hydrophobic micelle core. The hydrophilic components of the lignin form the micelle shell. The LNPs grow spherically through either molecular aggregation of polymer chains or by self-assembly via aromatic stacking [114, 121]. Lignin micellization is postulated to be driven by electrostatic interactions of the functional groups, hydrogen bonding, van der Waals and π-π interactions [107, 116, 122-126]. The length ratio of the hydrophobic core to the hydrophilic corona dictate the shape (i.e. a longer corona than core will be spherical) [122]. This mechanism suggests that the number of LNPs and the size of LNPs does not change once the critical micelle concentration (CMC) is reached, regardless of dilution rate [111].

A flow chart summarizing the different methods of forming LNPs and their corresponding mechanism can be seen below in **Figure** 2.12.
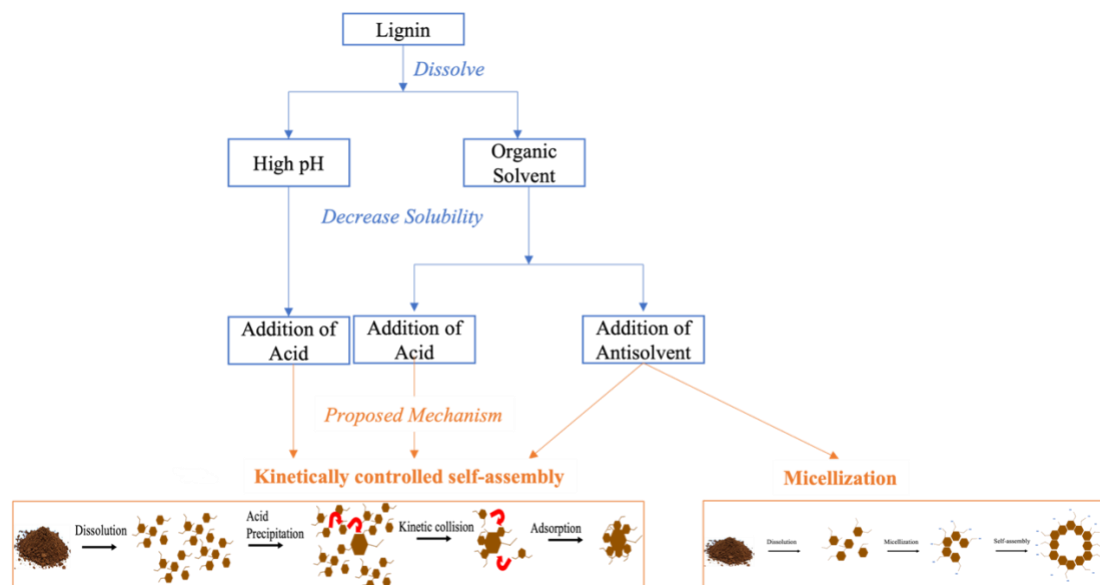
Figure 2.12. A summary of the conditions and potential mechanisms of formation of nanoparticles from lignin.

Recently, hydrotropic salts, such as p-toluene sulfonate, have been used to dissolve lignin. Hydrotropic salts are capable of solubilizing hydrophobic compounds in an aqueous solution. Lignin dissolved in a hydrotropic solution has its solubility decreased with water until the concentration is under the minimum hydrotropic concentration, at which point the salts start aggregating [127]. High yields (>90%) of LNPs with diameters around 500 nm and moderate stability as measured by a zeta potential of~ -25 mV have been produced by adding water to a hydrotropic salt solution [127].

2.6.2 Tunability of Lignin Nanoparticles

There is little research on the effect of lignin source and native structure on LNP synthesis and characteristics. It is unclear what factors control LNP characteristics and if these factors can be tuned to target the formation of LNPs of a particular size, shape, or charge. The literature reports a wide range of studies about LNPs derived from different types of lignin (source and extraction) and under different conditions making it difficult to determine the relationship between

structure and function. **Table** 2.5 summarizes the starting lignin (source and extraction), the method, reagents used, and properties of the resulting LNPs. There have been extensive studies on Kraft lignin and on the solvent/antisolvent method. We aim to elucidate rigorously the effects of lignin source and extraction method on LNP formation under the ambient conditions of our biorefining process.

Table 2.5. A summary of lignin source, method, reagents, and properties of LNPs from selected papers.

Lignin (source, extraction)	Method	Reagents	Size	Other
Softwood, Kraft [104]	Solvent/ antisolvent	Ethylene glycol/ hydrochloric acid	<100 nm	Stable pH 1-9, stable 30 days
Softwood, Kraft [104]	Acid precipitation	Sodium hydroxide/ nitric acid	85 nm	Amorphous shape, stable in pH < 3. Stable for 5 days
Hardwood, Organosolv [112]	Solvent/ antisolvent	DMSO/ water	195 nm	Stable pH 4-12
Softwood, Kraft [109]	Solvent/ antisolvent	THF/water	320 nm	Stable 60 days, zeta= -60 eV
Hardwood, Organosolv[111]	Solvent/ antisolvent	Acetone/ water	80 nm	Zeta = -45 eV
Softwood, Kraft [111]	Solvent/ antisolvent	Ethylene glycol/ nitric acid	45-250 nm	Zeta = -20 mV
Hardwood, Alkaline (Acetylated)[116]	Solvent/ antisolvent	Acetone/water+NaCl	50-1000 nm	
Softwood, Kraft[127]	Solvent/ antisolvent	Ethanol/water	300 nm	75% yield, zeta=-25.8 mV
Softwood, Kraft [127]	hydrotropic	Na-PTS	540 nm	90% yield, zeta = -24.3 mV

We determined that LNPs appear to self-organize in the BCD product mixture over two weeks at room temperature. Over this time the pH decreases from pH 10.8 to pH 8. Additionally, we can accelerate the aging effects by decreasing the pH with phosphoric acid. We initially found LNPs that ranged between 80 nm and 500 nm. We also found that after two weeks, the LNPs closed mass balance on the lignin depolymerization products. The SEM images below in Error! Reference source not found. confirm the size distribution as well as the spherical shape.
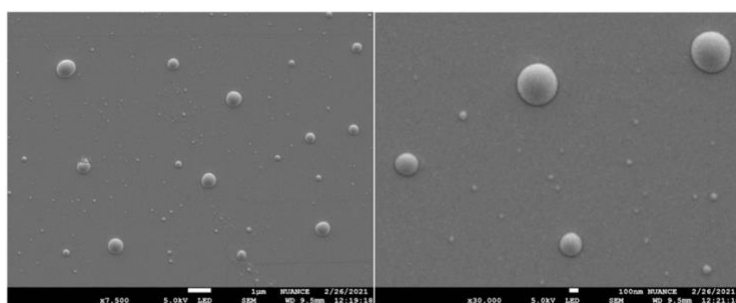
Figure 2.13 SEM micrographs of LNPs formed through neutralization of depolymerized Organosolv corn stover. Left: 7,500 x magnification. Right: 30,000 x magnification.

The LNPs in Error! Reference source not found. were formed from Organosolv lignin derived from corn stover. Preliminary results from Milled Wood extracted from a corn stover source neutralized and aged for two weeks do not show the production LNPs. This observation suggests that β-O-4 bonds (as previously determined via FTIR) are easily cleaved to make smaller lignin units that do not form critical nuclei that are necessary for LNP production. When we produced LNPs from Klason lignin extracted from a corn stover source, we saw similarly sized and stable LNPs to the Organosolv LNPs, albeit with greater aggregation to pieces of unreacted lignin.

Although anecdotal, there are a few insights to be gained from reports about how lignin extraction influences LNP characteristics. In a comparison of Organosolv lignin to lignin extracted

via the deep eutectic solvent (DES) method with DMSO and then dialyzed, similarly sized (195-197 nm) LNPs with similar properties were produced. There were, however, some differences in that the Organosolv LNPs had a higher number of phenolic hydroxyl groups at the LNP surface and there was greater polydispersity with the Organosolv lignin than the DES lignin (0.17 vs. 0.08, respectively) [112]. In another study LNPs were formed from Kraft and Organosolv lignin through flash precipitation methods. According to the researchers, Kraft LNPs remained stable at high ionic strength suggesting LNP stabilization by a combination of repulsive electrostatic interactions, steric repulsions, surface roughness, or other short range repulsion [111]. In contrast, the Organosolv lignin was stabilized mainly by electrostatic interactions, as determined by the relatively low ionic strength at which colloidal destabilization occurs (aggregation at <100 mM NaCl) [111].

In addition to the effects of lignin structure, the effects of pH and salt on LNP stability are also important consideration. Most prior research found that LNPs are stable between a pH range of 4 through 12 and up to 100 mM NaCl. Salt and pH conditions may also play a role in tuning LNP properties. For instance, Frangville varied the concentration of acid added to precipitate LNPs over two orders of magnitude and saw LNPs less than 100 nm to 2 μm over that range [104]. However, there is not an extensive body of research compiled thus far on how the starting and ending pH affect the resulting LNP properties.
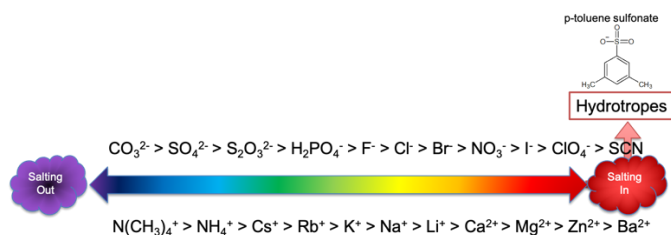
Figure 2.14. Reactivity of salt in accordance to the Hoffmeister scale [128].

The type and concentration of salts have myriad effects on LNP formation. For instance, biorefining process often require pH buffering. In our work, lignin depolymerization is conducted under the high ionic strength conditions set by the coupled MEC process requirements of a phosphate buffer. The high concentration of phosphate salts may trigger LNP formation through a salting out mechanism due to high ionic strength or the specific ion effects of phosphate anions. Salting out is defined as high ionic strength decreasing the solubility of a weak- or non-electrolyte by reducing the thickness of electrical double layers and therefore decreasing the electrostatic repulsion between the LNPs through electrostatic screening [129, 130]. Salting out varies as a function of the anion/cation type in accordance with the Hoffmeister series (**Figure** 2.14), with carbonate salts being the most reactive (most salting-out "power") and chlorides being the least. Phosphate salts are more reactive than chloride salts, which may also have an influence in the synthesis of LNPs [128]. A number of different salts can be used to create biocompatible conditions in place of phosphate in MECs, which paves the way for experimentation with different salts on the series to see the effect on solubilization and LNP synthesis [131, 132].

2.7. Potential Applications

Currently, the dominant commercial use of lignin is for fuel combustion. However, the potential of using lignin for high value products is showing greater promise and commercial

opportunity. Both discrete aromatics (2.5.3 BCD Products) and LNPs (2.6. Lignin Nanoparticles) have potential applications in fine chemicals, pharmaceuticals, personal care products, and agriculture. As previously discussed, the Borregaard process is a commercial method of producing vanillin (**Figure** 2.15.**a**) from lignin and is responsible for 15% of the world's vanillin production [133]. Syringaldehyde (**Figure** 2.15.**b**) is another fine chemical that is related to vanillin (with an additional methoxy group at the C5 position). Syringaldehyde is a valuable feedstock chemical in the pharmaceutic industry because it is a building block of the antibacterial agents ormetoprim (**Figure** 2.15.**c**) and trimethoprim (**Figure** 2.15.**d**) [134].
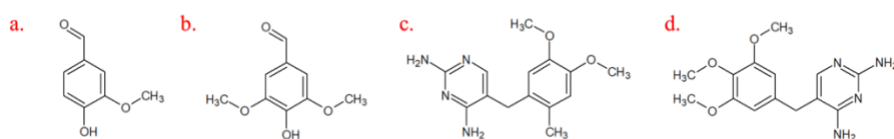
Figure 2.15. The structure of select compounds sourced from lignin. a. vanillin b. syringaldehyde c. ormetoprim (synthesized from syringaldehyde) d. trimethoprim(synthesized from syringaldehyde)

Other promising high value lignin derived products are flavonoids, which have antioxidant properties that may make them good candidates for various medicinal purposes. Lignin nanoparticles are non-toxic, biodegradable, inexpensive, and stable. These characteristics make LNPs favorable alternatives to carbon-based nanoparticles for a variety of uses such as drug delivery, hydrogels, sunscreen, food additives, and tissue repair [108, 135].

2.7.1 Pharmaceuticals and Personal Care Products

Lignin nanoparticles have been studied extensively for drug delivery and can be used for both hydrophobic and hydrophilic drugs[136]. LNPs can be coated with pH sensitive polymers to facilitate carrying hydrophilic drugs whereas the LNPs themselves increase the effects of

hydrophobic drugs [136]. LNPs have successfully encapsulated silver ions to be used for antimicrobial applications and cancer treatments [136]. LNPs were also tested in transporting methotrexate, an anti-rheumatoid arthritis drug, in rats [136]. LNPs were shown to be a good nanodrug carrier when combined through self-assembly with resveratrol and Fe_3O_4 [137]. The LNP carrier had a high drug loading efficiency, prolonged blood circulation time, and good cell uptake. LNPs were also tested as a carrier for curcumin, an antioxidant and anti-inflammatory agent, and showed a ten-fold increase in curcumin bioavailability [108].

LNPs can be tailored as hydrogels, which are hydrophilic polymeric networks with high absorption capacity, by combining them with other compounds to reverse lignin's inherent properties of hydrophobicity [138]. When LNPs were combined with polyvinyl alcohol (PVA) and cellulose nanofibrils, the resulting hydrogel showed promise in a variety of possible applications such as flexible pressure sensors, tissue scaffolds, and soft machines. Combining LNPs with PVA and chitosan imparted the material with antimicrobial properties well suited to drug delivery, food packaging, and tissue repair [108]. Combining LNPs with proteins may allow their use in tissue repair because of adhesive properties [139].

LNPs have also been used in sunscreen because of their UV absorption capabilities [110, 140]. It was found that a 10% weight solution of 50 nm Organosolv LNPs gives an SPF value of 15. The addition of 10% weight of mid-sized LNPs to sunscreen with UVA and UVB protection can increase the SPF from 10 to 47 [110].

2.7.2 Antioxidants

Flavonoids and other phenolic compounds, examples of which are listed in Error! Reference source not found., are antioxidants, which are substances that at low concentrations prevent or delay the oxidation of a substrate [1].

Table 2.6 Examples of flavonoids and phenolic compounds found in foods [1] .

Type of Antioxidant	Class of chemical	Name of chemical	Structure of chemical	Common Sources
Flavonoids	Flavonol	Quercetin		Citrus, apples, onions, parsley, sage, tea, red wine, dark berries.
	Flavone	Apigenin		Parsley, chamomile, celery, artichokes, and oregano.
	Flavonolol	Taxifolin		Olive oil, grapes, citrus fruits, onions
	Flavan-3-ol	Catechin		Red wine, tea leaves, beans, grapes, apricots, strawberries
	Flavonone	Hesperidin		Citrus fruits (oranges, grapefruits, lemons, tangerine)
	Anthocyanidin	Delphidin		Berries, red grapes, potatoes, red cabbage
	Isoflavone	Daidzein		Soy
Hydroxycinnamatic phenols		Ferulic acid		Rice, wheat, oats
		Caffeic acid		Coffee
		P-coumaric acid		Peanuts, beans, tomatoes, carrots, basil, garlic, barley grain

Oxidative stress occurs when there is an accumulation of reactive oxygen species. The risk of oxidation in the cell is that it can be the cause of inflammation, aging, and chronic diseases such as cancer, cardiovascular disease, neurological disease (Parkinson's, Alzheimer's, depression), respiratory disease (chronic obstructive pulmonary disease, asthma), arthritis, and kidney disease [141]. Because of the severity of these diseases, antioxidants play an important role in human health.

Oxidation in cells generally targets membranes, lipids, proteins and DNA[141]. The species that oxidize these compounds are often called reactive oxygen species (ROS) and reactive nitrogen species (RNS). Some examples of ROS are the singlet oxygen, superoxide anion radical, hydroxyl radical, alkoxyl radical, peroxyl radical, and hydrogen peroxide. Some of the mechanisms of oxidation that occur are: autooxidation, photosensitized oxidation, thermal oxidation, and enzymatic oxidation.

Broadly, there are two classes of antioxidants – enzymatic and non-enzymatic. Enzymatic antioxidants scavenge free radicals by converting ROS into water. Some examples of these types of antioxidants are superoxide dismutase, catalase, and gluthione peroxidase [142]. Non-enzymatic antioxidants, under which flavonoids are grouped, also disrupt the radical chain reaction in a number of ways. Non-enzymatic antioxidants found in nature include vitamin C, vitamin E, polyphenols, carotenoids, and glutathione, among others. Non-enzymatic antioxidants work by either breaking the free radical chain reaction as free radical scavengers (primary antioxidants) or acting preventatively (secondary antioxidants). Secondary antioxidants act via a variety of mechanisms such as deactivating metals, inhibiting lipid hydroperoxides, regenerating primary antioxidants, and quenching singlet oxygen [1]. Examples of the major antioxidant chemical classes, specific compounds that fall under those classes, and the mechanisms by which they function are summarized in **Table** 2.7**.**

Table 2.7. A summary of antioxidant classes, examples, and mechanisms by which they prevent oxidation [1, 143, 144].

Antioxidant Class	Antioxidant examples	Mechanism
Phenolic Compounds (* indicates sourced from lignin)	trolox, hydroxytrosol, gallic acid*, caffeic acid*, epicatechin*, kaempferol*, resveratrol*, flavonoids*, hydroxycinnamates*	free radical scavenging, chelating metals, singlet oxygen quenching
Carotenoids	lycopene, B-carotene, zeaxanthin, lutein, echinenone, astaxanthin	singlet oxygen quenching, inactivation of photosensitizers, free radical scavenging
Vitamins	vitamin C, ascorbic acid analogs, vitamin E	chelating metals, single oxygen quenching, free radical scavenging

Protein related compounds	hypoxanthine, xanthine, glycine, methionine, histidine, tryptophan, proline, lysine, ferritin, transferrition, carosine, glucose oxidase, superoxide dismutase, vatalase, gluthione peroxidase	enzymatic, cheating metals, free radical scavenging

Flavonoids, which can be extracted from lignin, primarily serve as antioxidants through free radical scavenging. Generally, this reaction mechanism is either, 1) a hydrogen atom transfer
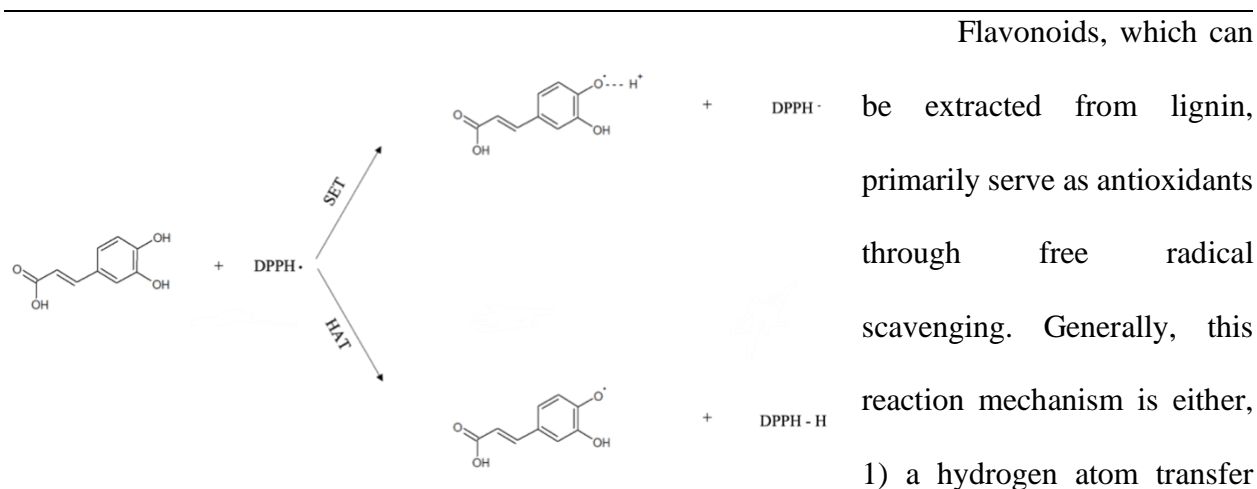
Figure 2.16. Caffeic acid undergoing a single electron transfer (SET) (above) and hydrogen atom transfer (HAT) (below) reaction with the DPPH free radical.

(HAT) reaction or 2) a single electron transfer (SET) (**Figure 2.16**). Phenolic reaction with ROS involves the transfer of the hydrogen cation from the phenol to the radical which forms a transition state of an H-O bond with one electron (free radical) [1]. Metals such as iron (II or III) and copper (II and I) are known to aggravate oxidative stress by reacting with hydrogen peroxide to produce the hydroxyl radical in the case of iron, and singlet oxygen in the case of copper. Antioxidants such as curcumin, capsaicin, and S-allylcystein that bind metals, successfully inhibit these oxidative stress reactions [144]. Singlet oxygen quenching occurs by energy transfer, when the energy of the quencher is very near or below that of the singlet oxygen. Carotenoids with 9 or more conjugated double bonds are well suited to this quenching mechanism [143]. Carotenoids with less than 9 conjugated double bonds prefer photosensitizer inactivations where the energy of the photosensitizer facilitates the transition from the singlet to triplet state of the carotenoid [143].

The antioxidant capacity of compounds can be determined through a variety of assays including: lipid peroxidation assay, DPPH free radical scavenging assay, chelating activity on ferrous ions, Fe^{3+} reducing power assay, hydrogen peroxide scavenging activity assay, superoxide radical scavenging activity , and ABTS scavenging activity [80-82, 145-153]. An illustration of how a flavonoid (anthocynidine) acts an antioxidant through metal chelating or free radical scavenging is shown in the **Figure** 2.17.
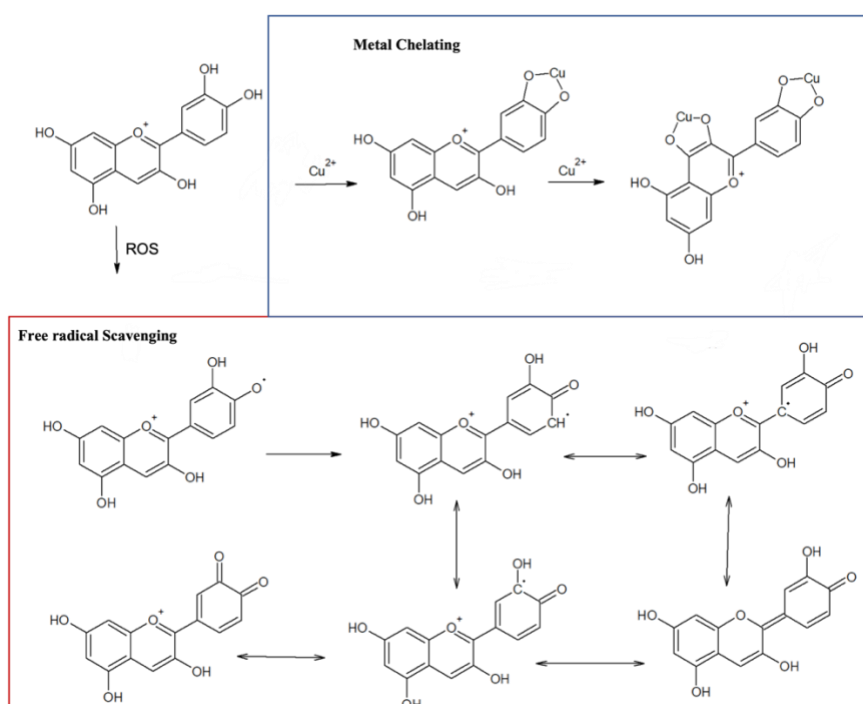
Figure 2.17. Anthocyanidin serving as an antioxidant via metal chelating and free radical scavenging [142].

2.7.3. Agriculture

LNPs have been used for the delivery of pesticides and herbicides in agricultural applications [106, 154]. Through the self-assembly mechanism of LNPs, hydrophobic pesticides or insecticides can be entrapped in the LNP interior [106]. The mechanism of entrapment is shown in the **Figure** 2.18 and is coupled to the micellular mechanisms of LNP formation. They can be

delivered to the roots through diffusion or they can be coated with a polymer such as chitosan or poly(di-allyldimethylammoniumchloride) (PDADMAC), to delay pesticide delivery [106]. LNPs can also be used for diagnostic and therapeutic uses related to plant disease and health such as nano-diagnostics, pesticide remediation, and induced resistance [154]. Graphite nanoparticles (another type of carbon nanoparticle) have been used to deliver fertilizer and decrease the amount of nitrogen leaching and this is another area for which LNPs may be similarly used [155].
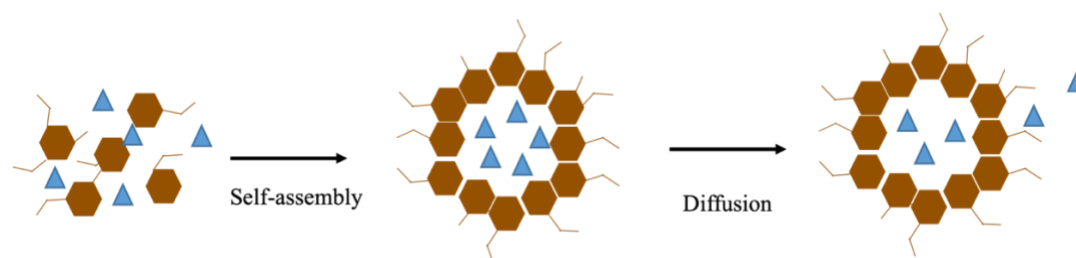
Figure 2.18. The mechanism of entrapment of a hydrophobic compound within an LNP.

2.8 Conclusion

Amid a climate emergency, there is renewed interest and motivation to explore the promise of lignin as far more than waste fuel and as a potential source of high value products. Unlocking this potential starts by studying and optimizing processing techniques. It is well understood that the source and the method of extracting lignin have significant effects on the structure of extracted lignin. It is also well understood that the structure of lignin has major effects on downstream processing. Many researchers stress that extraction methods should preserve the β-O-4 linkage in order to produce higher yielding monomers. What is not well understood, however, is how the structure of lignin affects other depolymerization products (e.g., mixture characteristics, yields,

etc.), such as flavonoids and LNPs, which may have similar or more value than the original targets of lignin depolymerization.

Biorefining has been around since mead was produced in 1700-1100 BC in Asia [156]. There are remains of wine, the fermentation of fruit, that are over 7,000 years old. Fermentation is the oldest type of biorefining and we have certainly expanded on that to produce products other than alcohol such as biofuels, bioenergy, biomaterials, and biochemicals. Biorefining is an important processing technique. In a world of limited resources there is immense value in being able to refine residual biomass. Although biorefining is not new, the potential for lignin processing is not fully explored or exploited.

Lignin processing generally falls into three categories: 1) extraction, 2) depolymerization, and 3) valorization. In this chapter we discussed that there is potential value in preserving the native structure of lignin through the extraction process. There are many ways that lignin can be depolymerized ranging from gasification and pyrolysis at high temperatures to yield syngas or bio-oil to catalysis that targets products such as vanillin in the Borregaard process. Base catalyzed depolymerization (BCD) of lignin typically occurs at elevated temperature and pressure and has had historically low yields and complicated mixtures.

The development of a biorefinery that couples wastewater treatment in a microbial electrolysis cell with lignin BCD is an innovative way to produce multiple product steams under ambient conditions (room temperature, atmospheric pressure, base from MEC catholyte). In addition to clean water, our work has detailed novel product yields at levels higher than previous reports. Flavonoids are compounds that have not been targeted in lignin valorization but have very high potential as antioxidants. LNPs are a relatively new (< 10 years) discovery having many

potential applications that have not yet been fully realized, ranging from drug delivery to cosmetics to applications in agriculture.

Lignin is an abundant and renewable source of materials and aromatic carbon that awaits inventive methods to open up opportunity in new and creative ways.

Chapter 3 : The valorization of lignin under mild conditions: biorefining flavonoids and lignin nanoparticles[2]

3.1 Introduction

Biomass is the only renewable source of organic carbon and, thus, a promising feedstock for obtaining chemicals and materials [157]. Furthermore, in a biorefinery, biomass processing can be integrated with the recovery of energy and materials from other waste streams, such as food waste or municipal wastewater to yield multiple high value product streams [158]. As the biopolymer of greatest aromatic content, lignin has 15-30% of the mass and 40% of the energy of lignocellulosic biomass and has long been a target for valorization [159, 160]. Yet, lignin is not commonly used in commercial production of chemicals or materials. For example, only 2% of the lignin obtained as a byproduct from paper production is used in other industries (mainly as dispersant or emulsifier), while the remainder is burned as a low-value fuel [161]. Moreover, in agricultural or urban settings, lignocellulosic biomass is typically considered a waste residue [162].

Efforts to obtain aromatic compounds from lignin began more than 70 years ago [163]. Many of those efforts were focused on energy-intensive thermochemical techniques (gasification, pyrolysis) that lead to a complex mixture of aromatic monomers which are difficult to separate [164]. The attempts to valorize lignin by other chemical routes began around the year 2000, and were first reviewed in 2010 by Zakzeski et al. [165], who pointed to a catalytic route as an essential way of

"efficient and selective lignin valorization." Motivated by the push for sustainable technologies, the number of publications about lignin valorization has grown exponentially over the last decade. During this time, literature reviews have appeared on various approaches such as biological methods [166], use of ionic liquids [167], electrocatalysis [68], and catalytic alternatives [167-171], which accelerate lignin depolymerization and reduce energy consumption [172]. Based on these reports, lignin is a potentially versatile feedstock for a wide range of products that include, in increasing order of economic value per ton: biofuels, BTX (benzene, toluene, xylene), activated carbon, phenolic resins, carbon fiber, food additives (mainly vanillin), fine chemicals, and pharmaceuticals [173]. Yet, it is also evident that there is not a recommended technological path for valorizing lignin, mainly because the methods having the highest yields suffer from elevated separation costs and are often energy-intensive and/or make use of relatively expensive, hazardous reagents.

Absent a price on net carbon emissions, the primary challenge for lignin valorization is its cost-competitiveness in the near term relative to petrochemically-derived alternatives. One approach to establish both the economic and technical advantages of lignin-derived products, is to identify a commercial niche around high-value and low-volume products such as pharmaceuticals, nutraceuticals, or engineered materials (e.g., nanoparticles).

Lignin extraction from biomass is well established [162, 172], but subsequent steps that solubilize and control its depolymerization to obtain desired products in sufficient yield for separation, purification, and ultimately valorization, remain technical challenges. Research on optimizing the fractionation and purification processes, such as the work done by Tindall et al, allows control over particular properties of lignin and may make the downstream valorization process simpler [42]. In principle, there are three basic approaches to lignin valorization [174]. In

the first case, lignin gasification produces synthesis gas or its pyrolysis creates a mix of small molecules (BTX, phenol) that can be used as drop-in replacements in the petrochemical supply chain. The second approach consists of an initial mild catalytic step to obtain oligomers that can be further depolymerized or functionalized into high-value chemicals. The third strategy is to use one harsh catalytic step to directly obtain valuable chemicals. The last two strategies, however, still require the development of new catalytic materials. In fact, the lack of effective catalysts with minimal environmental footprints is considered one of the main hurdles to the successful development of a lignocellulosic biorefinery [159, 172]. For example, base-catalyzed depolymerization (BCD) or hydrolysis of lignin could be a mild catalytic process if carried out at room temperature, but it is more often applied at higher temperatures (more than 150 ℃) and elevated pressures (more than 1 bar), and sometimes with additives such as organic solvents [172, 175]. On the other hand, for one-step processes, the catalysts are usually heavy-metal-based (Ni, Zn, Pd) and carbon-supported [172]. They are typically suspended in organic solvents (ethanol, methanol) and also require high temperatures and pressures [172].

As an alternative to these relatively energy-intensive and costly processes, we propose an integrated biorefinery strategy that couples a microbial electrolysis cell (MEC), treating organic-rich wastewaters, to lignin processing under mild conditions (room temperature, atmospheric pressure) [172, 176]. In this way, we seek to preserve the aromatic rings of lignin to produce feedstock chemicals, such as phenolics, or high value compounds for use in the food, nutraceutical, or pharmaceutical industries. This strategy is also plausible for producing carbon-based nanoparticles as alternatives to fullerenes or other graphene-based nanomaterials and for potential use in the personal care or agrochemical industries [108].

MECs are a counterpart to microbial fuel cells (MFCs) where biogenerated electrons are used in chemical reactions instead of being harvested as a source of electrical energy [176]. They rely on colonies (biofilms) of exoelectrogenic bacteria (e.g., S. oneidensis, G. sulfurreducens) for the treatment of wastewaters rich in volatile fatty acids (VFAs) [55]. In this work we use the microbial peroxide-producing cell (MPPC, a type of MEC) described by Griffin et al [4]. This cell generates H_2O_2 via the two-electron partial reduction of O_2 ($O_2 + 2H^+ + 2e^- \rightarrow H_2O_2$). In an acetate-fed MEC, this reaction is exergonic, although an external electrical potential is usually applied to increase the reaction rate [4]. It is important to note that protons are consumed in the reduction of oxygen, resulting in an increase in pH in the cathode chamber. In this way, the oxidation of VFAs in the anode produces an alkaline catholyte that can be controlled to produce H_2O_2.

The first goal of this work is to implement an MEC, as illustrated in **Error! Reference source not found.** to solubilize and depolymerize Organosolv lignin extracted from corn stover (a residue of bioethanol production) to obtain high-value aromatic chemicals and materials at ambient temperature and pressure. To achieve this goal we studied the effects of pH and the presence and absence of the phosphate buffer and H2O2 in the MEC catholyte on lignin depolymerization. The second goal is to quantitatively characterize the products of lignin solubilization and depolymerization using a variety of analytical tools on the solution and colloidal phases, including spectroscopic, chromatographic, microscopic and light scattering techniques. We show that the MEC can be simply operated to produce a caustic catholyte, in the pH range 10-11 without hydrogen peroxide, to solubilize over 90% of the lignin mass and to depolymerize it to yield two product fractions: approximately 11% of the lignin mass identified as discrete, high-value aromatic products (approximately 17% indicated by bulk measurements); and the balance as a colloid with particle sizes in the range of 50-500 nm.

3.2 Materials and methods

3.2.1 Lignin and other reagents

Lignin was kindly donated by Archer Daniels Midland (ADM), Decatur IL. ADM extracts lignin from corn stover by the acetosolv (Organosolv using acetic acid) process. Prior to use, it was ground in a mortar and pestle (< 0.4 mm), washed with ultrapure water until the washings showed minimal and stable absorbance at 260-280 nm, and then dried at 80 ˚C overnight.

Elemental analysis (Elementar Vario EL Cube) of the extracted lignin was made to determine the carbon, hydrogen, nitrogen and sulfur mass percentages of the sample. We estimated the oxygen content by taking the difference of the other reported elements from 100%. The washed Organosolv lignin was found to be approximately 58% C, 6% H, and 34% O by mass, with trace amounts of N and S. This corresponds to an average phenylpropanoid (C9) unit formula of $C_9H_{11}O_4$ with a molar mass of 183.18 g·mol^{-1}.

Reagent-grade acetic anhydride, potassium hydrogen phthalate, polystyrene (PS) beads, sodium hydroxide, and sulfuric acid, as well as the solvents pyridine (anhydrous), dichloromethane (DCM), tetrahydrofuran (THF), deuterochloroform (CDCl3), and deuterium oxide (D$_2$O) were purchased from Sigma Aldrich (now Merck) and used as received. Ethanol was 200 proof and anhydrous from Decon Labs. Reagent-grade Folin-Ciolcalteu reagent, gallic acid, and hexadecyltrimethylammonium bromide (CTAB), as well as HPLC-grade methanol were purchased from Fisher Scientific. Reagent-grade sodium carbonate, sodium nitrate, aluminum chloride hexahydrate, and rutin were purchased from Thermo Fisher.

3.2.2 Microbial electrolysis cell

We provide a brief summary of the MEC operational conditions used in this work. More details about the characteristics and performance of this MEC were previously published [4]. A detailed schematic of the MEC is shown in **Figure 2.5.** An acrylic cell, with a 200-mL anode chamber and a 100-mL cathode chamber, was separated by a 36-cm^2 anion exchange membrane (Ultrex AMI-7001, Membranes Intl.). The anode chamber was equipped with an Ag/AgCl reference electrode (BASI) and a 25-cm^2 piece of AvCarb carbon felt (Fuel Cell Earth) with a copper mesh current collector acting as the electrode. The cathode chamber had a 25-cm^2 exposed gas diffusion electrode, constructed using a carbon cloth membrane (GDL-CT, FuelCellsEtc) coated with PTFE on the air side and 5 mg cm^{-2} carbon black (Vulcan XC-72, Fuel Cell Earth) dispersed in Nafion on the liquid side. The spacing between the anode and cathode membranes was 3.4 cm, and there was a 1-cm gap between the anode and the reference electrode. The MEC was operated at room temperature under magnetic stirring in both chambers.

The anode chamber was inoculated with 20% (v/v) primary effluent from the O'Brien Water Reclamation Plant (Skokie, IL) and 80% (v/v) of a growth medium (synthetic wastewater) containing 1 g·L^{-1} (12.2 mmol·L^{-1}) of CH$_3$COONa in a 100 mmol·L^{-1} pH 7 phosphate buffer (2.9 g·L^{-1} NaH$_2$PO$_4$·H$_2$O and 11.3 g·L^{-1} Na$_2$HPO$_4$) also containing 0.03% (v/v) of a trace metal solution [177]. After an initial batch stage, the anode chamber was continuously fed with the same synthetic wastewater with a hydraulic residence time (HRT) of 5 h. The synthetic wastewater was constantly sparged with N$_2$ to avoid oxygen entering the system.

The cathode chamber was operated in batch mode. In order to control the pH increase, it was initially filled with a 179 mmol·L^{-1} pH 6 phosphate buffer (21.3 g·L^{-1} NaH$_2$PO$_4$·H$_2$O and 3.5 g·L^{-1} Na$_2$HPO$_4$). At least twice a day, the pH of the catholyte was monitored with a pH-meter (Mettler Toledo SevenCompact S210) and the H$_2$O$_2$ concentration was determined by the

ammonium metavanadate colorimetric method [4, 178]. The pH and the concentration of the bioproduced H_2O_2 of the catholyte were controlled by varying its residence time in the cathode chamber. The catholyte was harvested when it reached a pH between 10 and 11 (typically, after 24 h of operation) and stored at 4 °C until used. Then, the cathode chamber was replenished with fresh pH 6 buffer to start the process over.

An external potential of -0.25 V vs Ag/AgCl was applied to the anode (working electrode) by means of a Biologic VSP potentiostat (Biologic USA, Knoxville, TN), which was also used to monitor the cell current and the cathode (counter electrode) potential every 30 seconds. For settings and data storage, the potentiostat was connected to a laptop computer running the software Biologic EC-Lab.

3.2.3 Solubilization/depolymerization experiments

To examine the conditions in which lignin was solubilized/depolymerized we carried out experiments in a laboratory-scale slurry reactor. Dried Organosolv lignin (40 mg) and the appropriate reagents and solvents were combined in a beaker under magnetic stirring to a final volume of 40 mL (1 $g \cdot L^{-1}$ solid lignin initial concentration). Each beaker was wrapped in aluminum foil to avoid the incidence of light. The duration of the experiments was 60 min. One-mL samples were taken from the slurry and filtered through nylon syringe filters with a 0.2-μm pore size at 0, 5, 15, 30, and 60 minutes, although this paper reports the results at maximum concentration in solution, which occurs at 60 minutes. We denote the filtered liquid as the "liquid fraction" (< 0.2 μm), while the "suspended fraction" refers to all particles suspended in the beaker at the end of the experiment. Some lignin was not solubilized and this fraction was isolated through centrifugation

at 4000 rpm for 15 min. This was denoted as the "solid fraction", although at pH 10.8 the solid fraction was negligible.

We tested the effect of pH and the presence/absence of H_2O_2 in the solvent. For the MEC, these parameters were controlled by the catholyte harvesting procedure, as explained in the previous Section **3.2.2 Microbial electrolysis cel**. Due to limitations in the available volume of the MEC catholyte, we also developed a synthetic catholyte by increasing the pH of the cathode buffer solution, from 6 to the desired value, with NaOH. In the indicated cases, we also added a specific amount of commercial H_2O_2.

3.2.4 Characterization of products in solution

We determined the aromaticity and total carbon content of the liquid fraction by measuring the UV absorbance (Eppendorf BioSpectrometer) and the dissolved organic carbon (Teledyne Tekmar Co. Apollo 9000 TOC combustion analyzer), respectively. Quantification was achieved through calibration curves obtained from samples of untreated lignin dissolved in a pH 13 NaOH solution (**Figure** 3.1**).** For the UV absorbance measurements (280 nm), the pH was adjusted to different values (7, 10, 13) to account for shifts in the spectra. For the dissolved organic carbon (DOC) measurements, the pH of the lignin solutions was adjusted to 7 using H_3PO_4. All samples were filtered (0.2 μm nylon filters) before measurements.
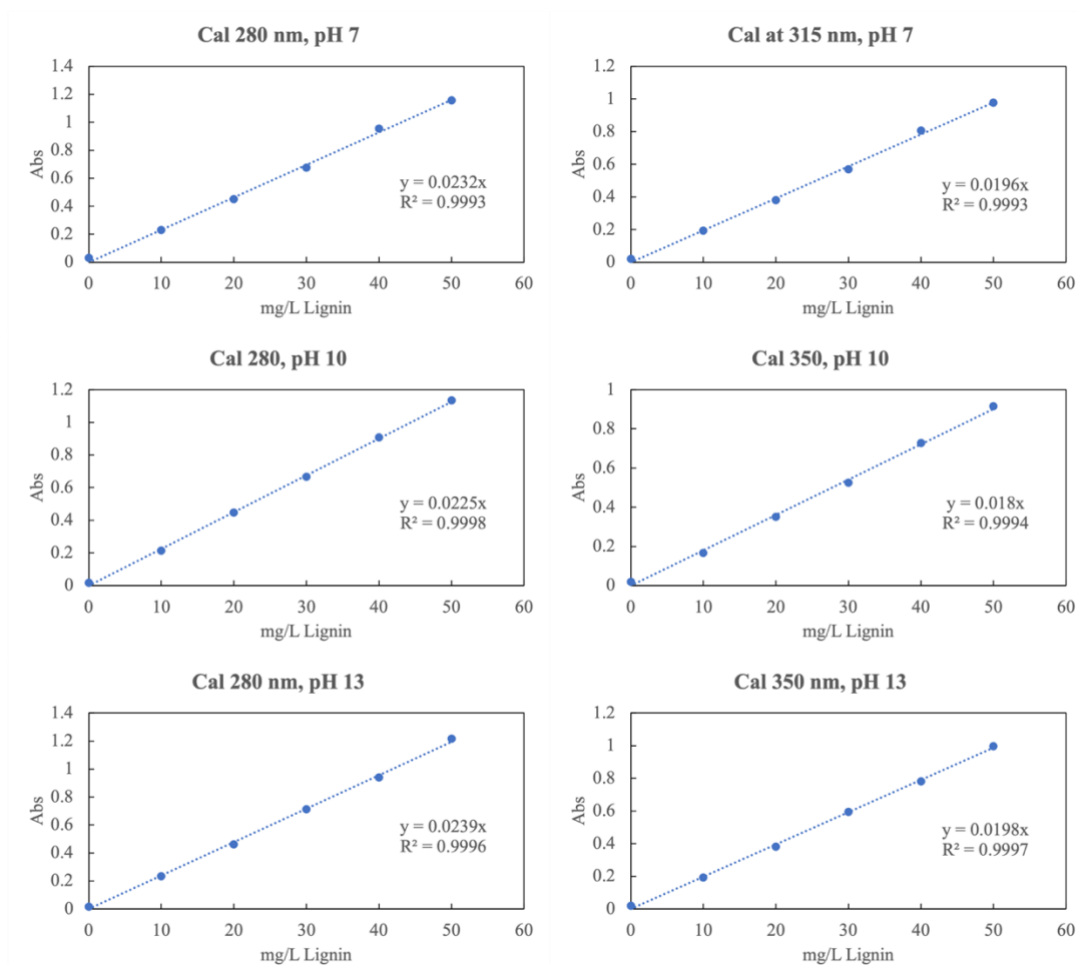
Figure 3.1 Calibration curves of untreated lignin dissolved in a pH 13 NaOH solution along with the calibration curves with the final pH adjusted to pH 10 and pH 7. The absorbances, measured by UV-vis spectrophotometry, where obtained at 280 nm and 350 nm.

To determine the total amount of phenolics and flavonoids in the liquid fraction, we ran the colorimetric Folin-Ciolcalteu method and the method by Zhishen et al, respectively [80, 82, 179, 180]. The former combines 100 μL of the solubilized mixture with 2 mL of a 2% sodium carbonate solution. After incubating at room temperature for five minutes, 100 μL of the Folin-Ciolcalteu reagent were added. Then, an absorbance measurement was made at 750 nm after incubating at room temperature for another 30 min. A calibration was performed with a solution of gallic acid (3, 4,5-trihydroxybenzoic acid) [180]. The calibration curve for the Folin-Ciolcalteu method was re-made each time the assay was ran. An example calibration curve is shown below

in **Figure** 3.2. The Zhishen method combines 300 µL of solubilized lignin, 3.4 mL of a 30 % methanol solution, 150 µL of a 0.5 mmol·L^{-1} sodium nitrate solution and 150 µL of a 0.3 mmol·L^{-1} aluminum chloride hexahydrate solution at room temperature. After 5 minutes, 1 mL of 1 mol·L^{-1} sodium hydroxide solution was added, and an absorbance value was obtained at 510 nm. The calibration curve was made using the flavonoid rutin, (3′,4′,5,7-Tetrahydroxy-3-[α-L-rhamnopyranosyl-(1→6)-β-D-glucopyranosyloxy]flavone) (**Figure** 3.2).
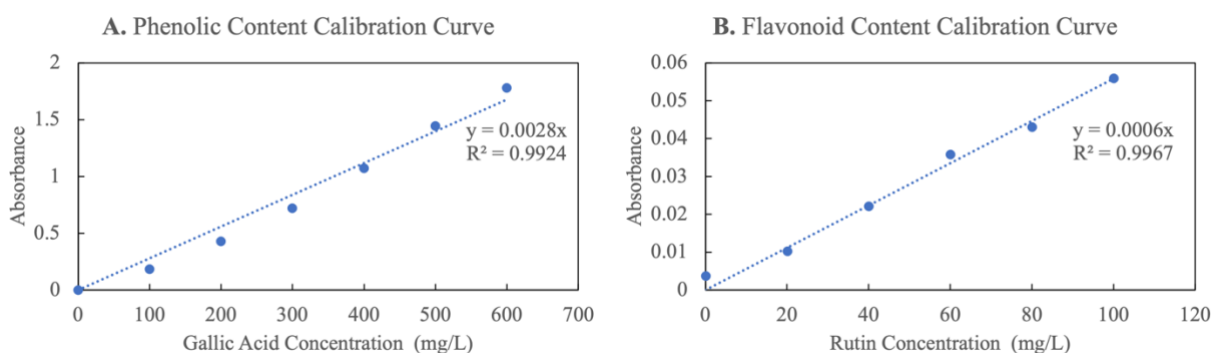
Figure 3.2. A. The calibration curve for the Folin-Ciolcalteu method, made with gallic acid (3, 4,5-trihydroxybenzoic acid) with absorbances obtained at 750 nm. B. The calibration curve for the Zhishen method, made with rutin (3′,4′,5,7-Tetrahydroxy-3-[α-L-rhamnopyranosyl-(1→6)-β-D-glucopyranosyloxy]flavone) with absorbances obtained at 510 nm.

The identification and quantification of the aromatic oligomers in solution (monomers to tetramers) involved reversed-phase high-performance liquid chromatography coupled to mass spectrometry (HPLC-MS or simply LC-MS). An Agilent 1260 Infinity binary LC system with an autosampler was coupled to a Bruker Amazon X ion trap with an electrospray ionization (ESI) source. The HPLC column was a Phenomenex Gemini C6-Phenyl, 250-mm long, with an internal diameter of 4.6 mm and a particle size of 5 µm. The HPLC instrument was also coupled to an Agilent G4212B diode array detector (DAD), which we used to complement the identification of compounds by means of their absorption spectra. Based on previously published works [181-183], we tested several isocratic and gradient methods at different temperatures using water and methanol or acetonitrile as mobile phase, with and without modifiers (formic acid or ammonium

acetate). For these tests we analyzed a mix of nine aromatic standards (see **Table 3.3** and **Figure 3.3** below). Based on the separation performance, we selected a gradient method mixing ultrapure water (solvent A) and HPLC-grade methanol (solvent B), both modified with 0.01% (v/v) acetic acid, at 40 ˚C column temperature, and a flow rate of 0.4 mL·min^{-1}. Following methods developed by Owen et al. [83, 184], we adjusted the pH by using a post-column addition of 5 mol·L^{-1} ammonium hydroxide at a rate of 1 mL·h^{-1}. The gradient setup was the following: from 30% (B) to 35% (B) in 15 min, from 35% (B) to 80% (B) in 5 min, from 80% (B) to 100% (B) in 5 min, then back to 30% (B) for re-equilibration.

Table 3.1 The nine aromatic standards used to create an HPLC method capable of separating the standards.

	Name	Formula	Structure		Name	Formula	Structure
A	4-Hidroxycinnamic Acid (P-Coumaric Acid)	C9H8O3		F	Acetovanillone	C9H10O3	
B	Ferulic Acid	C10H10O4		G	Acetosyringone	C10H12O4	
C	Cinnamic Acid	C9H8O2		H	Syringic Acid	C9H10O5	
D	Vanillin	C8H8O3		J	Syringaldehyde	C9H10O4	
E	Vanillic Acid	C8H8O4					
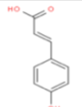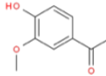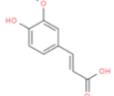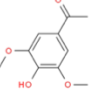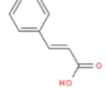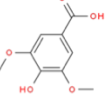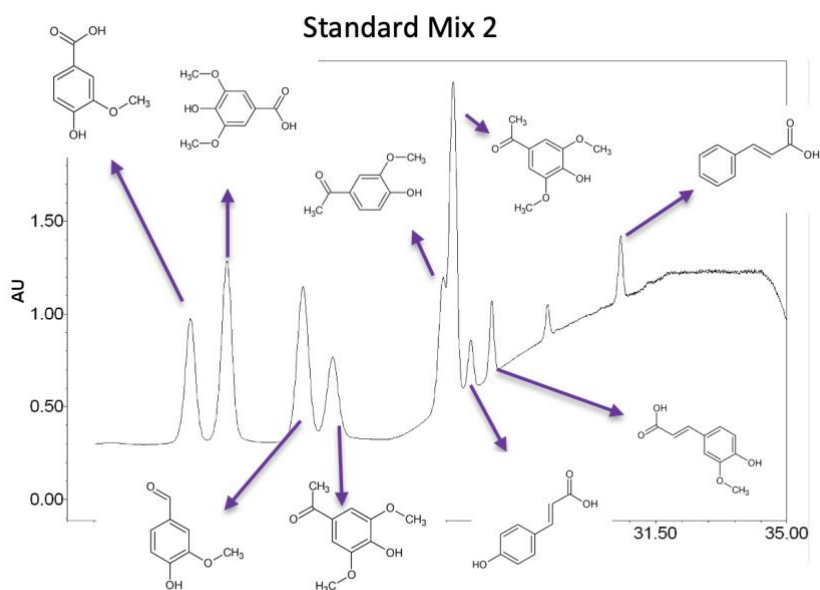
Figure 3.3 The HPLC chromatogram of the separated nine aromatic standards using the method described in the paper.

This method was also used for high resolution MS (HRMS) and tandem MS (MS^2) as well on the Bruker Impact – II spectrometer. The MS was run in negative ESI mode and calibrated prior to use, with the nebulizer set to 0.3 bar and the dry gas to 4.0 bar, in high precision calibration (HPC) mode with a tuning mix containing the following 10 compounds: $C_2F_3O_2$ (ref. m/z 112.9856), $C_6HF_9N_3O$ (ref. m/z 301.9981), $C_{12}HF_{21}N_3O$ (ref. m/z 601.9790), $C_{20}H_{18}F_{27}N_3O_8P_3$ (ref. m/z 1033.9881), $C_{26}H_{18}F_{39}N_3O_8P_3$ (ref. m/z 1333.9689), $C_{32}H_{18}F_{51}N_3O_8P_3$ (ref. m/z 1633.9489), $C_{38}H_{18}F_{63}N_3O_8P_3$ (ref. m/z 1933.9306), $C_{44}H_{18}F_{75}N_3O_8P_3$ (ref. m/z 2233.9115), $C_{50}H_{18}F_{87}N_3O_8P_3$ (ref. m/z 2533.8923), $C_{56}H_{18}F_{99}N_3O_8P_3$ (ref. m/z 2833.8754). This calibration was also done internally in the Bruker Compass DataAnalysis 5.1 software before analysis. After the calibration step, the nebulizer was set to 4.0 bar and the dry gas to 10.0 bar. Multiple reaction monitoring (MRM) was used to target the MS^2 of m/z values of interest. A 30-mV voltage was applied for MS^2.

3.2.5 Characterization of products in suspension

The formation and properties of lignin nanoparticles (LNPs) were interrogated via two experiments. In the first one, the treated lignin mixture was acidified with phosphoric acid to pH 7, yielding neutralized lignin nanoparticles (n-LNPs). In the second one, the depolymerized lignin suspension was unmodified and produced basic lignin nanoparticles (b-LNPs). Samples were collected every three to four days over a two-week period to be analyzed for concentration, size, pH and zeta potential. LNP formation via acid precipitation has been postulated before; this mechanism and another, micellization, are discussed in detail in Section **3.3.3 Characteristics of the colloidal/nanoparticle fraction.**

The LNP product fraction was characterized by a combination of nanoparticle tracking analysis (NTA), zeta potential, and scanning electron microscopy (SEM). NTA (Malvern Panalytical NanoSight NS300) was used to estimate both the concentration and size distribution of the suspended particles, and to close mass balance. The stability of the detected nanoparticles was determined by measuring their zeta potential and their shape was established by scanning electron microscopy.

To determine concentration by NTA, we modified the Parsons et al method [185]. We used dilutions of a suspension of mixed PS particles (sizes: 100 nm, 300 nm, and 460 nm) and measured the associated relative standard error (RSE) of the measured sizes. At a certain dilution, the RSE of the sizes reaches a minimum and at this point the concentration from the NTA is the closest to the actual (known) concentration (**Figure** 3.4). At the lowest RSE, the detected concentration is only 1.1 times greater than the actual concentration and thus, we used this concentration to track LNP formation.

Samples were prepared for zeta potential measurement (Malvern Panalytical Zetasizer Nano ZS) by diluting them 10 times. Then, 1 mL of sample was placed in a DTS1070 disposable zeta potential cuvette. Three measurements were taken for each sample with up to 100 zeta runs per sample. For these runs the refractive index of lignin was set at 1.61 [186].
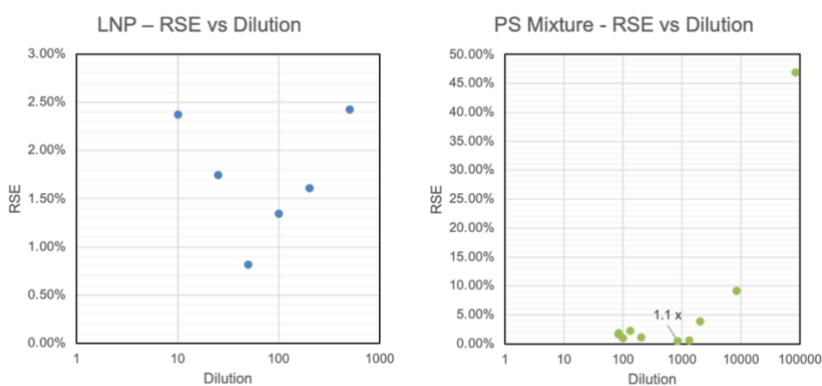
Figure 3.4 Residual standard error for a polystyrene suspension and for lignin nanoparticles versus the dilution factor.

The SEM micrographs were obtained using a JEOL JSM-7900FLV microscope equipped with an Oxford Ultimax 65 energy-dispersive x-ray spectroscopy (EDS) accessory. The voltage was set to 5 kV and the current to 8 mA. The SEM was run using the lower electron detector (LED). The software AZtecLive was used for live elemental mapping. SEM samples were prepared by diluting the suspensions 10-fold with a surfactant (5% CTAB solution) and sonicating them for 30 min. The surfactant was proven to be necessary to avoid aggregation of the LNPs. **Figure** 3.5 shows an image of the LNPs sans CTAB. Three surfactants were tested under 5 different dilutions to determine which gave the most stable zeta potential and achieved the best image under the SEM. The surfactants were dodecyl sulfate surfactant salt (DSS) (a negative surfactant), Triton-X,(a neutral surfactant) and hexadecyltrimethylammonium bromide (CTAB) (a positive surfactant). The following **Table** 3.2 summarizes the experimental conditions tested and

their results. **Figure** 3.6 shows images under SEM of the LNPs dispersed with 5% DSS and 5%

CTAB. We see much better separation with CTAB
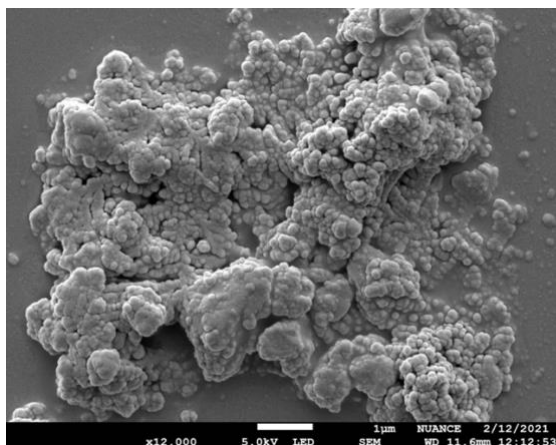
Figure 3.5. A picture of aggregated LNPs under the SEM without the use of surfactant to achieve separation.

Table 3.2 Summary of surfactants and resulting zeta potential in LNP solution

Surfactant (Charge)	Concentration (%)	Zeta (mV)
DI water	-----	-37.8
DSS (-)	0.1	-37.9
DSS (-)	0.5	-40.2
DSS (-)	1.0	-42.7
DSS (-)	5.0	-----
Triton-X (0)	0.5	-27.2
Triton-X (0)	1.0	-18.4
Triton-X (0)	5.0	-6.53
CTAB (+)	0.5	14.5
CTAB (+)	1.0	20.5
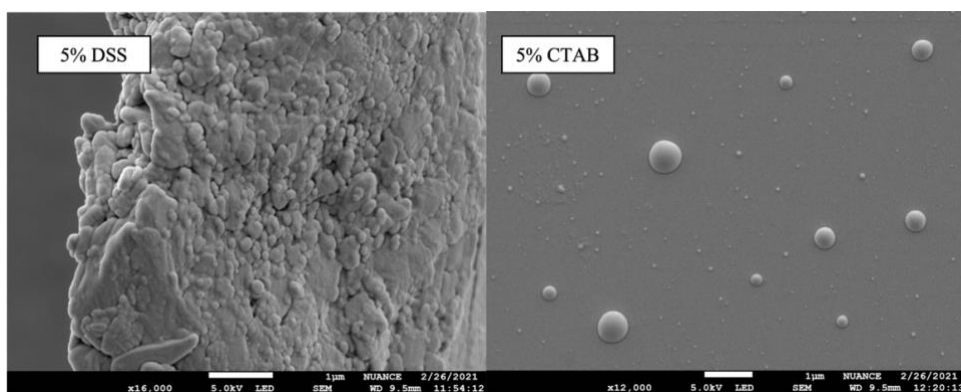
Figure 3.6. SEM images of LNPs with DSS and CTAB as the surfactant.

The samples were spin-coated (Laurel Technologies) onto a silicon wafer for 1 min. with an acceleration of 1 rpm·s^{-1} and a maximum rotation speed of 2000 rpm. For enhancing conductivity, a 10-nm AuPd layer was deposited over the sample via the Denton III Desk Sputter Coater

3.3 Results and discussion

3.3.1 Bulk characteristics of the products obtained from solubilization/depolymerization experiments

In Error! Reference source not found., we present the concentration of aromatic compounds in solution/ suspension, obtained by UV spectrophotometry, as a fraction of the initial solid lignin concentration (1 g·L^{-1}). Unless otherwise stated, the results correspond to experiments using the synthetic catholyte after one hour reaction at room temperature and atmospheric pressure. We observe that the increase in the concentration of aromatic compounds in solution/suspension with pH is exponential over the pH range we studied (pH 7-12). The results in the inset of Error! Reference source not found. show that there are no significant differences between treatments with the MEC catholyte and the synthetic catholyte at pH 11. Although we do not see the effect of just pH 11 sodium hydroxide on lignin depolymerization, note that without the addition of salt, sodium hydroxide will only depolymerize lignin up to 20%.

Since the cathode can be operated to produce H_2O_2, an intermediary of O_2 reduction (see Section **3.2.2 Microbial electrolysis cel**), we
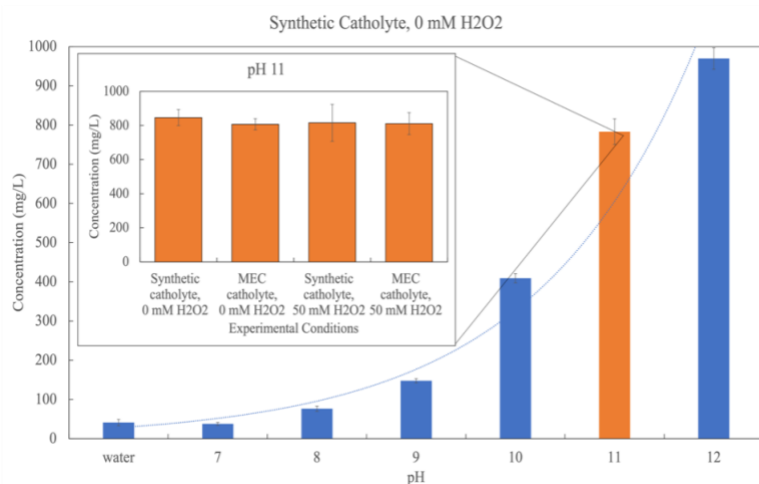
Figure 3.7 A comparison of solubilized/depolymerized lignin concentrations based on different pH values, hydrogen peroxide concentrations, and catholytes. The dotted blue line shows a fitted exponential trend.

tested the effect of H_2O_2 on lignin conversion to find no effect. There are two reasons that explain this observation: 1) hydrogen peroxide derives its oxidation potential from the perhydroxyl anion (which in turn is what produces the hydroxy radical as illustrated below). Without a catalyst, radical formation is slow due to the acid/base equilibrium shifted to H_2O_2 in reaction a (the pKa of hydrogen peroxide is 11.6) [187-191].

a) $H_2O_2 <-> H^+ + HO_2^-$ (pKa 11.6)

b) $HO_2^- + H_2O_2 -> HO_2\bullet + HO\bullet + OH^-$

c) $HO\bullet + H_2O_2 -> HO_2\bullet + H_2O$
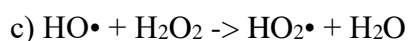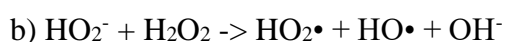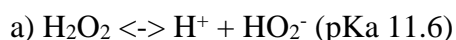
Our depolymerization runs at pH 10.8 and hydroxyl radical yield is not favored at that pH. 2) hydrogen peroxide is stabilized by phosphates, and we run our experiments in a phosphate concentration of almost 0.2 M. The phosphate, then, further stabilizes the hydrogen peroxide preventing the production of the perhydroxyl anion [192-194]. In order to confirm that H_2O_2 is not reactive under our experimental conditions, we also tested (via the metavanadate method) whether hydrogen peroxide was being consumed under our experimental conditions and it was not. We then tested strictly base catalyzed depolymerization (pH 12 (NaOH solution), with no phosphates, in the presence of 50 mmol$\cdot$L^{-1} H_2O_2 and absence of H_2O_2 and found via the metavanadate method that hydrogen peroxide is consumed and that when hydrogen peroxide is activated it destroys aromaticity, which is also not what we observe in our experiments (see **Figure** 3.8), but is consistent with literature reports that hydrogen peroxide is responsible for ring cleavage [195].
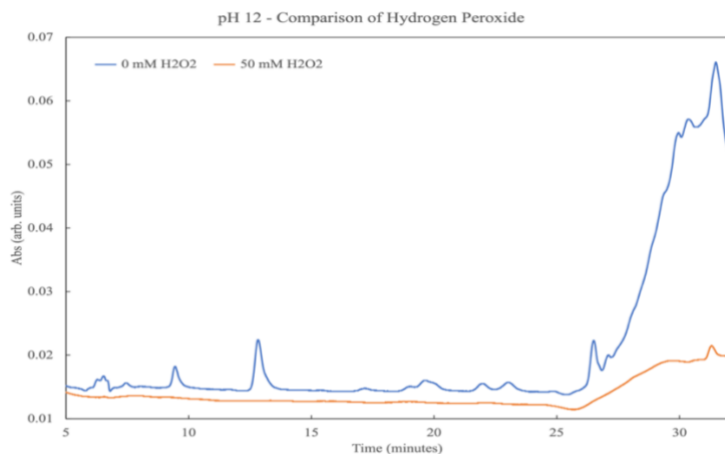
Figure 3.8. The difference in the HPLC chromatogram for lignin treated with a pH 12 NaOH solution with or without H$_2$O$_2$. It can be inferred that the H$_2$O$_2$ disrupts the aromatic rings based on the loss of most peaks.

This finding indicates that the mechanism of depolymerization is primarily hydrolysis and the MEC only needs to be controlled for pH, maintaining it at approximately pH 11. We also noted that the presence of phosphates stabilizes the catholyte pH (although it is out of its buffering range). To confirm this, we carried out an experiment with a pH 11 NaOH solution (no H$_2$O$_2$), for which we obtained a rapid pH decrease and less than 5 mg·L^{-1} of aromatic compounds in solution/suspension (compared to 800 mg·L^{-1} for the synthetic effluent, see Error! Reference source not found.). The results in Error! Reference source not found. corresponding to pH 11 show that the concentrations of the liquid and colloidal fractions, as determined by DOC, account for at least 85% and up to 90% of the initial solid lignin, where the remaining 10-15% may be explained due to measurement uncertainties. Of this total, we determined that our solubilized lignin at pH 11 contains up to 48% phenolics and 17% flavonoids (see the Section **3.2.4 Characterization of products in solution**). These product yields are much greater than those previously reported in the literature. The phenolic content of lignin via the Folin-Ciocalteu method has previously been reported to range between 10.5 and 16.7% [80]. While flavonoid content by the Zhishen method has not been determined with extracted lignin, this method has been performed on a plant, red

clover, that is sold as a supplement due to the medicinal properties of isoflavones. The plant itself contains between 0.61 and 2.66% flavonoids, indicating that, comparatively, our extracted lignin has substantial flavonoid content [180].

3.3.2 Identification and quantification of valuable aromatic products in solution

Discrete aromatics in solution were identified and quantified in accordance with the workflow illustrated in **Figure** 3.9. First, the compounds were separated by LC (detailed in the Section on "Characterization of products in solution" in Materials and methods). Using the UV chromatogram in combination with the molecular weight and double bond equivalence from MS, initial identifications were made. These identifications were further confirmed by the fragmentation pattern from tandem MS. Final identifications were made with standards, or, for compounds that do not have standards available, the identification of one potential structure that matches the aforementioned characteristics.
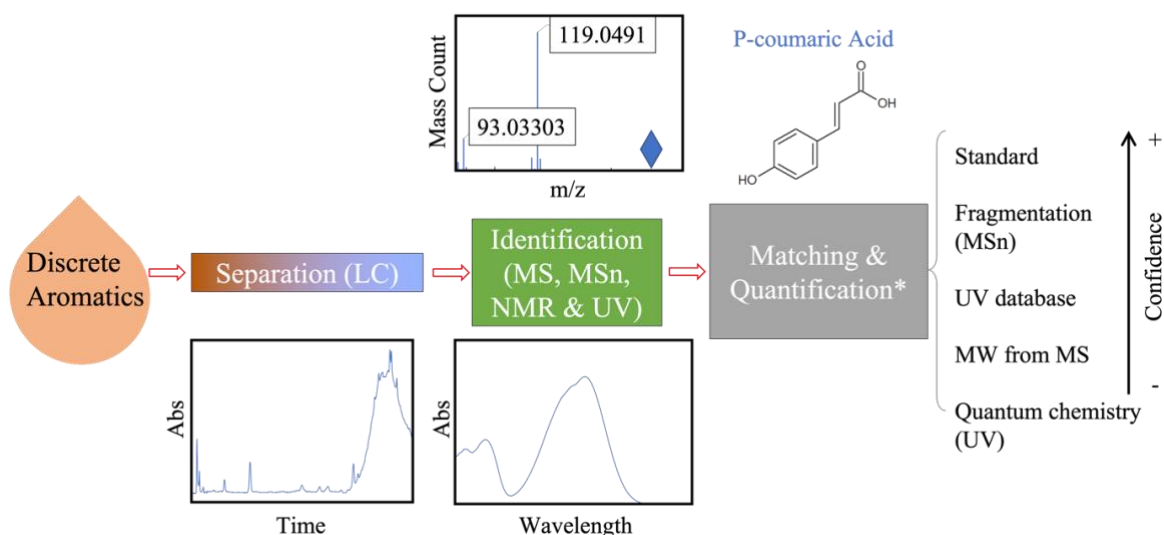
Figure 3.9 The workflow for identification and quantification of discrete aromatics from our depolymerized solution.

Figure 3.10 compares the percent yield of the fourteen unique compounds isolated and identified via LC-MS and also includes the bulk phenolic and flavonoid amounts. Once an identification was made, we confirmed the identity of the compounds, when possible, with commercial standards. Seven monomers (1-5, 8-9), five dimers (6-7, 10-12), including three flavonoids (10-12), and two tetramers were identified (13-14). The names, m/z, fragmentation patterns, and method of quantification are listed in **Table 3.3**. The structures of all identified compounds can be found in **Figure** 3.11**.**
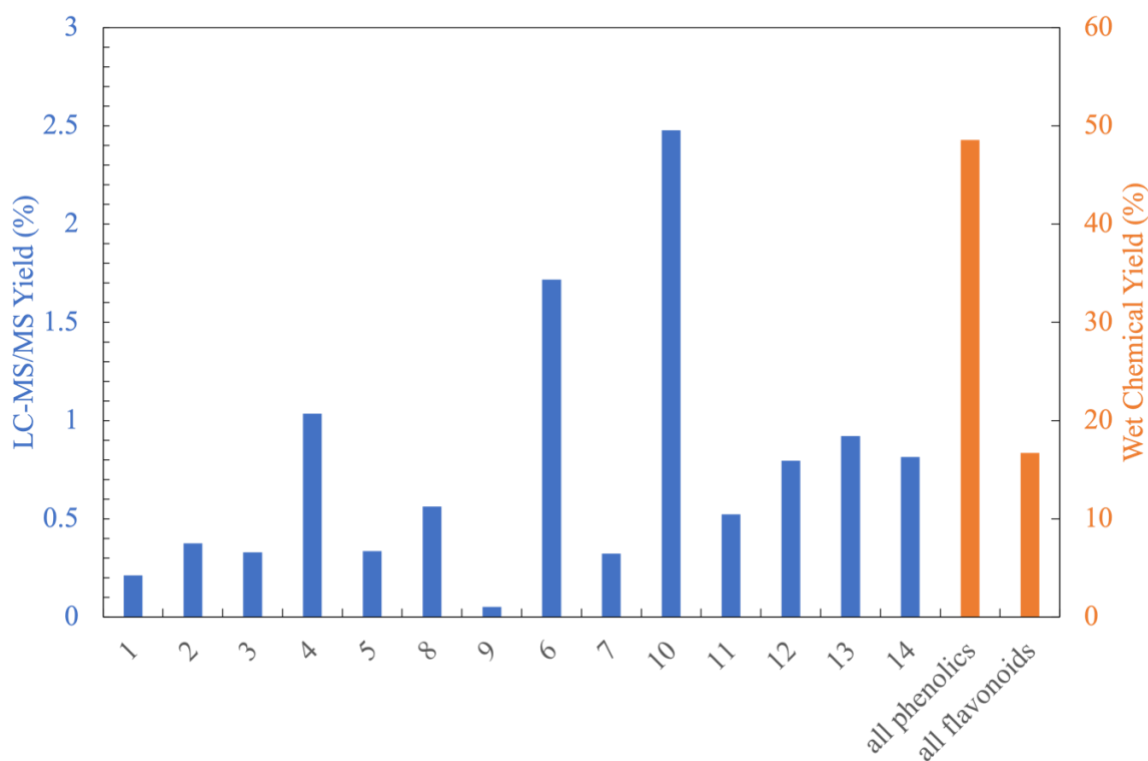
Figure 3.10 The yield (as % mass relative to the initial lignin mass) of the 14 identified discrete compounds. As well as the total phenolic and total flavonoid concentration, as determined by wet chemical assays. Compounds 1-5, 8, and 9 are monomers, 6 and 7 are dimers, 10-12 are flavonoids, and 13-14 are tetramers.

Table 3.3. T**he name, m/z, fragmentation pattern, and method of quantification for 14 identified discrete compounds.**

	Compound (m/z M-H)	Fragmentation	Calibration Curve Type
1	m-Hydroxybenzaldehyde (121.0279)	108.0202 (25.1%), 95.0127 (49.6%), 92.0259 (100%)	Standard available
2	Vanillin (151.0390)	136.0146 (14.4%), 108.0204 (100%)	Standard available
3	p-Coumaric acid (163.039)	119.0490 (100%), 93.0334 (22.2%)	Standard available
4	Dihydrocaffeic acid (181.0489)	151.0034 (53.8%), 135.0448 (12.7%), 123.0086 (100%), 95.0132 (30.9%)	Standard available
5	Ferulic acid (193.0500)	105.0124 (100%), 76.9802 (14.5%)	Standard available
6	4-methyl-2-(2-phenoxyethyl)phenol (227.1070)	182.9549 (5.2%), 138.9639 (44.3%), 94.9742 (100%)	Dihydroresveratrol calibration curve used
7	Dihydroresveratrol (229.0860)	123.0437(100%),81.0335 (9.9%)	Standard available
8	Cinametic acid (237.0447)	145.0293 (100%), 119.0500 (29.7%), 117.0344 (96%)	Averaged from monomeric calibration curves
9	Integerriminol (321.0970)	210.8877 (29.5%), 180.9541 (61.9%), 138.9440 (82%), 96.9560 (100%)	Averaged from monomeric calibration curves
10	Tricin (329.0660)	299.0163 (79.7%), 271.0219 (37.3%), 229.0841(100%), 123.0439 (27.2%)	Standard available
11	Antiarone F (383.1130)	319.7609 (27.4%), 262.9863 (100%), 160.0540 (30.8%), 78.9559 (38.8%)	Tricin calibration curve used
12	7-[(9-hydroxynonyl)oxy]-3-[4-(9-hydroxynonyl)phenyl]-4H-1-benzopyran-4-one (521.3196)	341.0617(100%), 326.0383 (63.4%)	Tricin calibration curve used
13	Orizavitol (727.2383)	581.1937 (4.1%), 163.0374 (11.2%), 145.0270 (9.7%)	Dihydroresveratrol calibration curve used
14	(2S)-rel-2-[4[(4R,5S)-5-(2,6-dimethoxyphenoxy)-2,2-dimethyl-1,3-dioxane-4-yl]-2,6-dimethoxyphenopxy]-1-[3,5-dimethoxy-4-(phenylmethoxy)phenyl]-1,3-propanediol (735.2960)	227.1050 (6.2%), 112.9845 (100%)	Dihydroresveratrol calibration curve used
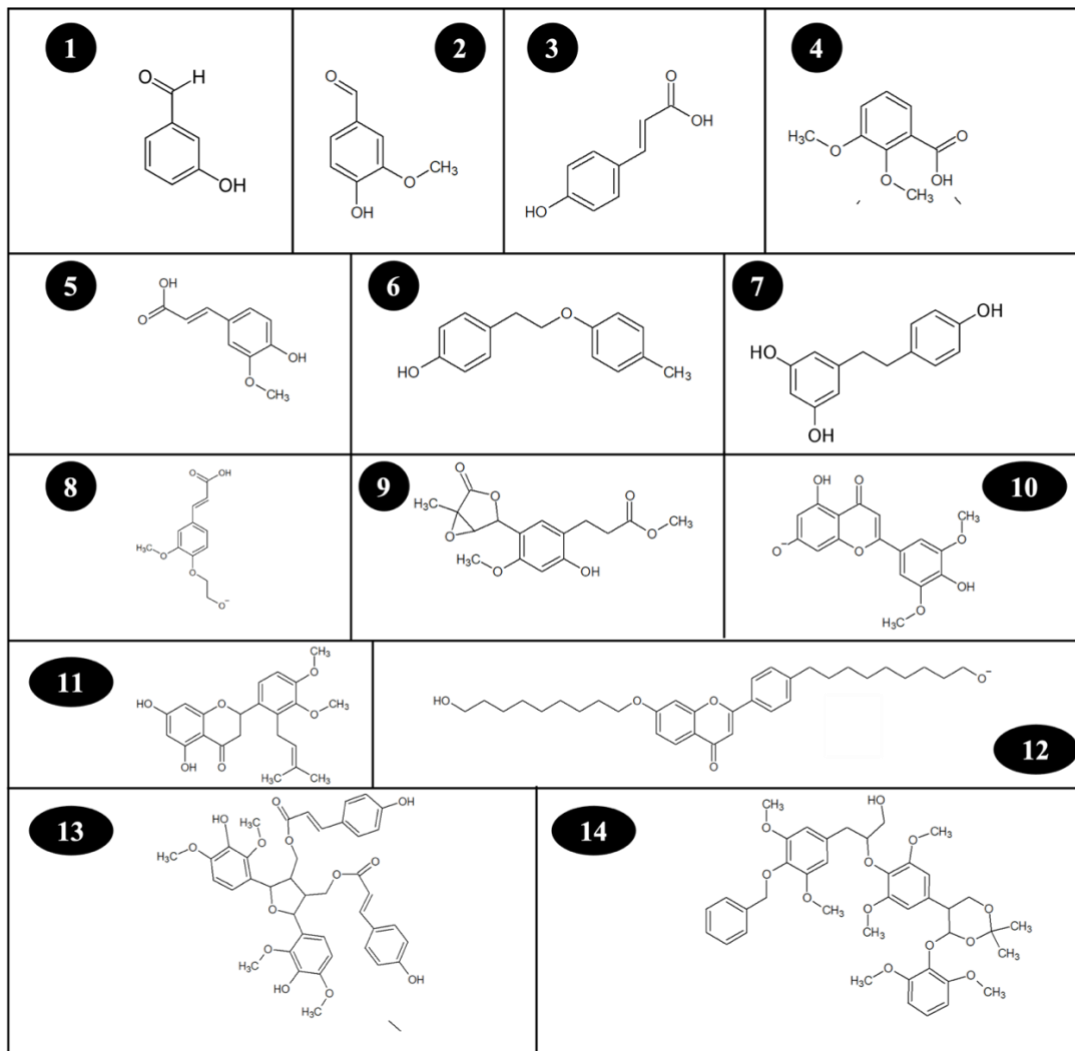
Figure 3.11 A list of the structures of the identified compounds present in the depolymerized mixture. The numbers correspond with the numbers in Table 3.3– **which contains further information on the compounds.**

Purchased standards were used to build calibration curves for determining compound concentrations. If a standard was not available, the target compound concentration was estimated using an average of the slope of the calculated calibration curves, as follows: for monomers (*) the average calibration of the standards belonging to compounds 1-9 (**Table 3.3**) was used; for non-flavonoid dimers/tetramers (**), the calibration curve for compound 7 (Dihydroresveratrol) was used; the calibration curve for compound 10 (tricin) was used to quantify those flavonoids without available standards (***) (**Figure 3.12**). Standards were not available for 6 of the identified

structures: 4-methyl-2(2-phenoxyethyl)phenol**, cinametic acid*, antiarone F***, 7-[(9-hydroxynonyl)oxy]-3-[4-(9-hydroxynonyl)phenyl]-4H-1-benzopyran-4-one***, orizavitol**, and (2S)-rel-2-[4[(4R,5S)-5-(2,6-dimethoxyphenoxy)-2,2-dimethyl-1,3-dioxane-4-yl]-2,6-dimethoxyphenopxy]-1-[3,5-dimethoxy-4-(phenylmethoxy)phenyl]-1,3-propanediol**. This estimation method accounts in part for the discrepancy in yields as determined by the wet chemical analysis (Folin-Ciocalteu and the Zhishen method) and the discrete compound analysis. The fragmentation pattern analysis (from MS^2) can also be found below for selected compounds that were not confirmed with standards (**Figure** 3.13).
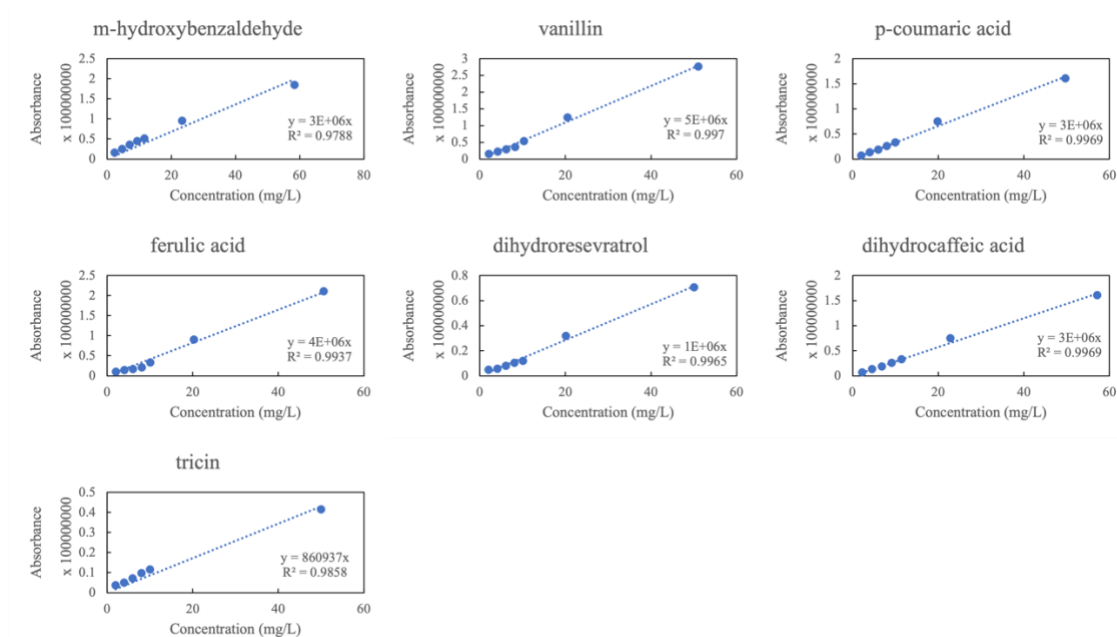
Figure 3.12 Calibration curves for compounds that were identified in the depolymerization. mixture. These calibration curves are made using the HPLC.
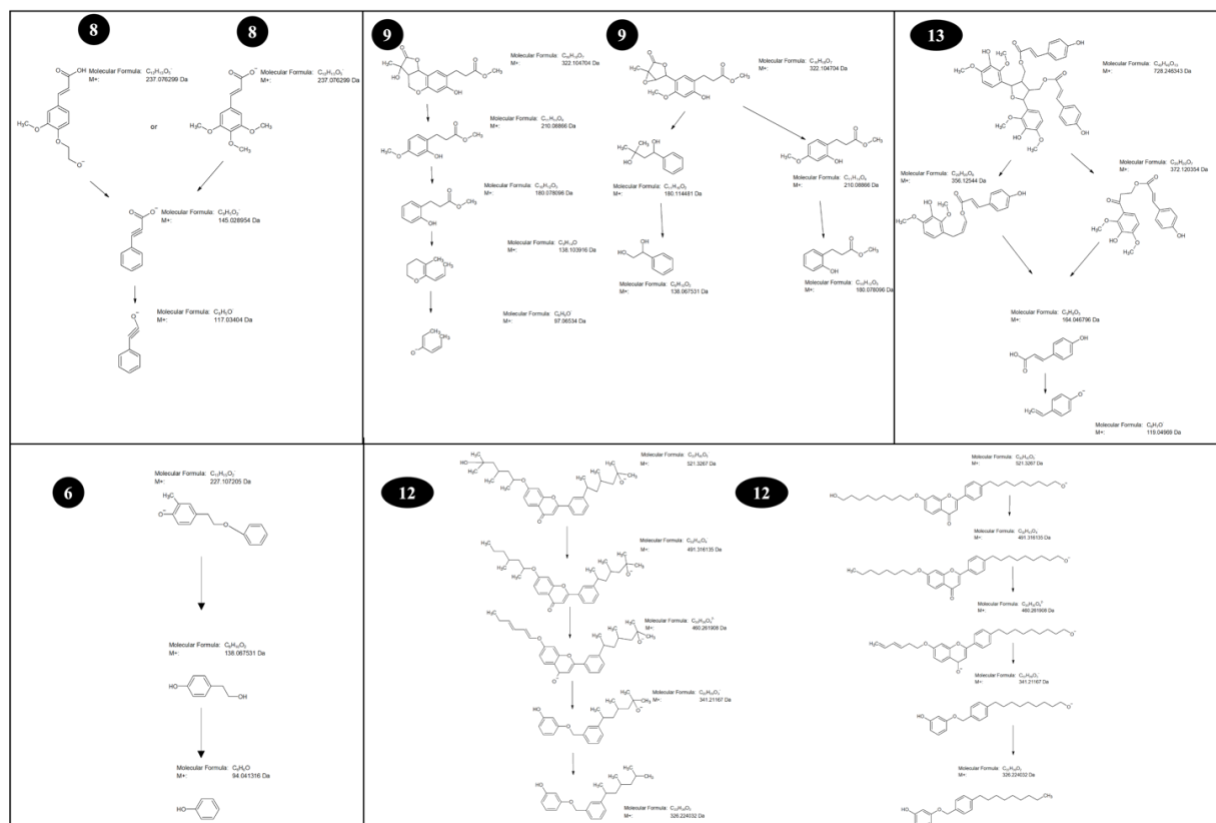
Figure 3.13. MS^2 Fragmentation analysis for select compounds that did not have standards available. This was done with ACD Labs 2019 ChemSketch. Structure 8, 9, and 12 shows how two potential structures may be possible without the confirmation from a standard. Antiarone F is not included as it was identified via quantum chemistry techniques.

Based on this analysis the total yield for identified discrete aromatics is approximately 11%. Our results differ substantially in both quantity and quality from those reported by others [176, 196, 197]. We measure a significant fraction of flavonoids, which have not previously been targeted in lignin depolymerization. In previous work, researchers have found BTX compounds present in a range of 0.1-5.8% and fine monomers (e.g., vanillin) in a range of 0.02-2.80%. Flavonoids and/or other oligomers (e.g., tricin) have not been identified [176, 196, 197]. In contrast, we observed no BTX, about 3% of fine monomers, and close to 8% of flavonoids/oligomers.
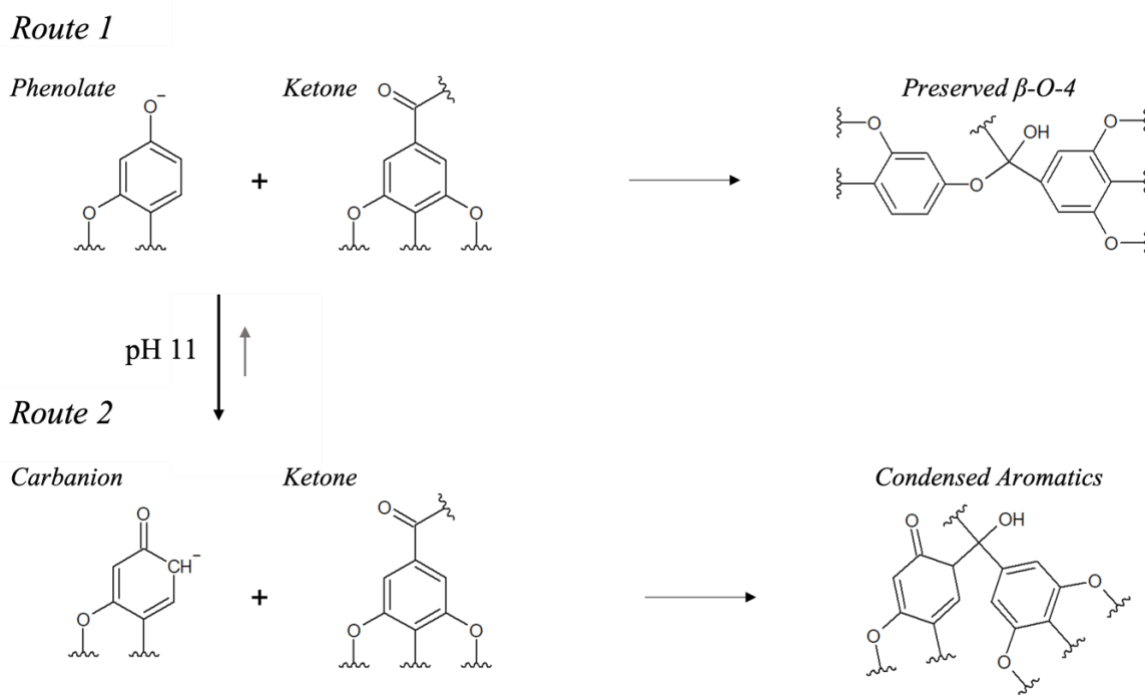
Figure 3.14 The rearrangement between a phenolate and carbanion, which is initiated by deprotonation, and the subsequent condensation reaction (Route 2) [196].

We propose that flavonoids are formed by repolymerization, a reaction that is noted by other researchers studying BCD [196]. We illustrate a hypothetical pathway in **Figure** 3.14. The general mechanism of repolymerization is initiated by a hydrogen abstracted from the hydroxyl group of a phenolic compound to form a phenolate (Route 1, **Figure** 3.14), which is in resonance with the carbanion (Route 2, **Figure** 3.14.). The phenolate can react with a ketone to re-create the β-O-4 linkage in the form of a hemiacetal (Route 1, **Figure** 3.14). The formation of the hemiacetal, however, is less favorable at pH 11 and equilibrium between the resonance structures is shifted to the carbanion making Route 2, which is also referred to as condensation, the predominant reaction. This has been shown empirically in the literature by attempting to run a second round of BCD on the "unreacted" lignin and only obtaining up to 2% more monomer mixture [196]. This is because when the carbanion reacts with a ketone to form a carbon-carbon bond, it has a higher bond

dissociation energy than the original ether bond, making it more difficult to break via BCD. Route 2, then, suggests a pathway by which flavonoids, as well as other oligomers and LNPs, may be formed. Previous lignin valorization research has focused more on how to avoid these condensation phenomena in order to produce monomers, but by promoting conditions under which we produce flavonoids, we synthesize products with high-value applications in the pharmaceutical or nutraceutical industries as antioxidants and supplements.

We propose that the reaction mechanism in **Figure** 3.14 provides a general pathway by which flavonoids may be formed. We tested if repolymerization occurs under our experimental conditions by combining select monomer standards -vanillin (ketone), *p*-coumaric acid, ferulic acid, catechol (phenolate/carbanion at caustic pH), and o, m, p-cresol- in the synthetic pH 11 phosphate catholyte and measured flavonoid production with the Folin-Ciocalteu method at yields (>3%) greater than that observed naturally in other plant sources. It is imporatnt to note, however, that the reaction in **Figure** 3.14, is a general reaction scenario and there are many other possible reactions in a process as complicated as lignin depolymerization.

3.3.3 Characteristics of the colloidal/nanoparticle fraction

Identified discrete aromatics from the depolymerization experiments with synthetic catholyte effluent at pH 10.8 account for approximately 11% of the initial lignin mass. In the same depolymerized mixture, the remainder of the mass can be accounted for with LNPs. Our method of producing LNPs is different from what has been previously reported by other researchers. Generally, the conventional route of LNP production begins with dissolving lignin in an organic solvent or at high pH (pH 14), followed by decreasing the solubility through the addition of an anti-solvent (water) or the addition of acid (to a final pH of around 2). Our method is a one-pot

depolymerization/LNP production that utilizes a salt, pH 10.8 catholyte generated by the MEC. We find that by adding small amounts of acid (to reach neutral pH), we can tune the resulting LNPs, in terms of average size and maximum concentration.

We compared two methods to produce LNPs (see **Section 3.2.5 Characterization of products in suspension**): the basic LNP (b-LNP) pathway and neutralized LNP (n-LNP) pathway. Both methods begin by depolymerizing lignin with a pH 10.8, 179 mM phosphate buffer. After 24 hours, the pH of the depolymerized lignin is either adjusted to pH 7 (n-LNPs) or left unadjusted (b-LNPs). The dependence in time of the concentration and zeta potential of the produced LNPs is shown in **Figure** 3.15. For n-LNPs, the amount immediately following the neutralization step is around 30% of the initial lignin concentration (**Figure** 3.15**,** closed circles), whereas the amount of b-LNPs is initially around 18% (**Figure** 3.15**,**, closed triangles). Both types of LNPs take two weeks after the pH adjustment to reach their maximum concentrations. The n-LNPs reach a higher maximum concentration than the b-LNPs over the same time period. After two weeks, the concentration of LNPs measured by NTA begins to decrease, which is likely the result of aggregation. The lignin nanoparticles range in size from 70 nm to 450 nm based on our NTA results with the average size being 241 nm for b-LNPs and 231 nm for n-LNPs.
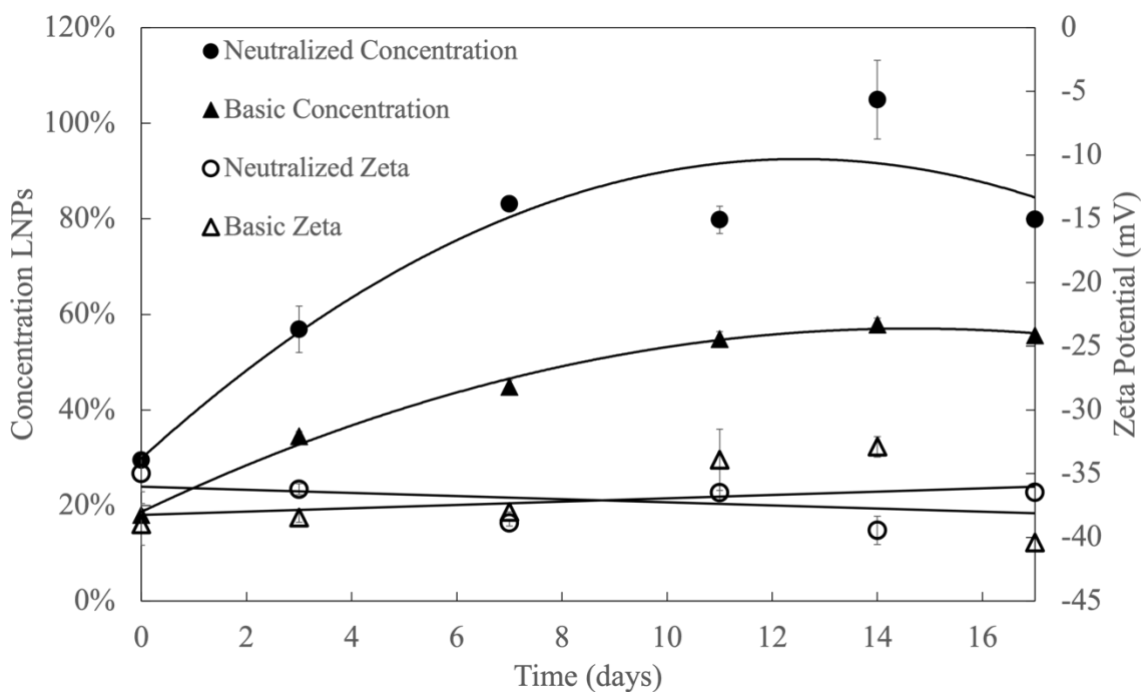
Figure 3.15 . The concentration and zeta potential as a function of time of neutral and basic LNPs over a two-week period. Open and closed symbols represent the zeta potential and concentration, respectively. Circles and triangles represent neutralized and basic LNPs, respectively.

The zeta potential of both of the LNPs varied between -33 and -40 mV which indicates moderate stability (**Figure** 3.15, open symbols) and more negative values than previously reported in the literature (typically around -25 mV). The pH for the n-LNPs remained stable around 7. For the b-LNPs, the pH of the suspension decreased from 10.5 to around 9.0 over the first 48 hours and was stable over the remaining 15 days of the experiment.

The SEM analysis confirmed that both n- and b-LNPs are spherical. We show the n-LNP SEM micrograph in **Figure** 3.16. The sizes observed in the SEM micrographs are in accordance with the NTA size distribution, as seen in the top inset in **Figure** 3.16, with three different sized groups: 50 nm, 150 nm, and 500 nm. EDS (bottom inset of **Figure** 3.16), confirmed that the nanoparticles were composed of carbon and oxygen exclusively.
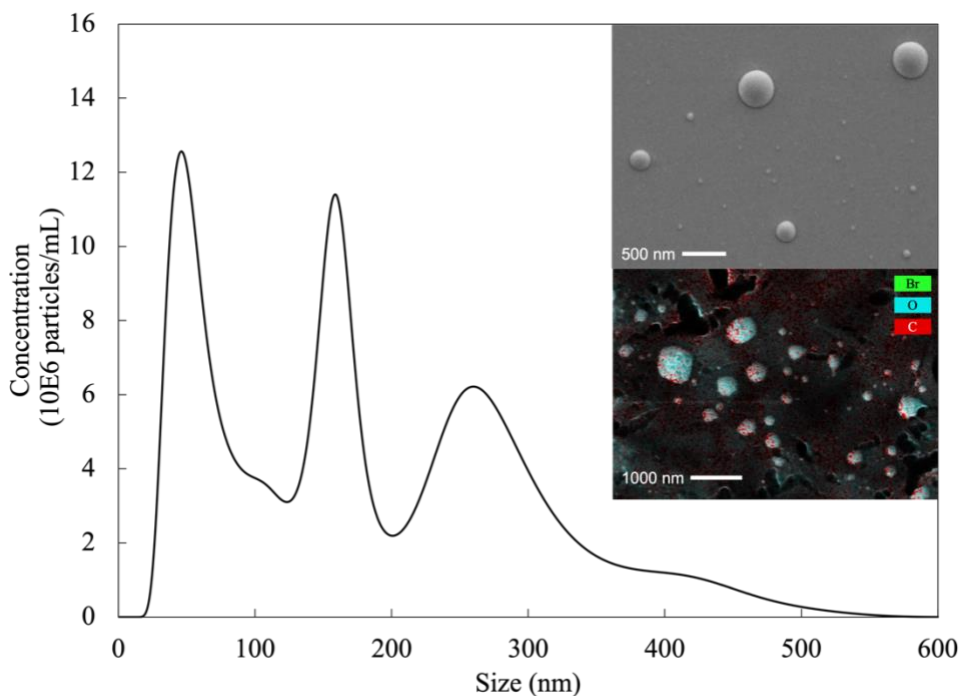
Figure 3.16. The size distribution of n-LNPs. Top inset: SEM micrograph of n-LNPs. Bottom inset: EDS of n-LNPs. The colors represent the following: green – bromine, blue – oxygen, and red – carbon. Bromine is a component of CTAB (Cetyltrimethyl ammonium bromide) so we show that the surfactant is not incorporated into the LNPs.

Although both b- and n-LNPs are similar in size, shape, and stability, the difference in concentration indicates that they may be subject to different mechanisms of formation. It has been previously reported that LNP formation can occur by either micellization or precipitation. The mechanism of micellization involves alignment of the hydrophobic and hydrophilic parts of the lignin fragments depending on the solvent characteristics [127, 198]. According to other researchers, lignin first depolymerizes in an organic solvent followed by the addition of an aqueous phase[117, 198] where the subunits aggregate to form a hydrophobic micelle core. The hydrophilic components of the lignin form the micelle shell. The LNPs grow spherically through either molecular aggregation of polymer chains or by self-assembly via aromatic stacking [114, 118, 119]. Lignin micellization is postulated to be driven by electrostatic interactions of the functional groups, hydrogen bonding, van der Waals, and pi-pi interactions [127, 198].

The precipitation mechanism for LNP formation was first proposed by Frangville [199] and is initiated by the molecular weight dependent precipitation of the dissolved subunits of lignin. Large lignin depolymerization products precipitate first to form a critical nuclei (40-70 nm). This is followed by collision-driven particle growth and adsorption [200].

We believe that both mechanisms may be at play under the conditions of our system and lead to similar products. For n-LNPs we observed a temperature dependence that is consistent with the micellization mechanism. We observed that n-LNPs do not form at temperatures less than room temperature. This is consistent with what has been seen in literature for LNPs [201] as well as with the concept of a Krafft point or the minimum temperature at which a surfactant can form micelles [202]. Precipitation, on the other hand, tends to occur at lower temperatures. For b-LNPs we witnessed a decrease in pH that is consistent with precipitation. It is important to note that our procedure deviates from those in literature as it does not utilize an organic solvent to initiate the lignin dissolution step, rather the high salt/pH 10.8 MEC effluent triggers dissolution for both proposed mechanisms.

3.4 Conclusions

The feasibility of a biorefinery that couples wastewater recovery in an MEC to lignin valorization by chemical depolymerization relies in part on a dependable, local flow of feedstock materials. If we consider waste feedstocks in urban/agricultural settings, a city like Chicago produces a total of approximately 4.5 million tons of solid waste per year (including municipal and construction & demolition wastes), of which 17% (765 k tons) is lignocellulosic material (newsprint paper, woody yard waste, woods) [203], containing an average of 25% lignin (191k tons) [204]. Based on the United States Department of Agriculture National Agricultural Statistics Service (USDA-NASS), Illinois has approximately 72,000 farms [205]. In Illinois an average farm

(approximately 140 hectares) produces 360 tons of collectable corn stover per year [160] containing an average of 18% lignin [206]. This adds up to almost 200,000 tons of lignin waste in Chicago and 4.7 million tons from farms in Illinois each year. Corn stover is also feedstock for cellulosic ethanol production [204]. Volatile fatty acids, which promote high MEC current densities, are abundant in urban settings principally from food processing industries (for example, breweries) and in agricultural settings from animal feeding operations (for example, feedlots) [207, 208]. Thus, based on these data, there are ample, potential opportunities for creating distributed, small-scale production facilities where biomass conversion yields high value products.

Despite this potential in feedstock volume and the many attempts to unlock the value of lignin, the commercial viability of lignin conversion has rarely been achieved. Ninety-five percent of lignin continues to be burned for energy [209]. This project illustrates the efficacy of an integrated biorefinery. By combining two waste streams under ambient conditions, we can close the mass balance of lignin derived products with valuable aromatic monomers and flavonoids as well as lignin nanoparticles.

Our biorefinery approach is novel in several ways: 1) it focuses on four product streams simultaneously – two (a treated wastewater effluent having reduced biochemical/chemical oxygen demand and a caustic catholyte) from the MEC and two (aromatics and nanoparticles) from the lignin biomass which close mass balance; 2) it is an approach that integrates an output stream from an MEC without introducing heat or pressure; and 3) the reaction conditions promote condensation pathways for the synthesis of higher molecular weight, high-value products.

Our approach also improves on the sustainability of conventional BCDs. The depolymerization step of our process is from 4 to 20 times more energy efficient than other BCDs. This estimate is based on the energy consumption of heating, pressurizing, and stirring, taking into

account the yield of the water-soluble fraction after depolymerization in our system compared to previous published works [72, 210]. Our process also has advantages according to the 12 principles of green chemistry due to its integration with a MEC. For the caustic catholyte, the atom economy of the overall reaction for OH^- production in a membrane-cell chlor-alkali process is 32%, while it is 51% for an acetate-fed MEC [211]. MEC production of caustic is also advantageous as it entails less hazardous chemical synthesis and, since no chlorine is produced, it is inherently safer chemistry from an accident prevention perspective [211].

The high value of the products we obtain comes from their potential applications. Flavonoids are well-known antioxidants and are being studied for other pharmaceutical, nutraceutical, and medical applications due to their potential antibacterial, anti-cancer, cardioprotective, and anti-inflammatory effects and for cosmetic products due to their UV absorbing capabilities [212]. Since flavonoids are formed at much higher concentrations than can be extracted from plant biomass, in combination with their hydrophobicity and stability making separation relatively simple, compound purification, always important downstream processing and cost concerns, may not pose a high hurdle to accessing these commercially useful antioxidant and nutraceutical properties relative to incumbent sources. Lignin nanoparticles may also have personal care and cosmetic applications as sunscreens and are strong candidates for drug and pesticide delivery and controlled release due to their outstanding adsorption properties and biodegradability. In addition, lignin nanoparticles have also raised interest for biomedical (tissue engineering) and environmental (antifouling materials) applications [108].

Chapter 4 : The effects of lignin source and extraction on the composition and properties of biorefined depolymerization products

4.1 Introduction

Lignin is an amorphous, aromatic 3D biopolymer composed of three monomeric units: coniferyl alcohol (G), *p*-coumaryl alcohol (H), and sinapyl alcohol (S). [21, 23]. It plays an essential structural and functional role in plants and is the largest store of renewable aromatic carbon. Despite the potential chemical value of the aromatic subunits, lignocellulosic biomass is rarely processed commercially for products other than low-value combustion fuels. This is due, in part, to the technical challenges associated with depolymerizing this complex polymer.

The ratio of monolignols varies with plant species. Generally, hardwood lignin, such as birch and poplar, are composed of S and G monolignols, whereas softwood lignin, such as pine and spruce, are composed exclusively of G monomers. Herbaceous lignin found in switchgrass and corn stover, for example, typically contains all three monolignols, but the H content is low (below 5%) [23, 24]. The amount of lignin varies between 10 and 35% by plant species with softwood typically containing the highest percentage of lignin and herbaceous containing the lowest percentage of lignin [21, 23]. The monolignols are bonded through 14 unique linkages, the most common being the β-O-4 linkage [29]. The bond dissociation energy (BDE) of the β-O-4 linkage is between 221 and 295 kJ/mol making it easier to break compared to the 5-5 (carbon-carbon) bond with nearly double the BDE [9, 10]. The abundance of the β-O-4 bond, as well as the relatively lower BDE, makes this bond a common target of depolymerization processes.

Lignin extraction or fractionation from biomass has a significant effect on its structure. Extracted lignin is often referred to as technical lignin. Some methods produce a technical lignin that conserves the natural (native) structure of lignin including milled-wood lignin (Bjorkman process), ionic liquid lignin and cellulolytic enzyme lignin [9, 23]. The most industrially common method of extracting lignin without severe structural modification is the Organosolv method, which is used to separate cellulose for second generation bioethanol production, producing the second largest lignin stream [30]. The Kraft process, employed in paper production, is the largest commercial lignin stream comprising 85% of total technical lignin produced in the world [31, 32]. The Kraft process does not aim to preserve the β-O-4 linkages, resulting in lignin that varies immensely from its native structure and is highly condensed and difficult to use as the feedstock in a downstream biorefinery.

Biorefinery research primarily focuses on "lignin first fractionation," the goal of which is to preserve the structure of native lignin because of the difficulties working with some forms of technical lignin and the lack of β-O-4 linkages [33]. Research in this area centers on: 1) analytical methods to determine and preserve the structure of native lignin [213-218], 2) genetic modification to allow easier separation and more structural preservation of lignin [34, 35], 3) stabilization of the low molecular weight lignin to avoid repolymerization [36], and 4) determination of fractionation methods to better conserve the structure of native lignin [37-44].

We previously demonstrated a proof of concept biorefinery to depolymerize lignin into high value products. In this biorefinery we coupled a microbial electrolysis cell (MEC) that oxidizes the organic content of wastewater (as modeled by acetate) at the anode reducing BOD by 60% and producing a high pH, high salt effluent at the cathode which is then used to depolymerize

an extracted lignin stream [18]. Under the ambient temperature and pressure conditions of our biorefinery, base catalyzed depolymerization of an Organosolv herbaceous (corn stover) lignin preserves the aromatic structure to yield discrete aromatics such as monomers (e.g., vanillin, p-coumaric acid) and flavonoids at approximately 20% of the initial lignin mass and lignin nanoparticles (LNPs) to close mass balance. These products have many potential commercial applications in the food, pharmaceutical, nutraceutical, personal care and agricultural industries.

Since the native structure of lignin varies as a function of its source and is further modified by the method of extraction, it is unclear how the biorefining of lignin is altered as a function of these factors. The purpose of this research, then, is to investigate how lignin source, particularly lignin content, bond type, and monolignol composition, and extraction influence our biorefinery's performance as characterized by the composition and properties of the depolymerized product mixture. Specifically, we study the products: phenolic content, flavonoid content, and lignin nanoparticles, and the properties of the product mixture including: shape, size, stability, polydispersity, and the antioxidant capacity. We also evaluate the relationship between the products and their properties.

4.2 Materials and Methods

4.2.1 Materials

Sources of biomass include corn stover (herbaceous), white spruce (softwood), and bitternut hickory (hardwood) which were donated by the author's family from Cadott, Wisconsin. Archer Daniels Midland (ADM), Decatur IL kindly donated lignin extracted from corn stover via the acetosolv process (Organosolv using acetic acid). Other materials used were acetone (HPLC plus, Sigma Aldrich) , sulfuric acid (certified ACS plus, Fischer), DMSO (Dimethyl sulfoxide)

(certified ACS, Fischer), NMI (N-methyl Imidazole) (97%, Aldrich), sodium phosphate dibasic (Fischer) , potassium phosphate monobasic (USP analytical test, JT Baker), Folin-Ciolcalteu reagent (Sigma Aldrich), sodium carbonate (ACS, VWR), gallic acid (97.5%, Sigma Aldrich), aluminum chloride hexahydrate (Alfa Aesar), sodium nitrite (98%, Alfa Aesar), sodium hydroxide (certified ACS, Fischer), phosphoric acid, rutin (>94%, TCI), Trolox (abcam), ABTS (TCI), potassium persulfate (certified ACS, Fischer), DMSO-d6 (99.9%, ACROS organics), 1,4 dioxane (>99.5%, Honeywell), Methanol (HPLC grade, Fisher), hexadecyltrimethylammonium bromide (CTAB) (>98%, Sigma Aldrich), acetic acid (ACS, EMD), potassium bromide (Spectograde, International Crystal Labs).

4.2.2 Lignin source and extractions

Lignin was extracted from corn stover via three methods: Milled Wood, Organosolv (ADM) and Klason; lignin from softwood and hardwood was extracted via the Klason method. Prior to extraction, biomass was prepared for extraction using methods: TAPPI T 257 cm-85 (2000) – "Sampling and Preparing Wood for Analysis", and TAPPI T 264 cm-97 – "Preparation of Wood for Chemical Analysis". The white spruce and bitternut hickory samples were acquired as 100-gram blocks. They were turned into saw dust with a power saw. The saw dust was sifted through a 40-mesh screen. The corn stover was dried over night at 40°C. It was then ground in an electric grinder and sifted through a 40-mesh screen. All samples were purified through a Soxhlet extraction. The fine material was placed in a glass extraction thimble (~20 g), the extraction thimble was placed in position in the Soxhlet apparatus. 200 mL of solvent (95 acetone: 5 water v:v) was placed in a 250 mL extraction flask. The extraction ran for 6-8 hours with the liquid

boiling briskly. After the extraction the sample was washed with boiling DI water. The sample was filtered with Whatman No. 5 paper and dried in the oven at 105°C overnight.

Lignin was extracted via the Milled Wood process according to the Bjorkman method, which involves milling biomass in a planetary ball mill and extracting lignin with an organic solvent [219]. The milling was done using a SPEX 8000D Mixer/Mill equipped with a 50 mL ZrO_2 grinding jar and 10 x 10 mm ball bearing set at 600 r.p.m. The milling protocol for the corn stover was 5 minute runs, 5 times, with 5 minute pauses in between for a total of 45 minutes [91]. The milled corn stover was dispersed in dioxane: water (96:4, v:v) and magnetically stirred for 24 hours [220]. After 24 hours the suspension was centrifuged, the supernatant was saved and the solids were resuspended in fresh dioxane:water for 24 more hours. The mixture was centrifuged and the supernatants from days 1 and 2 were combined and freeze dried (Labconco -84 C 4.5L PTFE coated benchtop freeze dryer) to produce Milled Wood lignin (MWL).

Lignin was extracted via the Klason method for the herbaceous, hardwood, and softwood sources in accordance to TAPPI T 222 om-98 - Acid Insoluble Lignin in Wood and Pulp. In a beaker, 1 gram of biomass was stirred with 15 mL of 72% sulfuric acid for 2 hours. After 2 hours, the material from the beaker was transferred into a flask with 300-400 mL DI water and more water was added to a final volume of 575 mL. The solution was boiled for 4 hours, frequently adding hot water to keep the volume constant. After four hours the material was allowed to settle overnight. The supernatant was decanted off. The lignin was washed with hot water, filtered and left to dry over night at 105°C. The total amount of acid insoluble (Klason) lignin in the biomass was calculated according to:

$$Lignin, \% = \frac{A}{W} * 100$$

Where A is the weight of the lignin in grams and W is the weight of the initial biomass.

4.2.3 Lignin Depolymerization Experiments

Lignin depolymerization was carried out as described in Obrzut et al. [18]. Synthetic MEC catholyte was used for the experiments and prepared with a 227 mM phosphate solution (0.2 g·L^{-1} KH$_2$PO$_4$·H$_2$O and 32 g·L^{-1} Na$_2$HPO$_4$) adjusted with sodium hydroxide to a final pH of 10.8. Lignin (250 mg) was combined with the phosphate solution (250 mL) in a beaker under magnetic stirring. The beakers were wrapped in aluminum foil to avoid light exposure. Two types of experiments were run; a basic set of experiments following the above protocol and a neutral set of experiments following the above protocol except the pH was adjusted to 7 with dilute phosphoric acid after 1 hour (7 mL of 10x diluted phosphoric acid). The latter experiment had previously been more successful in producing a higher yield of LNPs. Both methods had produced similar yields of phenolics and flavonoids. The experiments ran for 14 days, with 50 mL samples taken out at 60 minutes (0 days), 1 day, 4 days, 7 days, and 14 days for characterization. Each set, basic and neutral, was run in duplicate. Table 4.1 summarizes the source, extraction, pH, time and name of each experiment. In bold and underlined, we show at which time each experiment reached maximum solubilization. These are the data that will be reported in Figures 3-6. We chose maximum solubilization over the 14-day average for these values because 1) the day of maximum solubilization corresponded with the minimum IC50 (maximum antioxidant capacity) and a lower residual standard error than if we chose the 14-day average since both the solubilization and antioxidant capacity increase significantly over the 14-day period (solubilization under basic conditions increased 2-5 fold over 14 days, antioxidant capacity increased similarly). **Table** 4.2

and **Table** 4.3 compare product and property values over a 14-day average, at maximum

solubilization and maximum antioxidant capacity.

Table 4.1. Summary of experimental matrix; lignin source, extraction method, pH, time of sampling, and experiment label. Each experiment was conducted in duplicate. For a total of 88 experiments.

Source	Extraction	pH	Time (# days)	Experiment Label
Herbaceous	MWL	Basic (10.8)	**0**, 7	MWL-B
Herbaceous	MWL	Neutral (7.0)	**0**, 7	MWL-N
Herbaceous	Organosolv	Basic (10.8)	0, 1, 4, **7**, 14	HO-B
Herbaceous	Organosolv	Neutral (7.0)	0, 1, 4, **7**, 14	HO-N
Herbaceous	Klason	Basic (10.8)	0, 1, 4, 7, **14**	HK-B
Herbaceous	Klason	Neutral (7.0)	0, 1, 4, 7, **14**	HK-N
Softwood	Klason	Basic (10.8)	0, 1, 4, 7, **14**	SK-B
Softwood	Klason	Neutral (7.0)	0, 1, 4, 7, **14**	SK-N
Hardwood	Klason	Basic (10.8)	0, 1, 4, 7, **14**	HaK-B
Hardwood	Klason	Neutral (7.0)	0, 1, 4, 7, **14**	HaK-N

Table 4.2 Solubilization (sol), LNP conc. (concentration), size, PDI, PC (phenolic content), FC (flavonoid content), zeta (potential), and IC50 data along with its associated error for Klason extractions of herbaceous (HK), softwood (SK), and hardwood (HaK) lignin at basic (B) and neutral (N) conditions for a 14 day time average, the time at which max solubilization occurs, and the time at which minimum IC50 occurs. In the case of the Klason extractions, maximum solubilization and minimum IC50 occur at the same time – day 14.

		time (days)	Sol. (mg/L)	LNP conc. (mg/L)	Size (nm)	PDI	PC (mg/L)	FC (mg/L)	Zeta (-mV)	IC50 (g/L)	RSE Sol.	LNP conc.	Size	PDI	PC	FC	Zeta	IC50
HK-B	AVG	-----	503.7	144.9	1495.3	0.68	146.0	50.6	31.0	113.9	11%	18%	32%	8%	9%	14%	-4%	6%
	Max depol.	14	620.9	212.9	3417.1	0.48	186.1	52.3	33.5	107.4	6%	9%	36%	15%	6%	22%	-1%	2%
	lowest IC50	14	620.9	212.9	3417.1	0.48	186.1	52.3	33.5	107.4	6%	9%	36%	15%	6%	22%	-1%	2%
SK-B	AVG	-----	26.1	9.1	3760.8	0.88	66.3	73.8	31.4	834.5	14%	30%	18%	6%	18%	15%	-2%	16%
	Max depol.	14	33.4	18.6	6252.8	0.81	109.8	110.5	31.8	505.3	46%	7%	24%	8%	23%	14%	-2%	14%
	lowest IC50	14	33.4	18.6	6252.8	0.81	109.8	110.5	31.8	505.3	46%	7%	24%	8%	23%	14%	-2%	14%
HaK-B	AVG	-----	263.0	117.3	2364.0	0.82	212.3	138.3	29.0	148.9	22%	42%	12%	9%	17%	25%	-4%	34%
	Max depol.	14	345.1	283.9	3379.8	0.56	318.6	231.0	29.8	72.3	1%	16%	15%	36%	2%	4%	0%	2%
	lowest IC50	14	345.1	283.9	3379.8	0.56	318.6	231.0	29.8	72.3	1%	16%	15%	36%	2%	4%	0%	2%
HK-N	AVG	-----	260.9	106.3	1303.7	0.76	137.8	82.1	29.0	201.1	6%	29%	11%	6%	10%	16%	-2%	8%
	Max depol.	14	295.4	109.3	751.0	0.60	155.7	107.2	29.9	167.2	6%	9%	36%	15%	6%	22%	-1%	2%
	lowest IC50	14	295.4	109.3	751.0	0.60	155.7	107.2	29.9	167.2	6%	9%	36%	15%	6%	22%	-1%	2%
SK-B	AVG	-----	12.0	9.4	3035.1	0.94	39.0	31.8	29.2	995.9	16%	30%	5%	4%	17%	52%	-5%	8%
	Max depol.	14	19.3	14.0	3296.7	0.88	49.4	87.4	25.9	729.8	46%	7%	24%	8%	23%	14%	-2%	14%
	lowest IC50	14	19.3	14.0	3296.7	0.88	49.4	87.4	25.9	729.8	46%	7%	24%	8%	23%	14%	-2%	14%
HaK-B	AVG	-----	32.9	16.9	2042.9	0.73	133.2	49.2	27.3	569.5	7%	48%	11%	17%	17%	41%	-2%	13%
	Max depol.	14	36.2	46.8	2043.3	0.32	191.0	123.1	26.0	385.6	1%	16%	15%	36%	2%	4%	0%	2%
	lowest IC50	14	36.2	46.8	2043.3	0.32	191.0	123.1	26.0	385.6	1%	16%	15%	36%	2%	4%	0%	2%

Table 4.3 Solubilization (sol), LNP conc. (concentration), size, PDI, PC (phenolic content), FC (flavonoid content), zeta (potential), and IC50 data along with its associated error for Milled Wood lignin (MWL), Organosolv (HO) and Klason(HK) extractions of herbaceous lignin at basic (B) and neutral (N) conditions for a 14 day time average, the time at which max solubilization occurs, and the time at which minimum IC50 occurs.

		Time (days)	Sol. (mg/L)	LNP conc. (mg/L)	Size (nm)	PDI	PC (mg/L)	FC (mg/L)	Zeta (- mV)	IC50 (g/L)	RSE Sol.	LNP conc.	Size	PDI	PC	FC	Zeta	IC50
MWL-B	AVG	-----	627.5	61.5	1849.0	0.95	48.6	28.2	43.0	316.5	7%	25%	4%	1%	2%	47%	8%	27%
	Max depol.	0	671.4	45.9	1771.7	0.96	47.5	15.0	46.6	230.3	4%	12%	13%	4%	6%	6%	2%	15%
	lowest IC50	0	671.4	45.9	1771.7	0.96	47.5	15.0	46.6	230.3	4%	12%	13%	4%	6%	6%	2%	15%
HO-B	AVG	-----	826.4	209.4	474.5	0.49	349.4	191.1	34.6	33.5	4%	31%	10%	5%	3%	17%	3%	5%
	Max depol.	7	935.9	465.3	446.4	0.47	373.3	295.1	38.5	34.4	10%	3%	3%	7%	2%	0%	1%	7%
	lowest IC50	0	720.2	138.8	424.4	0.47	349.8	234.0	34.8	29.7	4%	6%	3%	5%	3%	4%	2%	4%
HK-B	AVG	-----	503.7	144.9	1495.3	0.68	146.0	50.6	31.0	113.9	11%	18%	32%	8%	9%	14%	4%	6%
	Max depol.	14	620.9	212.9	3417.1	0.48	186.1	52.3	33.5	107.4	6%	9%	36%	15%	6%	22%	1%	2%
	lowest IC50	14	620.9	212.9	3417.1	0.48	186.1	52.3	33.5	107.4	6%	9%	36%	15%	6%	22%	1%	2%
MWL-N	AVG	-----	335.7	86.7	7521.8	0.78	48.3	35.3	35.4	475.8	2%	84%	37%	17%	4%	55%	11%	25%
	Max depol.	0	342.0	13.7	10282.3	0.92	46.6	15.9	39.4	357.1	1%	50%	7%	9%	0%	44%	3%	2%
	lowest IC50	0	342.0	13.7	10282.3	0.92	46.6	15.9	39.4	357.1	1%	50%	7%	9%	0%	44%	3%	2%
HO-N	AVG	-----	423.1	640.8	538.8	0.45	364.7	203.0	31.8	53.8	1%	27%	14%	12%	5%	14%	6%	6%
	Max depol.	7	431.7	996.5	504.7	0.38	390.8	310.0	35.5	58.1	11%	8%	5%	7%	2%	0%	1%	7%
	lowest IC50	0	441.3	165.3	767.0	0.56	350.8	215.0	24.5	50.0	3%	5%	4%	5%	3%	3%	2%	4%
HK-N	AVG	-----	260.9	106.3	1303.7	0.76	137.8	82.1	29.0	201.1	6%	29%	11%	6%	10%	16%	2%	8%
	Max depol.	14	295.4	109.3	751.0	0.60	155.7	107.2	29.9	167.2	6%	9%	36%	15%	6%	22%	1%	2%
	lowest IC50	14	295.4	109.3	751.0	0.60	155.7	107.2	29.9	167.2	6%	9%	36%	15%	6%	22%	1%	2%

4.2.4 Product Characterization

The initial biomass and lignin extractions were characterized by NMR and FTIR to determine the S/G ratio and β-O-4 content (NMR) and to look at changes to functional groups and aromaticity (diffuse reflectance infrared Fourier transform, DRIFT). For NMR the samples were acetylated. We followed a modified acetylation protocol by Mansfield et al [91]. For both the fine, extractive free biomass, and for the extracted lignin, 100 mg of the sample were suspended in 2 mL of DMSO. An additional 1 mL of NMI was added, and the solution was stirred constant with a magnetic stirrer for 24 hours. Then 0.5 mL of acetic anhydride was added, and the solution was stirred for another 24 hours. The solution was then transferred to 300 mL of deionized water and allowed to settle overnight. Most of the supernatant was decanted and the solution was centrifuged for 10 minutes at room temperature at 3,480 rpm. The precipitate was washed with 50 mL of water, 3 times. The sample was then dried overnight at 40°C. Once the sample was dry, 30-50 mg of acetylated biomass or lignin was dissolved in 0.5 mL of deuterated DMSO-d6 and the solution was transferred to an NMR tube (Kimble, 5MM, 7", 400 MHZ). The samples were run on a Bruker Neo 600 MHz system with QCI-F cryoprobe. The software used is TopSpin 4.04. The Bruker Pulse Program for the HSQC spectra is "hsqcetgpsisp2.2". The number of scans (NS) was set to give a total acquisition time of 3 hours for biomass and 30 minutes for lignin. DRIFT ~~FTIR~~ spectroscopy (Bruker Tensor 37) was run on initial biomass and lignin (diluted to 4% in KBr) as well as dialyzed (thermos scientific Slide-A-Lyzer Dialysis Cassette G2 – 2,000 MWCO, 15 mL capacity) and freeze dried (Labconco -84 C 4.5L PTFE coated benchtop freeze dryer) day 14 samples of solubilized lignin.

The lignin depolymerization slurry samples were characterized with the following analyses: pH, total solubilization, total phenolic content, total flavonoid content, antioxidant capacity, lignin nanoparticle (LNP) concentration, LNP size, polydispersity index (PDI), and zeta potential. These characterizations were conducted on centrifuged and non-centrifuged samples. Unless indicated with a "C", results are for the non-centrifuged samples. Centrifuging was done on 25 mL in 50 mL falcon tubes for 10 minutes at 7,000 r.p.m. The pH was measured with a pH-meter (Mettler Toledo SevenCompact S210).

We determined the total solubilized lignin, total phenolic content, and total flavonoid content by measuring the UV absorbance (Eppendorf BioSpectrometer). Total solubilized lignin is define as lignin that can be measured spectroscopically and typically includes monomer, dimer, and soluble polymers. Over time base catalyzed depolymerization and repolymerization transforms the smaller products into flavonoids/oligomers and LNPs. Quantification was achieved through calibration curves obtained from samples of lignin dissolved in pH 13 NaOH solution (**Figure 4.1**). Peak absorbance occurred between 288 and 291 nm. Solubilization was measured on centrifuged samples to remove any residual solids.
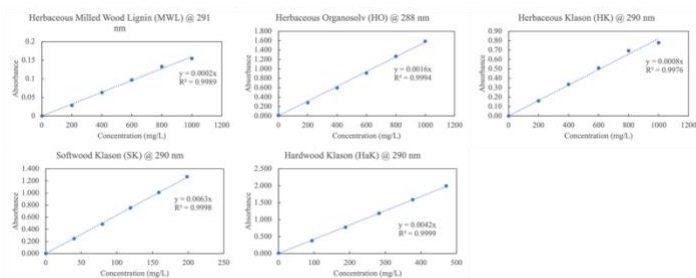
Figure 4.1 Calibration curves for the Milled Wood, Organosolv, and Klason extraction of herbaceous (corn stover) lignin and the Klason extractions of softwood (white spruce) and hardwood (bitternut hickory) lignin. The MWL and Organosolv calibrations were made with a 20x dilution, the herbaceous Klason was made with a 10x dilution, and the softwood and hardwood were made with a 2x dilution. The softwood and hardwood did not have full dissolution with pH 14 NaOH so the remaining solids were dried and weighed to determine the actual concentration in solution.

The total amount of phenolics and flavonoids were determined with the colorimetric Folin-Ciolcalteu method and the method by Zhishen et al, respectively [81, 82]. The former combines 100 μL of solubilized lignin with 2 mL of a 2% sodium carbonate solution. The mixture was incubated at room temperature for 5 minutes and then 100 μL of Folin-Ciolcalteu reagent was added and the mixture was incubated further for 30 minutes. The absorbance was measured at 750 nm. A calibration was performed with a solution of gallic acid (3, 4,5-trihydroxybenzoic acid) every time the experiment was performed [180] (**Figure 4.2 a**). For the Zhishen methods, 300 μL
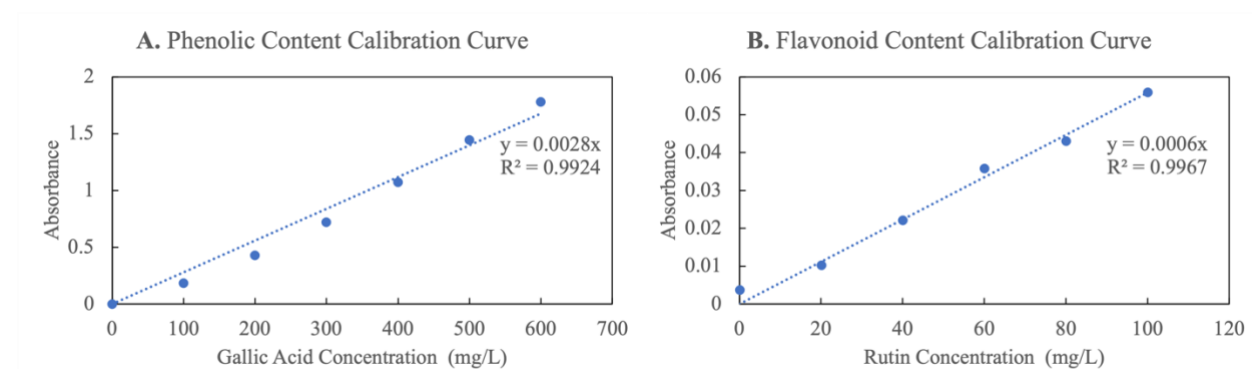
Figure 4.2 a) The calibration curve for the Folin-Ciolcalteu method, made with gallic acid (3, 4,5-trihydroxybenzoic acid) at 750 nm. b) The calibration curve for the Zhishen method, made with rutin (3′,4′,5,7-Tetrahydroxy-3-[α-L-rhamnopyranosyl-(1→6)-β-D-glucopyranosyloxy]flavone) at 510 nm.

of solubilized lignin was combined with 3.4 mL of a 30% methanol solution, 150 μL of a 0.5 mmol L^{-1} sodium nitrate solution and 150 μL of a 0.3 mmol L^{-1} aluminum chloride hexahydrate solution at room temperature. 1 mL of 1 mol L^{-1} sodium hydroxide was added after 5 minutes and the absorbance was immediately measured at 510 nm. The calibration curve was made using the flavonoid rutin, (3′,4′,5,7-Tetrahydroxy-3-[α-L-rhamnopyranosyl-(1→6)-β-D-glucopyranosyloxy]flavone) (**Figure 4.2 b**). A 100 mg/L sample of rutin was made with each set of experiments to confirm the accuracy of the calibration curve.

The antioxidant capacity was also determined by measuring the UV absorbance. We followed a modified version of the ABTS method first described by Cano et al. [221]. The ABTS$^+$ radical solution was prepared from 10 mL of 7mM ABTS$^+$ [2,2'-Azino-bis(3-ethyl-benzothiazoline-6-sulfonic acid)] solution in water and 10 mL of 2 mM potassium persulfate solution in water. The mixture was incubated in the dark at room temperature overnight. The ABTS$^+$ solution was diluted with water to an absorbance of 0.70 +/- 0.1 at 734 nm. Then 1 mL of different concentrations of lignin (0, 2, 6, 10, 14, 16, 18, 20, 40, 60, 80, 100, 140, 160, 200, 300, 400, 600, 800 mg/L) was added to 2.0 mL of ABTS$^+$ diluted solution. The mixture was incubated in the dark for 6 minutes and were measured at 734 nm. The scavenging was calculated with the following equation:

$$Scavenging\ effect\ (\%) = \frac{A_c - A_t - CF}{A_c - CF} x\ 100,$$

where A_C is the absorbance of the ABTS$^+$ diluted solution without any antioxidants added, A_t is the absorbance of the test, and CF was the correction factor due to pH. The correction factor for neutral samples is 0, the correction factor for pH 10.8 varies as a function of concentration and can be found in the supplemental information (**Figure** 4.3 and **Table** 4.4). The concentration required to inhibit the ABST$^+$ by 50% (IC50) was determined by linear regression analysis. Trolox (6-hydroxy-2,5,7,8-tetramethylchroman-2-carboxylic acid) was used as a standard to verify the method. The IC50 of Trolox was found to be 21.5 mg/L, consistent with literature [222].
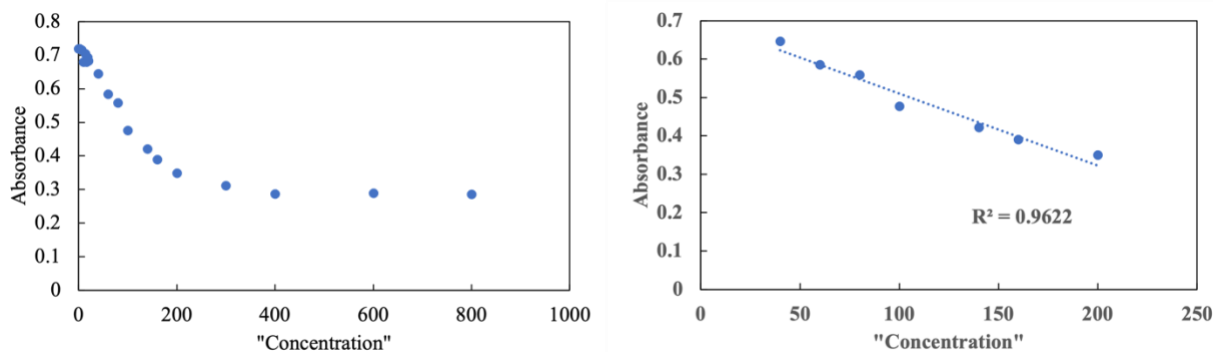
Figure 4.3 The inhibition of absorbance produced by the phosphate buffer at pH 10.8. Under 20 mg/L of buffer, the inhibition is negligible (SD < 0.01). Between 20-200 mg/L the inhibition increases linearly. Above 200 mg/L the inhibition is constant (SD < 0.01). The correction factors are listed in Table 4.4.

Table 4.4 The correction factors needed for ABTS scavenging calculations at basic pH. These values were used by subtracting the absorbance from Figure 4.3 from the initial absorbance of the ABTS without any buffer.

Concentration	Absorbance Correction
Between 0-20 mg/L	0.000
40 mg/L	0.054
60 mg/L	0.115
80 mg/L	0.141
100 mg/L	0.223
140 mg/L	0.278
160 mg/L	0.310
Over 200 mg/L	0.405

LNP concentration, size, PDI, and zeta potential were determined with Nanoparticle Tracking Analysis (NTA) and Zetasizer. The NTA (Malvern Panalytical NanoSight NS300) was used according to Obrzut et al. to estimate both the concentration and size distribution [18]. The limits for size distribution are between 10 and 1000 nm. The lignin solutions were diluted 50 times in water to be measured via NTA. Since the NTA cannot detect LNPs larger than 1000 nm, the

LNP concentration reported is for LNPs smaller than 1 micron. The concentration of LNPs larger than 1 micron is not known. The zetasizer (Malvern Panalytical Zetasizer Nano ZS) also has dynamic light scattering (DLS) capabilities to measure size and polydispersity index (PDI). DLS can measure the size up to 10.0 microns. The lignin solutions were diluted 10x for size, PDI and zeta potential measurements. Then, 1 mL of sample was placed in a DTS1070 disposable zeta potential cuvette or a plastic cuvette for DLS. Three measurements were taken for each sample with up to 100 zeta runs per sample. For these runs the refractive index of lignin was set at 1.61 [186].

High-performance liquid chromatography coupled to mass spectrometry was completed using previously published methods [18]. Briefly, an Agilent 1260 Infinity binary LC system with an autosampler was coupled to a Bruker Amazon X ion trap with an electrospray ionization (ESI) source. The HPLC column was a Phenomenex Gemini C6-Phenyl, 250-mm long, with an internal diameter of 4.6 mm and a particle size of 5 μm. The HPLC instrument was also coupled to an Agilent G4212B diode array detector (DAD). A gradient method with ultrapure water (solvent A) and HPLC-grade methanol (solvent B), both modified with 0.01% (v/v) acetic acid, at 40 ˚C column temperature, and a flow rate of $0.4 \ mL \cdot min^{-1}$ was used.

The SEM micrographs were obtained using a JEOL JSM-7900FLV microscope equipped with an Oxford Ultimax 65 energy-dispersive x-ray spectroscopy (EDS) accessory. The voltage was set to 5 kV and the current to 8 mA. The SEM was run using the lower electron detector (LED). SEM samples were prepared by diluting the suspensions 10-fold with 5% CTAB and spin-coated (Laurel Technologies) onto a silicon wafer for 1 minute with an acceleration of $1 \ rpm \cdot s^{-1}$ and a maximum rotation speed of 2000 rpm. For enhancing conductivity, a 10-nm AuPd layer was deposited over the sample via the Denton III Desk Sputter Coater.

4.3 Results

4.3.1 Structure

Table 4.5 summarizes the structural features of interest for each lignin source: % acid insoluble lignin as determined by the Klason extraction, and the % β-O-4 linkages and S/G ratio as determined by NMR. The results for the biomass characterization compare well with those in the literature [25]. Softwood biomass contains the highest lignin content, followed by hardwood, and then herbaceous, which has slightly more than half that found in softwood. For % β-O-4 linkages, herbaceous has the highest content, followed by hardwood, followed by softwood. S/G ratio is highest for hardwood and lowest for softwood, since softwood contains mostly the G monolignol. Herbaceous S/G ratio is around 0.5 and is only one of the sources that contains the H monolignol. The S monolignol lacks a free ortho-position, making it unable to form 5-5 or β - β carbon-carbon bonds [223]. For this reason, lignin with a high S/G ratio (hardwood) has less carbon-carbon bonds and has a more linear structure, whereas lignin with a low S/G ratio (softwood) has more carbon-carbon bonds and has a more branched structure, making it harder to delignify the biomass and for downstream depolymerization [224, 225]. The more linear structure of hardwood lignin allows more flexibility to form coiled structures, creating more density [226]. The extractions: MWL, Organosolv, and Klason, do not have a major effect on the S/G ratio of herbaceous lignin, however they have a large effect on the % β-O-4 linkages. The more mild extractions, Milled Wood lignin and Organosolv, remove only 19% and 32% of β-O-4 linkages, respectively. The Klason extraction was the only extraction done on all three sources because the Organosolv (acetosolv) and MWL extractions were unable to extract sufficient lignin from the samples, as previously noted in literature [227]. Klason, the harshest extraction, eliminates between 80 and 90% of the β-O-4 linkages present in the initial biomass.

Table 4.5 Lignin content, B-O-4 content, and S/G ratio of all three sources and three extractions. Herbaceous lignin also contains the H monolignol.

Source	Latin Name	Common Name	% lignin (determined via *Klason*)	β-O-4 (%)	S/G ratio	β-O-4 (%)	S/G ratio	β-O-4 (%)	S/G ratio	β-O-4 (%)	S/G ratio
Hardwood	Carya cordiformis	Bitternut Hickory	23.71%	68.67%	1.74	11.90%	1.64	N/A		N/A	
Softwood	Picea glauca	White Spruce	28.12%	37.42%	0.063	3.53%	0.056	N/A		N/A	
Herbaceous		Corn Stover	15.60%	83.46%	0.55	14.52%	0.52	56.50%	0.55	67.60%	0.50

The DRIFT spectra between 1750 – 1000 cm^{-1} of the MWL, Organosolv, and Klason extractions of herbaceous lignin and the Klason extractions of the hardwood and softwood lignin are shown in **Figure** 4.4. All of the sources and extractions share the characteristic peaks of lignin and are detailed in **Table** 4.6. We point out six key peaks in **Figure** 4.4. Peak 1 (~1712 cm^{-1}) and Peak 2 (~1680 cm^{-1}) correspond to unconjugated and conjugated carbonyl (C=O) stretching, respectively. Peak 3 (1506 cm^{-1}) corresponds to the aromatic skeletal vibration. Peak 4 (1220 cm^{-1}) corresponds to phenolic O-H plus ether C-O stretching, peak 5 (1087 cm^{-1}) corresponds to C-O deformation at C_β and aliphatic ether and peak 6 (1033 cm^{-1}) corresponds to C-O deformation at the C_α and aliphatic ether.

Table 4.6 FTIR assignments. The values in bold correspond to those that are highlighted in red in Figure 4.4

MWL	HO	HK	SK	HaK	
3507	3377	3294	3462	3416	O-H stretching
	3086	3086	3005	3005	C=H stretching
2963	2963	2963	2943	2943	C-H stretching

					(CH2 asymmetric vibration (guaiacyl-syringyl))
	2938	2920	2872		C-H stretching (methyl and methylene groups)
2885	2843	2851	2839	2839	C-H stretching
			2045		
1705	**1707**	**1711**	**1721**	**1707**	**C=O stretching unconjugated**
1602	**1628**	**1619**	**1629**	**1619**	**aromatic skeletal vibration + C=O stretching (conjugated)**
1509	**1512**	**1508**	**1505**	**1506**	**aromatic skeletal vibration**
1459	1459	1458	1460	1462	C-H deformation (methyl and methylene)
1422	1425	1425	1421	1422	C-H in-plane deformation with aromatic ring stretching
1325	1330	1329		1323	C-O of the syringyl ring
1267	1266	1267	1269	1259	C-O of the guiacyl ring
1217	**1235**	**1231**	**1223**	**1233**	**C-C + C-O stretch (phenolic O-H plus ether C-O)**
1163	1170	1165	1156	1163	C-O stretching in aliphatic groups
1135	1123	1124	1124	1122	aromatic C-H in plane deformation of guaiacyl ring
1074	**1086**	**1091**	**1087**	**1087**	**C-O deformations at C$_\beta$ and aliphatic ethers**
1046	**1033**	**1027**	**1032**	**1027**	**aromatic C-H in plane deformation (G>S), C-O deformation at C$_\alpha$ and aliphatic ethers**
920					=CH out-of-plane deformation in aromatic ring
885	837	856	880	880	C-H out of plane vibrations in 2,5,6 of guaiacyl units
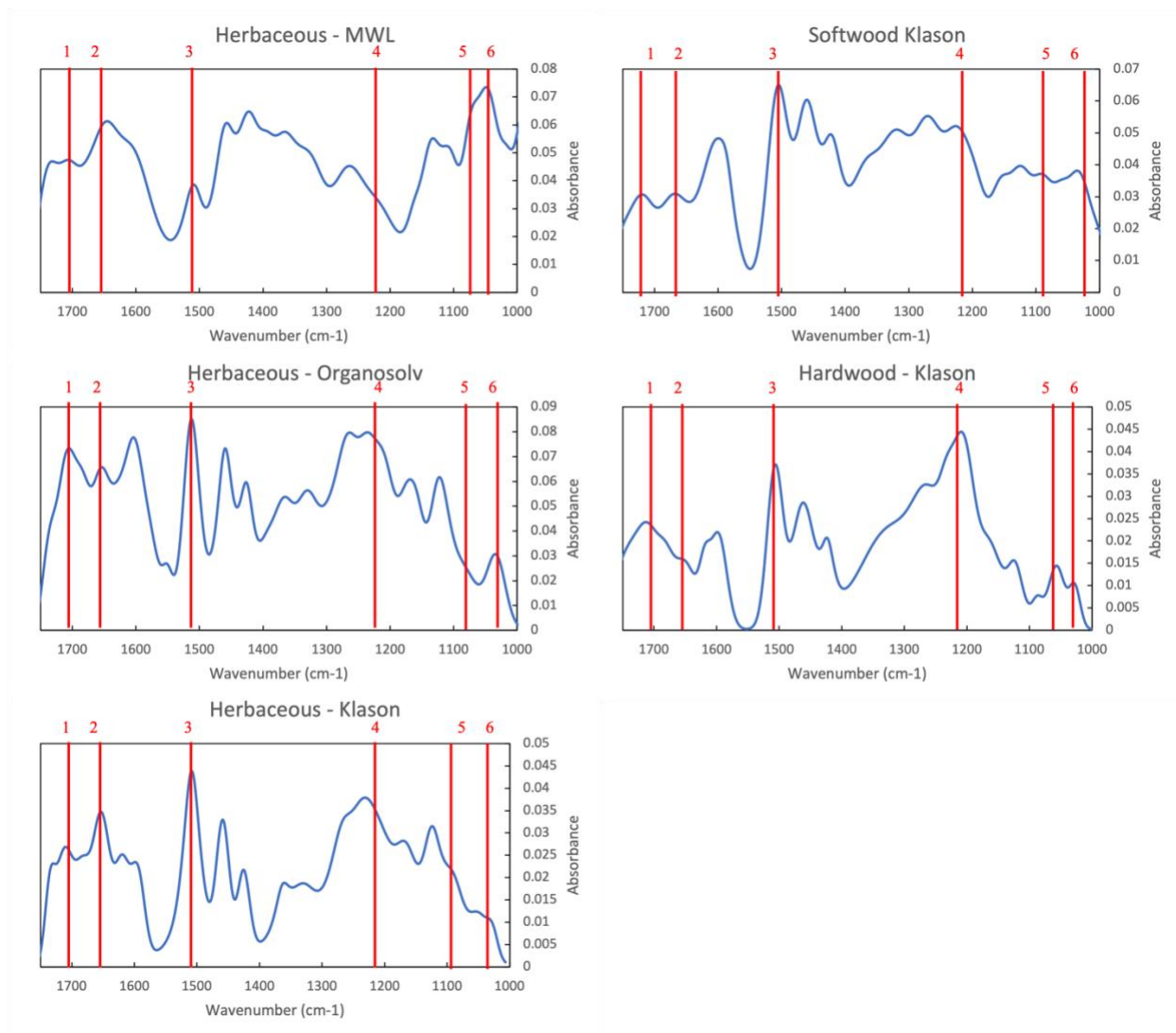
Figure 4.4 DRIFT spectra between 1750-1000 cm-1 for the five sources and extractions of lignin. 6 peaks are highlighted. Peak 1 (~1712 cm^{-1}): unconjugated C=O stretching, Peak 2 (~1680 cm^{-1}): conjugated C=O stretching, Peak 3 (1506 cm^{-1}) : aromatic skeletal vibration, Peak 4 (1220 cm^{-1}): phenolic O-H plus ether C-O stretching, Peak 5 (1087 cm^{-1}) : C-O deformation at C$_\beta$ and aliphatic ether, and Peak 6 (1033 cm^{-1}) : C-O deformation at C$_\alpha$ and aliphatic ether.

The proportions of the peaks vary between sample and extractions. In order to compare the differences between the samples we followed the analysis method of Wang et al. and Pandey [45, 228]. **Figure** 4.5 shows the relative absorbance (I_w/I_{ar}) of the five oxygen containing functional groups: C=O conjugated, C=O unconjugated, OH + C-O, C-O at C$_\beta$ and C-O at C$_\alpha$. I_{ar}

corresponds to the aromatic skeletal vibration peak (Peak 3) and I_w corresponds to the intensity of a particular wavenumber. Here we see that MWL (gray triangle) and Organosolv (yellow square) have the highest proportions of oxygen containing groups compared to the Klason extractions (circles). Of the Klason extractions we see that softwood (dark blue) contains the lowest proportion of carbonyl bonds.
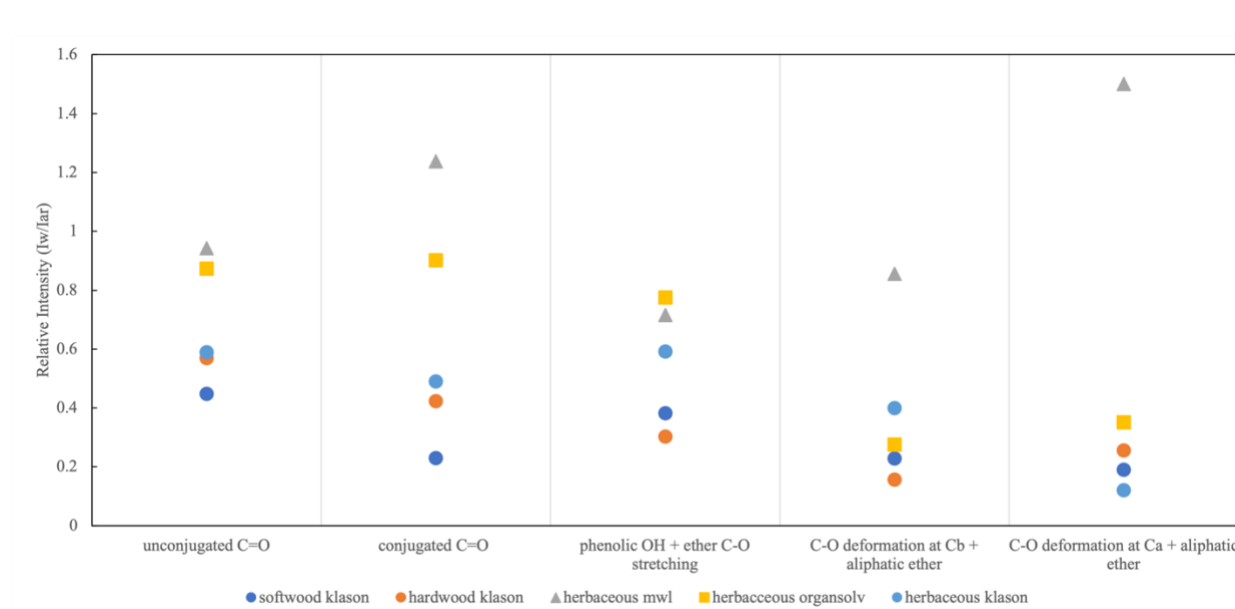
Figure 4.5. Relative intensities of typical functional groups for softwood Klason, hardwood Klason, herbaceous Klason, and herbaceous Organosolv lignins.

4.3.2 Source Influence

To look at the influence of lignin source, we chose one extraction across all three lignin sources. The Klason extraction has a few benefits over the others 1) The Klason extraction produces the most lignin without contamination from cellulose and hemicellulose; 2) It is the most harsh extraction, removing most of the β-O-4 linkages, which mirrors how lignin is typically

extracted industrially (i.e. Kraft, soda, etc.); 3) The Klason extraction is robust and reproducible;

it works on all three of the sources; and 4) there is no introduction of sulfur or other elements.
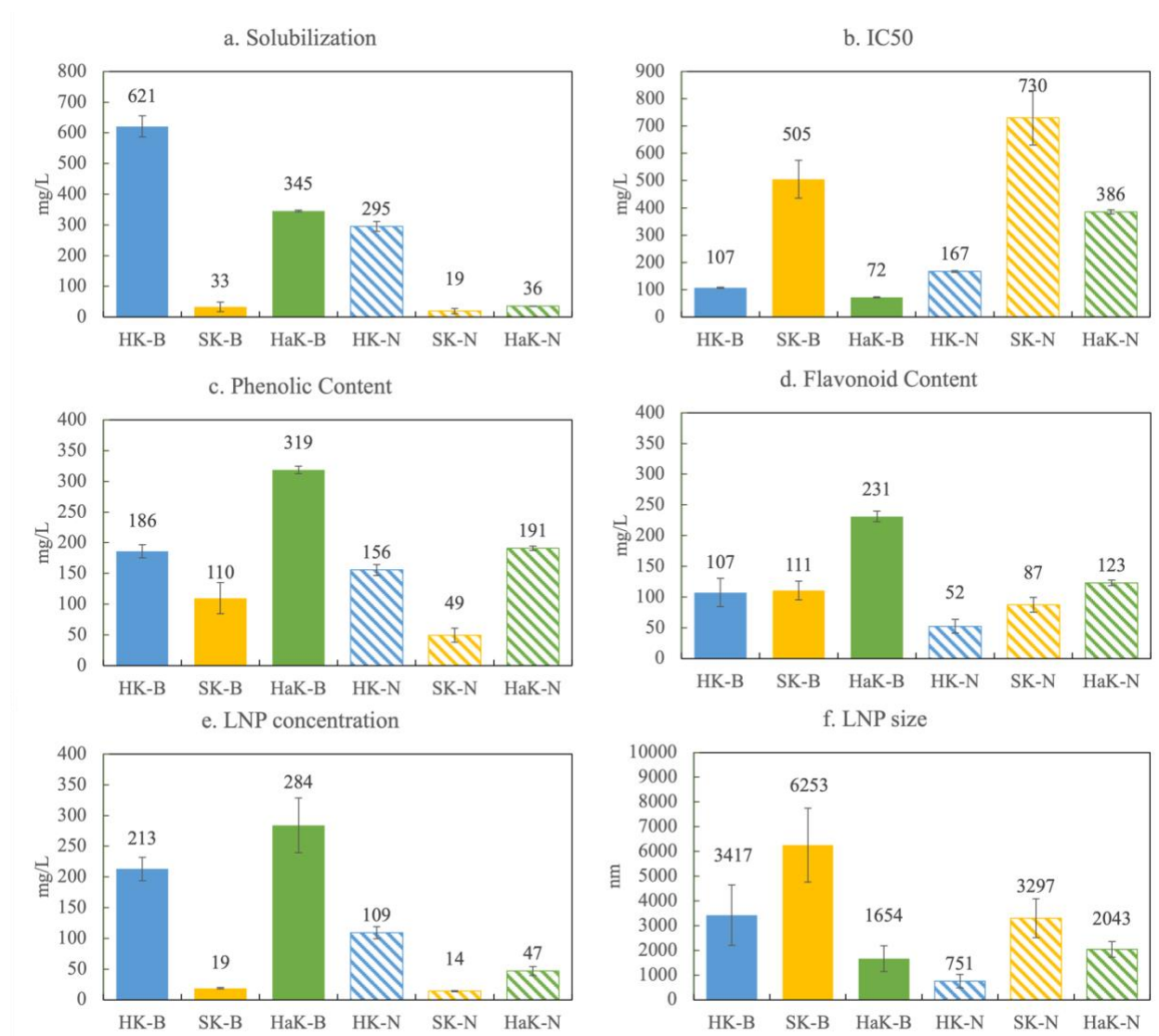
Figure 4.6. We show the a) solubilization (centrifuged), b) IC50, c) Phenolic Content, d) Flavonoid Content, e) LNP concentration, and f) LNP size for the Klason extractions of herbaceous (HK), softwood (SK), and hardwood (HaK) lignin in both basic (B) and neutral conditions.

In **Figure** 4.6**,** we present solubilization, antioxidant capacity, phenolic content, flavonoid content, LNP concentration and LNP size for the Klason extraction of herbaceous, softwood, and hardwood lignin. **Figure** 4.6**a** shows that in basic conditions, Herbaceous Klason (HK) lignin solubilizes to the greatest extent, 62% of the starting lignin concentration (1g/L). Hardwood Klason (HaK) reaches slightly more than half of that at 35%, and Softwood Klason (SK) solubilizes around 3%. In neutral conditions, we see that solubilization is much lower, 50-80% lower than in basic conditions. This indicates that in the case of Klason extraction of lignin, neutralizing the samples at 60 minutes prevents further solubilization, and as we will see subsequent products formation. In basic conditions, of the solubilized lignin, HaK produces more phenolics and flavonoids than either HK or SK (**Figure** 4.6**c** and **Figure** 4.6**d**). We see HaK, produces up to 32% phenolics and 23% flavonoids. HK and SK only reach a max of 19% and 11% phenolics and 10% and 11% flavonoids respectively. We see that SK has more flavonoids and phenolics than the amount solubilized – we hypothesize that this is due to the attachment of phenolics and flavonoids to LNPs or residual solids. To confirm this, we ran the phenolic assay and flavonoid assay on a centrifuged sample to find that the phenolic and flavonoid content both decreased to less than 2%. We see similar trends for the other sources. We believe, however, that making the phenolic and flavonoid measurements without centrifugation is justified because we measure the antioxidant capacity on the entire solution and there is a relationship between the phenolics and flavonoid and antioxidant capacity, whether they are free or associated with LNPs.

With regard to antioxidant capacity (**Figure** 4.6**b),** HaK has the lowest IC50 of 72 mg/L, meaning that the lowest concentration of lignin is required to scavenge 50% of the ABTS radical relative to the other lignin sources and thus, HaK exhibits the highest antioxidant capacity. Trolox, an analog of the industrially relevant antioxidant, vitamin E, has an antioxidant capacity of 21

mg/L. Although HaK, shows about a third of that antioxidant capacity, there has been a push for more natural sources of antioxidants [229]. We see that HK follows closely with an IC50 of 107 mg/L, and SK has the highest IC50 – 505 mg/L, making it a less effective source of antioxidant than the other lignin types. The antioxidant capacity trend is similar to that of phenolic content. Antioxidant capacity is thought to be influenced by many factors, including the -OH groups on phenolics and flavonoids, as well as the surface area to volume ratio of LNPs. It is worth noting that antioxidant capacity also decreases (higher IC50) with all of the sources under neutral pH conditions, relative to that of basic pH conditions. This can be explained by less solubilized lignin yields less phenolics, flavonoids, and LNPs in neutral conditions which simply decreases the concentration of antioxidants in solution. We confirm this by conducting the antioxidant assay on the three extracted lignins in water and finding no antioxidant activity due to no solubilization (**Figure 4.7**). The other explanation has to do with the mechanism in which solubilized lignin scavenges free radicals. Typically phenolic compounds scavenge free radicals either through, 1) a hydrogen atom transfer (HAT) reaction or 2) a single electron transfer (SET) [1]. At high pH, the SET reaction is predominant, which is the specific mechanism that ABTS tests for [221, 230].
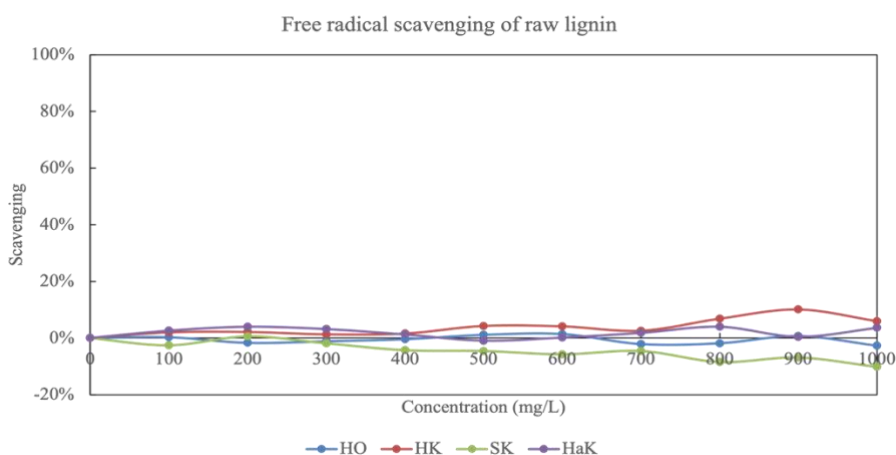
Figure 4.7 ABTS scavenging for herbaceous Organosolv (HO) and the Klason extractions of herbaceous (HK), softwood (SK), and hardwood (HaK)lignin in water. We see no antioxidant activity.

The production of lignin nanoparticles follows a trend similar to that observed with other products. HaK and HK produce the most LNPs at 30% (284 mg/L) and 20% (213 mg/L) (**Figure** 4.6**e)**, respectively. The DLS data show that HaK has the smallest LNP size at around 1600 nm and HK has LNPs around 3400 nm (**Figure** 4.6**f).** SK produces essentially no LNPs in the measurable size range of the NTA (up to 1000 nm) and DLS shows the size to be 6200 nm. In contrast to previous observations, neutralizing the samples fails to increase the LNP yield [18]. The low solubilization for neutral samples, as illustrated in **Figure** 4.6**a**, indicates that there is not enough lignin in solution for the first step of LNP formation, which is dissolution**.**

Figure 4.8 below shows SEM images of the LNPs. In basic conditions, HK produces small LNPs that grow to about 200 nm and at 14 days aggregate into a large, amorphous mass or may be attached to a larger fragment of solid, unreacted lignin. SK produces large, disc like particles. However it is not clear whether this is self-assembled nanoparticle or a solid lignin remnant. HaK produces spherical and non-aggregated LNPs bearing a hole (pointed out by arrows in

Figure 4.8 **c**) which has been seen previously in the literature for LNPs produced from hardwood [231]. The zeta potential (**Figure** 4.9**a**) for all of these LNPs indicates moderate stability (< -30 mV). The PDI for all of the LNPs indicates that they are polydisperse (>.05), although the polydispersity for SK is much greater, > 0.8 indicating extremely high polydispersity (**Figure** 4.9**b**).
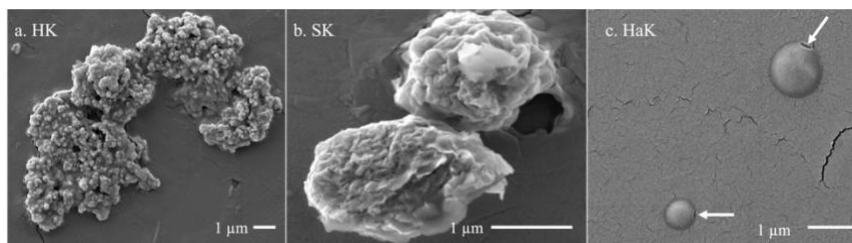
Figure 4.8. SEM images Klason extraction (basic pH) of herbaceous, softwood, and hardwood lignin. All taken at day 14 for the basic experiments.
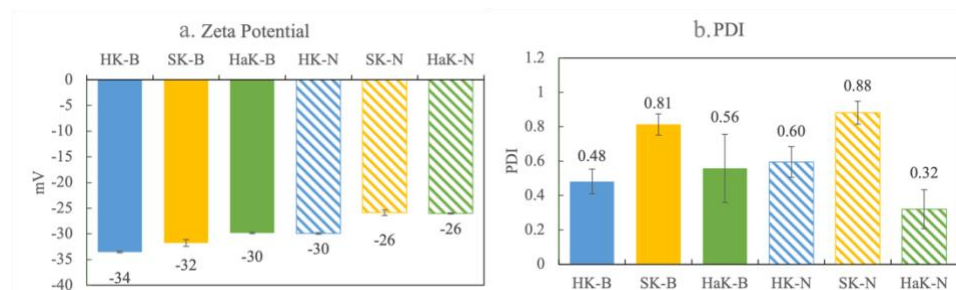
Figure 4.9 a) The zeta potential in mV for HK, SK, and HaK in basic and neutral conditions. Zeta potential indicates moderate stability in basic conditions. b) The PDI for HK, SK, and HaK in basic and neutral conditions. PDI indicates polydisperse sample. PDI of <0.05 indicates a monodisperse sample. PDI > 0.7 indicates highly polydisperse sample.

4.3.3 Extraction Influence

To evaluate extraction effects, Milled Wood, Organosolv, and Klason extractions of the herbaceous lignin were compared. Only the herbaceous source could be extracted by the acetic acid based Organosolv and the Milled Wood methods to yield a sufficient quantity of lignin mass.

Figure 4.10**a** shows that herbaceous Organosolv (HO) material solubilizes to the largest extent, up to 94% (936 mg/L), whereas the Milled Wood herbaceous lignin (MWL) and HK solubilize to a lesser extent, around 65% (671 and 621 mg/L, respectively). Solubilization decreases in all conditions at neutral pH. HO also produces the most phenolics and flavonoids, 37% (373 mg/L) and 30% (295 mg/L) respectively, and these values remain constant at both basic and neutral pH. Lower bulk phenolic and flavonoid yields are observed with HK-B (186 and 107 mg/L, respectively) and they decrease in neutral conditions. Much lower product yields are observed with MWL (48 and 15 mg/L of phenolics and flavonoids, respectively) and these values do not change with pH.

Consistent with these trends, HO has the lowest IC50 (highest antioxidant capacity), followed by HK, and then MWL. HO and MWL are the only examples of the antioxidant capacity decreasing over time. In the case of HO, the IC50 at maximum solubilization (day 7) is 34.4 mg/L and at day 0 it is 29.7 mg/L. Although the total phenolic and flavonoid content for HO increases over the 7 days (349 to 373 mg/L and 234 to 295 mg/L, respectively), the centrifuged phenolics and flavonoids decrease (333 to 288 mg/L and 180 to 133 mg/L). This indicates two things, 1) that phenolics and flavonoids become incorporated into LNPs over time, and 2) that phenolics and flavonoids may have a higher antioxidant capacity as free rather than attached to LNPs. Similar to HaK and SK, the antioxidant capacity always decreased at neutral pH.
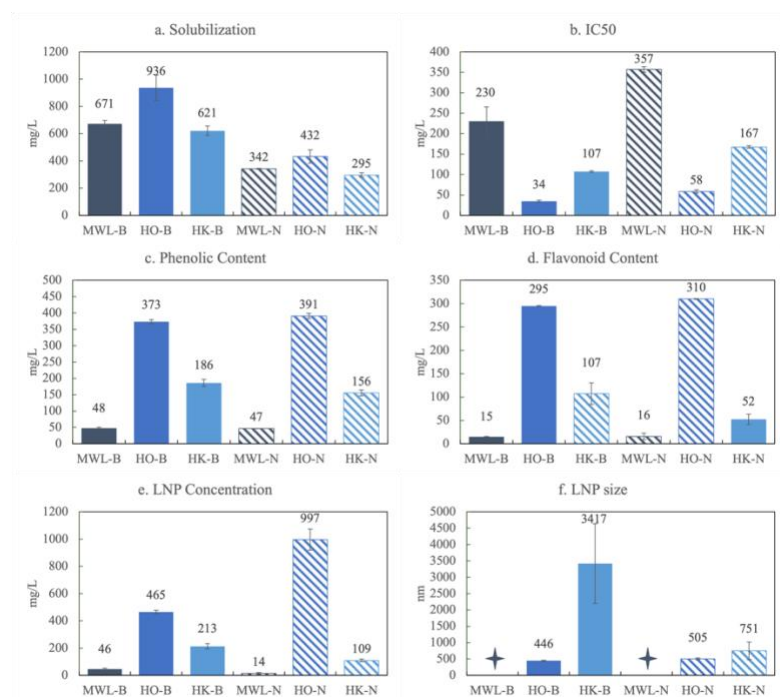
Figure 4.10. We show the a) solubilization (centrifuged), b) IC50, c) Phenolic Content, d) Flavonoid Content, e) LNP concentration, and f) LNP size for the Milled Wood (MWL), Organosolv (HO), and K lason (HK) extractions of herbaceous lignin in both basic (B) and neutral conditions.

Figure 4.10**e** shows that in basic conditions MWL has an LNP concentration of less than 5% (46 mg/L) and HK has an LNP concentration of 20% (213 mg/L), both of which decrease in neutral conditions. HO has a concentration of 46% (456 mg/L) which more than doubles (>99%) in neutral conditions, indicating that essentially of the lignin is in the LNP form. The average size of the HO LNPs are also much smaller than HK, 446 nm in basic conditions and slightly larger at 505 nm in neutral conditions. The zeta potential of HO is slightly larger than that of HK at -39 mV, compared to -34 mV, indicating moderate stability **(Figure** 4.11**a**). The PDI in basic conditions is similar between 0.47 and 0.48, indicating a polydisperse sample (**Figure** 4.11**b**). In neutral conditions the PDI of HO drops to 0.38, which is in polydispersity category but may be more suitable for certain applications. PDIs around 0.2-0.3 may indicate LNPs are suitable for drug delivery [232]. **Figure** 4.12 shows SEM images of: a. MWL, b. HO, and c. HK. The SEM image for MWL does not show the presence of LNPs, which is consistent with the DLS and zetasizer results. Given the high concentration of ether bonds in MWL, the molecular weight of the solubilized MWL lignin may not be large enough to micellize or self-assemble into LNPs. Many of the interactions that LNP formation relies on are molecular weight dependent, such as, the hydrophobic effect, van der waals, and chain entanglement [121]. The mass spec data indicate peaks of non-aromatic compounds **(Figure 4.13**), and given that the MWL extraction does not exclude carbohydrates, there may be interferences that disrupt LNP formation. However, the HO LNPs are spherical and well dispersed. As previously shown (

Figure 4.8**a**), the HK LNPs are highly aggregated into large clusters.
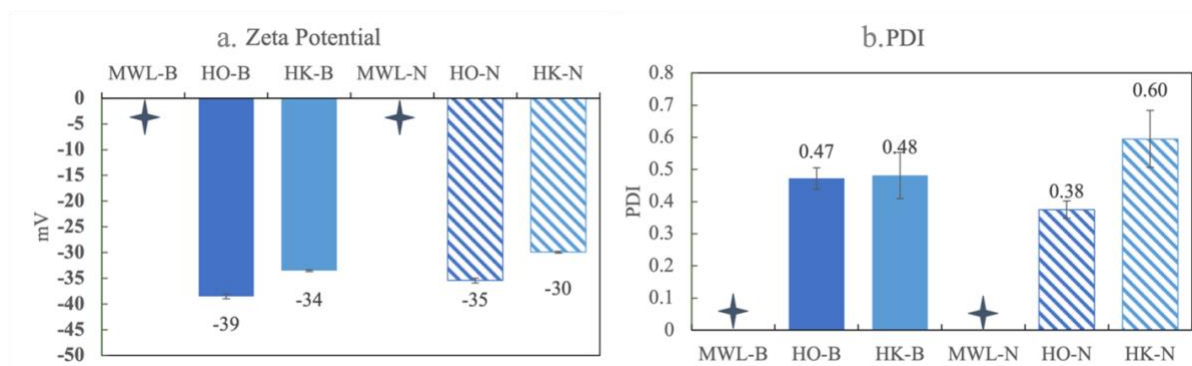
Figure 4.11 a) The zeta potential in mV for HO and HK in basic and neutral conditions. Zeta potential indicates moderate stability in basic conditions. A reading could not be done for MWL. b) The PDI for HO and HK in basic and neutral conditions. PDI indicates polydisperse sample. PDI of <0.05 indicates a monodisperse sample. PDI > 0.7 indicates highly polydisperse sample. A reading could not be done for MWL
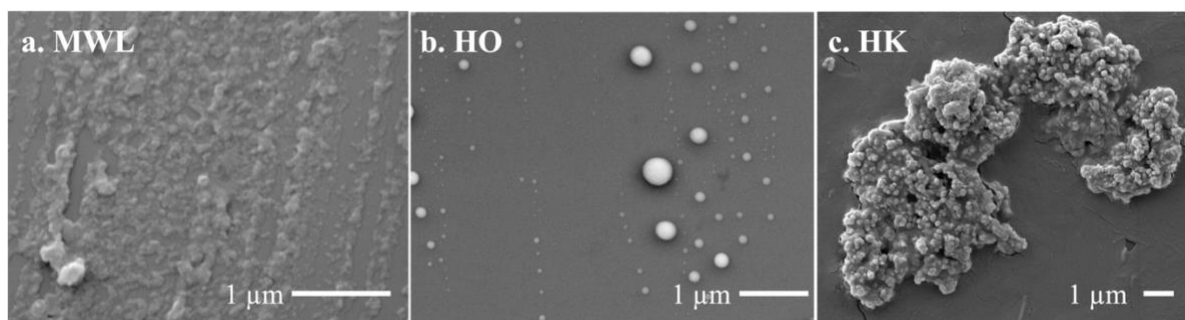
Figure 4.12. SEM images of MWL, HO, and HK in basic conditions. Day 7 for MWL, day 14 for HO and HK.

Milled Wood extraction of the herbaceous biomass produces a small lignin yield, recovering only about 4-6% of the material's lignin content. In addition, MWL has low purity as revealed by its mass spectra showing a peak at m/z of 179.055, which corresponds to glucose (**Figure 4.13**). Despite the recalcitrant nature of lignin as a carbon source and the antimicrobial properties of LNPs [233, 234], MWL LNPs appeared to support microbial growth due to coextracted impurities that may be as much as 15% carbohydrates [220]. Although Milled Wood extraction is mild and preserves the highest amount of β-O-4 linkages, the method gives low yields
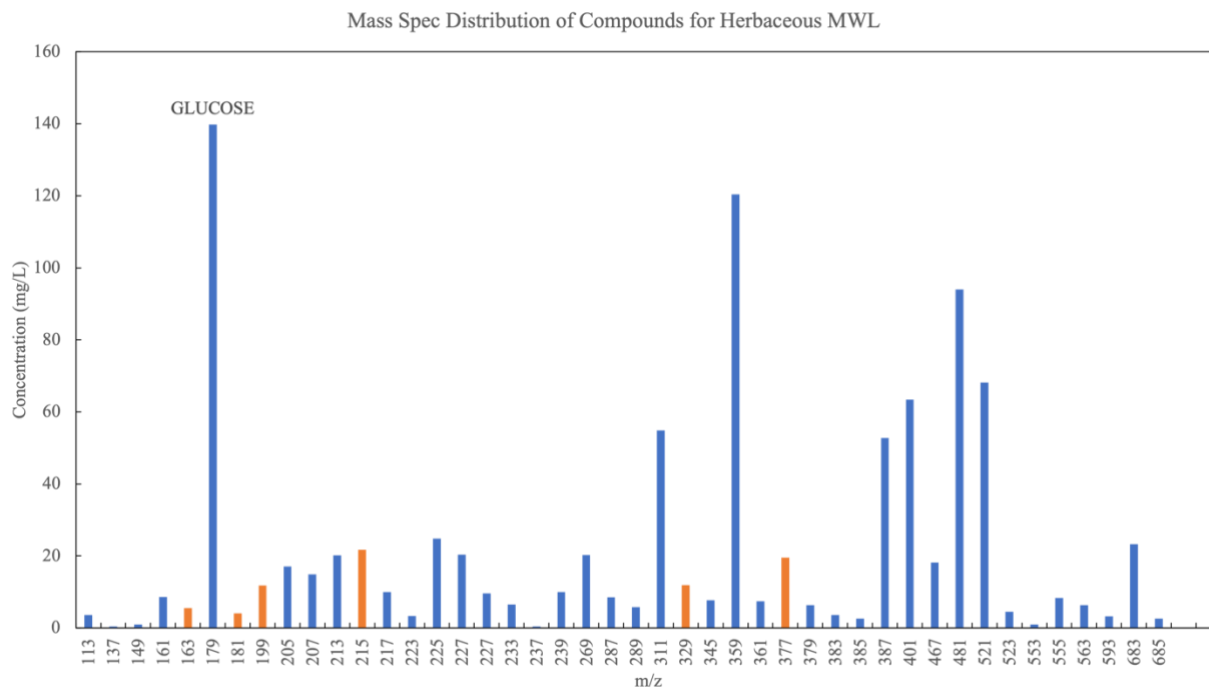
Figure 4.13 The distribution of compounds from solubilized MWL. The orange indicate compounds that are aromatic.

of pure lignin, phenolics, flavonoids and LNPs - and is not a viable route to process lignin in our

biorefinery.

4.4 Discussion

Lignin structure is determined by its source, and this structure is further modified by the method of extraction. Neither of these factors, however, has been rigorously interrogated relative to the type and quantity of products created by a particular depolymerization process. Our aim is to compare how, under the conditions of our biorefinery (MEC catholyte - 220 mM phosphate, pH 10.8), the product composition, yields and properties vary for representative models from each of the three types of lignin source and three examples (harsh, medium, mild) of extraction. We also probe which factors can predict product yields and properties.

The three sources of lignin, softwood, hardwood, and herbaceous, differ relative to lignin content, the percentage of β-O-4 linkages, and the S/G ratio. Extraction modifies the β-O-4 content. The Milled Wood isolation process is a mild extraction technique with poor yields and low purity but it preserves most of the β-O-4 linkages. Organosolv is a medium extraction process that degrades the lignin to a limited extent but still preserves many of the β-O-4 linkages. Organosolv is typically used in the bioethanol industry. Klason is a harsh extraction method, akin to Kraft (which is industrially used in the paper and pulp industry alongside lignosulfonate) without introducing sulfur. Klason cleaves most of the β-O-4 linkages, but is efficient in extracting the highest quantity and purity of lignin from biomass. We found that the herbaceous biomass was the only source that could be extracted by all three methods and that the Klason extraction was the only method among those evaluated that worked well on all three sources. We then determined and compared the products and properties of the five biorefined extracted lignin samples, specifically the amount of soluble lignin, bulk phenolic/flavonoid yields, and the antioxidant capacity, as well as the concentration of LNPs and their shape, size and polydispersity.

Table 4.5 presents salient characteristics of the raw biomass. The lignin content indicates the maximum amount of lignin in the biomass that can be extracted. Based on this, softwood lignin with up to 35% lignin content would seem a promising target for depolymerization. Yet, its β-O-4 bond content, which is a good indicator of the ease of depolymerization with preservation of the aromatic structure, is less than half that of the other sources, making extracted softwood lignin a poor candidate for biorefining high value aromatic products. Rather, herbaceous lignin has the greatest β-O-4 content, roughly twice that of softwood and about 20% more than that of hardwood lignin. Taking into account both the total lignin (8% more than herbaceous) and β-O-4 content

(30% more than softwood), we might also expect hardwood lignin to be a favorable choice for depolymerization.

The ease of depolymerization and product yields, however, also depend on the monolignol composition. When we compare monolignol proportions, softwood contains primarily the G monolignol, herbaceous has roughly two G monolignol for every S monolignols, with a small amount of H monolignol as well. In contract, hardwood contains roughly two S monolignols for every G monolignol. It is significant that herbaceous lignin is the only source that contains a detectable amount of the H monolignol which is likely responsible for some of the discrete aromatic products in the depolymerized corn stover that we identified in our previous work, including the monomer p-coumaric acid (making up to 0.5% of the depolymerized lignin mixture) and the flavonoid tricin (making up to 2.3% of the depolymerized lignin mixture) [18]. These compounds were not detected by LCMS in depolymerized hardwood and softwood samples from our biorefinery.

The S/G ratio influences the branching and cross linking density of the lignin structure. High methoxy content, such as found in hardwoods with high S/G ratios, shows reduced tendency to form branched or crossed linked structures, whereas the opposite is true of softwoods with small S/G ratios and more highly branched and cross linked structures with fewer ether linkages [226]. A high S/G ratio has been hypothesized to increase the β-O-4 content in lignin because the S monolignol contains a methoxy in the 5 position of the aromatic ring, which prevents the formation of 5-5 and β-5 carbon-carbon bonds [223] In contrast, G units promote more carbon-carbon bonds, which are much less labile, and fewer ether linages, making softwood lignin a poor candidate for depolymerization. Recent work, however, challenges the notion that the S/G is the major determinant of monomer yield in lignin depolymerization [25].

The structural feature that most informs lignin solubilization and subsequent product formation under our biorefinery conditions is the β-O-4 content. In **Figure** 4.14, a linear relationship is illustrated between the β-O-4 content and various product characteristics. A strongly positive correlation exists between increasing β-O-4 content and increasing soluble lignin, phenolic content, flavonoid content, and LNP concentration. An inverse relationship is observed between β-O-4 content and LNP size and polydispersity which decrease with increasing percentage of β-O-4 linkages.
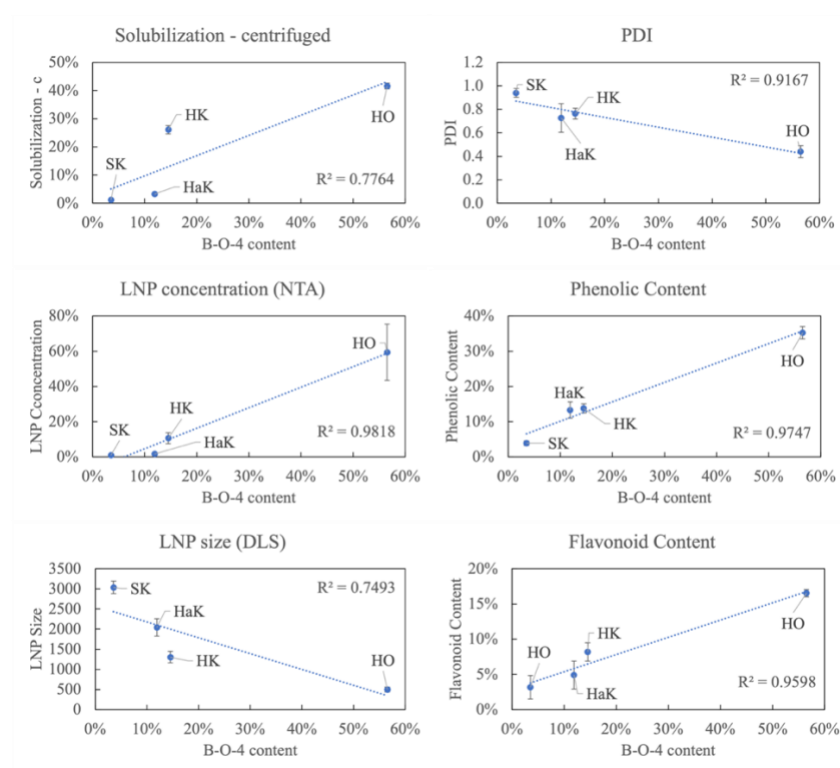
Figure 4.14 Relationships between β-O-4 content and various products in neutral conditions for each lignin source. Each data point is labeled with the corresponding lignin it represents. Table 4.7 and Table 4.8 show the R² for all factors and products.

Table 4.7 The R^2 values between various parameters and products in basic conditions. The higher the value and the darker the shade indicate stronger relationships.

	B-O-4	S/G	Sol.	C-Sol.	NTA conc	DLS size	PDI	phenolics	flavonoids	zeta	IC50
S/G	0.00										
Sol.	0.59	0.13									
C-Sol.	0.82	0.00	0.80								
NTA conc	0.34	0.22	0.82	0.50							
DLS size	0.74	0.03	0.30	0.51	0.11						
PDI	0.89	0.01	0.68	0.75	0.52	0.22					
phenolics	0.83	0.15	0.72	0.68	0.53	0.27	0.62				
flavonoids	0.46	0.27	0.31	0.16	0.27	0.01	0.25	0.61			
zeta	0.60	0.43	0.00	0.09	0.00	0.02	0.18	0.05	0.00		
IC50	0.38	0.31	0.67	0.56	0.49	0.26	0.37	0.53	0.18	0.00	

Table 4.8 The R^2 values between various parameters and products in neutral conditions. The higher the value and the darker the shade indicate stronger relationships.

	B-O-4	S/G	Sol.	C-Sol.	NTA conc	DLS size	PDI	phenolics	flavonoids	zeta	IC50
S/G	0.00										
Sol.	0.65	0.03									
C-Sol.	0.78	0.04	0.88								
NTA conc	0.98	0.03	0.44	0.59							
DLS size	0.75	0.02	0.78	0.81	0.47						
PDI	0.92	0.06	0.45	0.45	0.49	0.59					
phenolics	0.97	0.01	0.62	0.74	0.58	0.75	0.69				
flavonoids	0.96	0.01	0.62	0.70	0.45	0.64	0.71	0.78			
zeta	0.57	0.46	0.07	0.12	0.28	0.05	0.00	0.06	0.00		
IC50	0.59	0.03	0.75	0.77	0.35	0.87	0.55	0.66	0.69	0.01	

Softwood, which has the highest lignin content, but the lowest β-O-4 bonding, is difficult to extract except with the harsh Klason method that further reduces the β-O-4 content to under 4% making it resistant to solubilization/depolymerization under the conditions of our biorefinery. Since the extracted softwood lignin (SK) shows limited solubilization, its product yields are also limited. NMR results confirm that the softwood lignin is composed of mostly the G monolignol linked with few β-O-4 bonds (**Figure** 4.15). The DRIFT data in **Figure** 4.4 reveal that the relative intensity of oxygen containing functional groups in SK is typically less than that of the other sources extracted in the same way. These observations also explain why SK does not form nanoparticles. There are many specific interactions responsible for the mechanisms of LNP formation including, 1) hydrophilic-lipophilic interactions, 2) π-π interactions, 3) hydrogen bonding, 4) chain entanglement, 5) van der Waals forces, and 6) hydrophobic interactions [121]. The lower oxygen content in softwood hinders dissolution in a polar solvent and explains the low solubility in **Figure** 4.6**a**. Low dissolution, then, inhibits LNP formation since this is the initial step in the mechanism. In addition, SK does not form LNPs due to the lack of the syringyl monolignol and relatedly, lower methoxy content. Since the non-covalent π-π interactions between aromatic rings follow the order of Syringyl (S) > Guiacyl (G) > p-Hydroxyphenyl (H) [235], the lower methoxy content of SK diminishes π-π interactions preventing LNP formation.
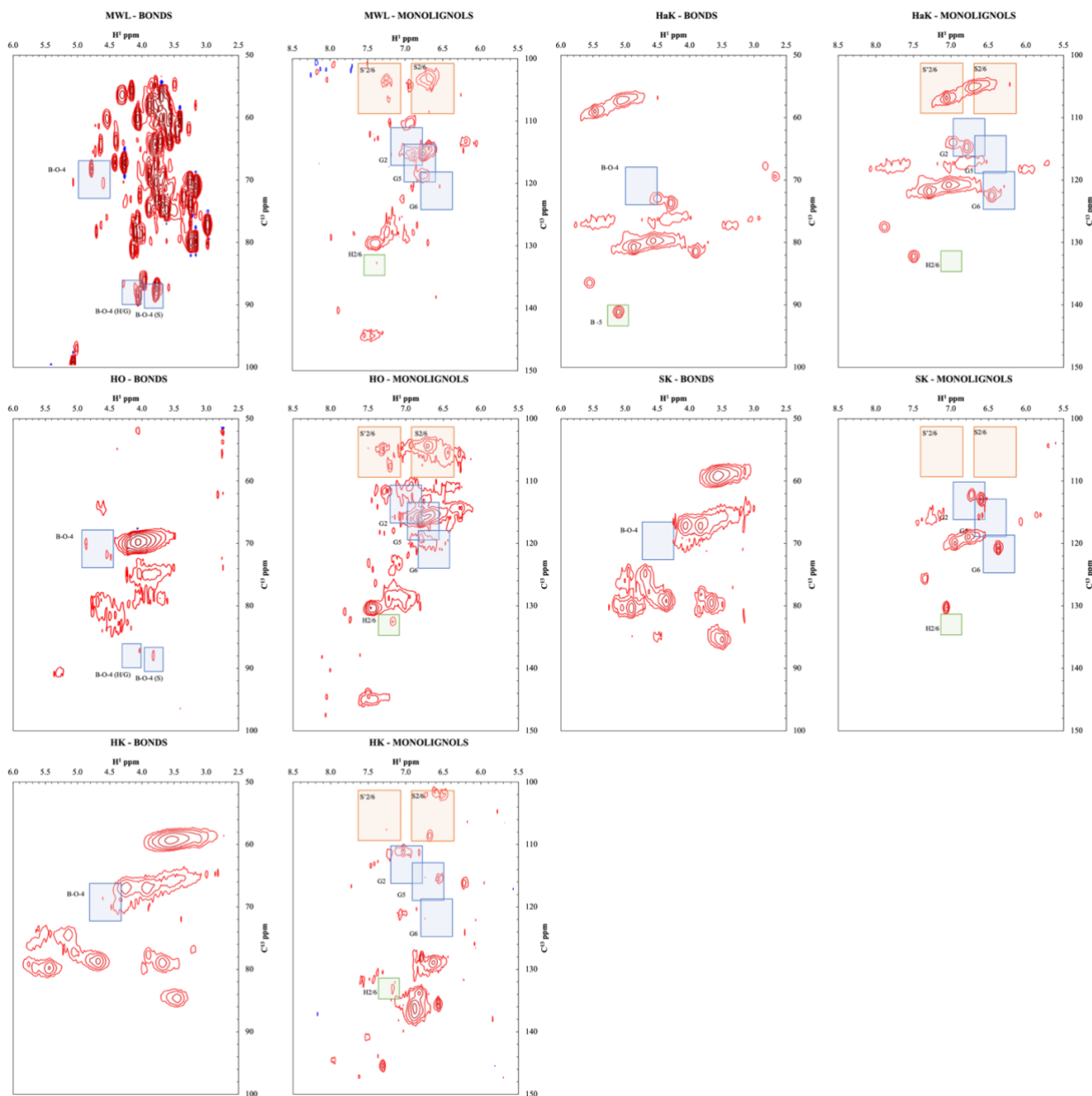
Figure 4.15 NMR spectra for aromatic and aliphatic regions for all lignin extractions.

As noted previously, based on the lignin content and amount of β-O-4 linkages in the native biomass, hardwood appeared to be a promising lignin source for biorefining, except that it can only be extracted by the Klason (harsh) technique, which then removes most of the ether linkages. Under our biorefinery conditions, HaK lignin produces only half the soluble lignin compared to

Klason extracted herbaceous lignin (HK). Yet, the soluble HaK lignin has significantly greater phenolic and flavonoid content, and hence a higher antioxidant capacity (lower IC50) than HK, suggesting that differences between the S/G ratio of hardwood and herbaceous sources may play a role. We also see that the depolymerization of hardwood lignin in our biorefinery produces the most LNPs compared to the other Klason extracted material. These LNPs are spherical and dispersed but larger and fewer (failing to close mass balance) than the highly aggregated LNPs of the Organosolv extracted herbaceous lignin. HaK lignin can be biorefined to soluble products with antioxidant properties but in lower amounts compared with Organosolv herbaceous lignin. Thus, the biorefinery conditions do not fully solubilize HaK lignin resulting in limited product yields.

Under the conditions of our biorefinery, the Organosolv extraction of herbaceous lignin produces the maximum amount of soluble lignin (< 90%) and the highest aromatic product yield (30-40% phenolics/flavonoids) having the greatest antioxidant potential (close to the commercial standard), as well as the most LNPs – accounting for all of the soluble mass. In general, the herbaceous source can be extracted by all the methods that we studied to provide higher soluble lignin than other sources. We observe the effects of extraction and processing most vividly with respect to the LNPs, which are small, spherical, and produced at the highest concentration with the Organosolv herbaceous lignin. As discussed, MWL does not form LNPs. Although the Klason extraction has a strong effect on the native structure of lignin, it preserves lignin aromaticity (see peak 3 in **Figure** 4.4) and gives the highest quantities of pure lignin, albeit with large losses in the β-O-4 content, which is critical to the ease of depolymerization. Furthermore, the Klason extraction of herbaceous lignin does not form small and well dispersed LNPs.

Figure 4.16 illustrates the relationship between flavonoid content and IC50 (antioxidant capaicy) across all of the sources and extractions. The phenolics, flavonoids and LNPs produced

in our biorefinery have the valuable property of serving as antioxidants. Antioxidants combat oxidative stress in cells and tissues which occurs when there is an accumulation of reactive oxygen species (ROS) and can be the cause of inflammation, aging, and chronic diseases such as cancer, cardiovascular disease, neurological disease, respiratory disease, arthritis, and kidney disease [141]. Antioxidants play an important role in maintaining human health. Although synthetic antioxidants have been used for decades in a variety of applications, there has been a push for more natural sources of antioxidants due to consumer demand for all natural ingredient, as well as some safety concerns about synthetic antioxidants [229]. We show that although there is a relationship between flavonoids and antioxidant capacity in **Figure** 4.16, the relationship becomes stronger when aggregated by source, indicating that the amount of bulk flavonoids produced in our depolymerization method is not the only factor responsible in antioxidant capacity. Other factors may also contribute to antioxidant capacity, we see in the Spearman correlation matrix (**Figure** 4.17) that soluble lignin, phenolic content, LNP concentration have a positive effect on antioxidant capacity and that LNP size and PDI have a negative effect on antioxidant capacity. These relationships can also be seen in a PCA (**Figure** 4.18), with solubilization, phenolic content, flavonoid content, LNP concentration, and antioxidant capacity pointing in the positive PC1 direction and LNP size and PDI pointing in the negative PC1 direction.

128
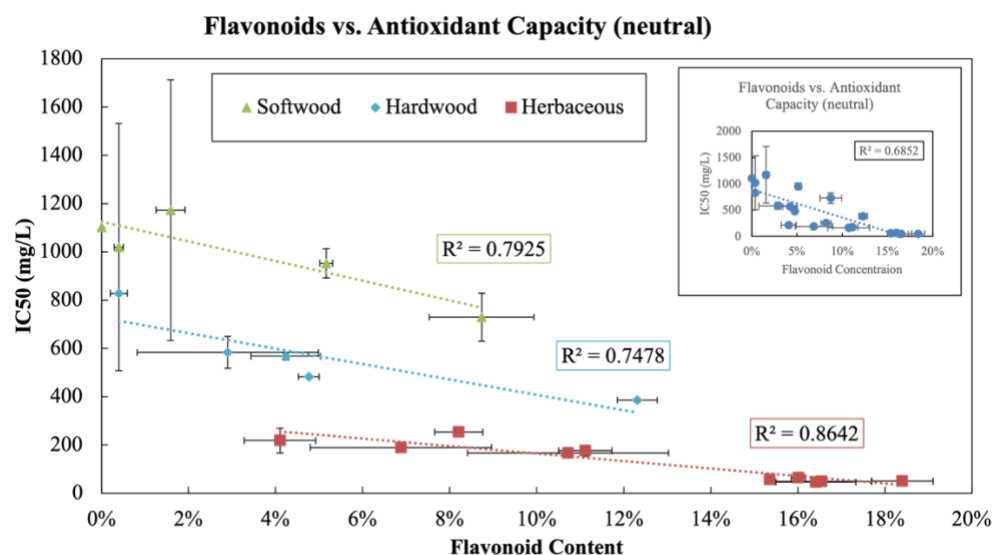
Figure 4.16. The relationship between flavonoid content and antioxidant capacity in neutral experiments. The top right inset shows the overall linear relationship. The main graph has the linear relationship segmented by the source of lignin.
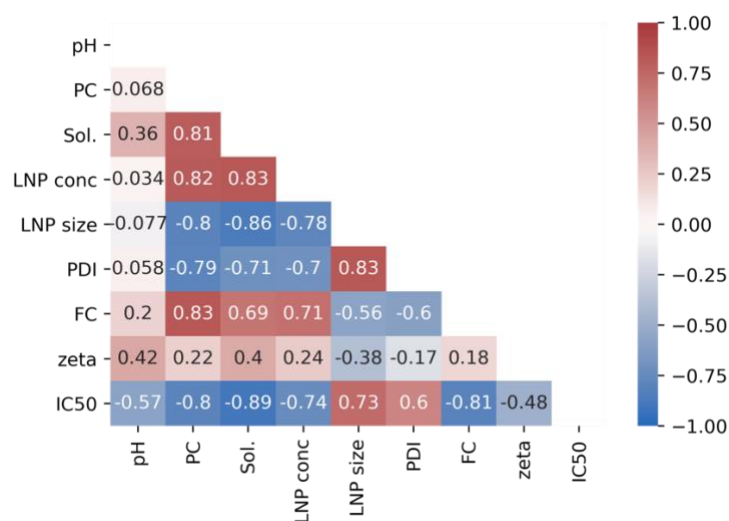
Figure 4.17 The Spearman correlation between various parameters. The higher the value (and darker the shade), the stronger the correlation. Red indicates a positive relationship and blue indicates a negative relationship. Note that IC50 is inverse to antioxidant capacity. Therefore a blue value with IC50 indicates a positive correlation with antioxidant capacity.
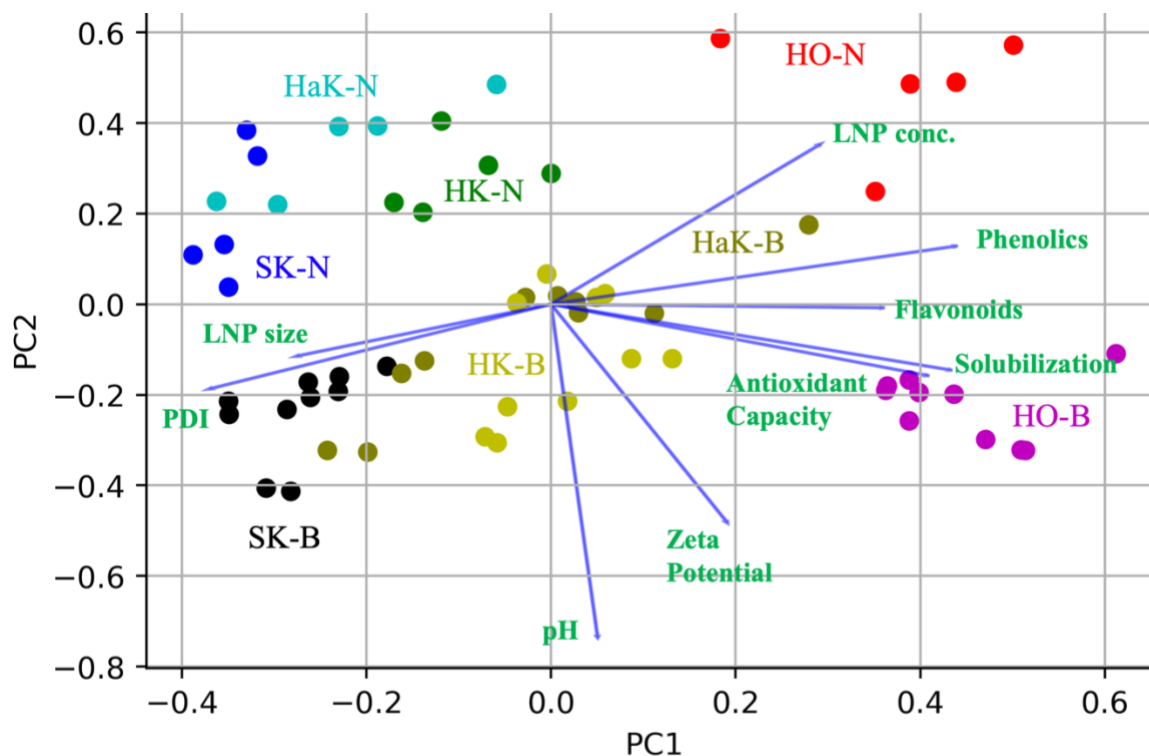
Figure 4.18 PCA of all depolymerization experiment of HO, HK, SK, and HaK in neutral and basic conditions. The arrows represent various product characteristics and the dots represent individual experiments.

4.5 Conclusion

The goal of this research was to investigate if an MEC-mediated biorefinery is equally effective with different lignin streams and to determine what factors impact product yields. The biorefinery approach to depolymerizing lignin was originally employed on herbaceous Organosolv lignin, but was found to work on both different sources and extractions to a varying degrees of success. Lignin source has a large effect on the efficacy of extraction method. The Klason extraction was the only extraction to successfully extract lignin from all three sources, although it severely modifies the lignin structure by eliminating β-O-4 linkages, which ultimately diminishing lignin solubility and depolymerization.

We found that under the caustic and high salt conditions of our biorefinery, herbaceous lignin extracted via the Organosolv method produces the highest amount of soluble lignin, phenolic/flavonoid content, and antioxidant capacity as well as a greater LNP concentration, with smaller and less polydispersed particles. The Organosolv extraction preserved a high amount of the β-O-4 linkages which is found to be strongly correlated with many of these products and properties.

Klason extractions of herbaceous and hardwood biomass solubilize lignin to a lesser extent (60% and 35%, respectively) than Organosolv, but still produce good yields of phenolics, flavonoids, and LNPs with a moderate antioxidant capacity. Klason extracted softwood, however, is not solubilize/depolymerized in this biorefinery to produce products (phenolics, flavonoids, LNPs). This is likely due to the lack of S monolignol subunits and the paucity of β-O-4 linkages in this type of lignin. Only the herbaceous lignin could be extracted with the mild Milled Wood extraction to produce very small lignin quantities of low purity. Despite the fact that the β-O-4 linkages were highly persevered by this method, limitations in the amount of pure lignin extracted prevented the biorefining of high-value products.

In conclusion, at the present time our biorefinery is best suited to process the type of lignin recovered in the cellulosic ethanol industry from herbaceous (corn stover) biomass and extracted with the Organosolv method. This industry produces the second largest industrial lignin stream [30]. This biorefinery may also be well suited at smaller, distributed scales, targeting herbaceous yard waste or perennial grasses.

Chapter 5 : The effect of salt type, concentration, and pH on lignin depolymerization products and their properties

5.1. Introduction

Lignin, despite being the only source of renewable aromatic carbon, is traditionally burned for low-value energy. There has long been research on transforming lignin into higher value products, still, the products often remove the aromaticity of lignin, produce low yielding aromatic products, and use harsh conditions (high temperature, high pressure, high/low pH, expensive catalysts etc.). We previously found that we can depolymerize lignin with the renewable caustic effluent of a MEC (a byproduct from wastewater treatment) preserving aromaticity in high value products. We have established that lignin extracted via the Organosolv process from a herbaceous source (corn stover) is solubilized to a high extent (80% within an hour, 100% within a week) under the conditions of our biorefinery, producing phenolics and flavonoids that can be identified as discrete compounds and that can be incorporated into lignin nanoparticles (LNPs). The reason for such high solubilization is the caustic MEC effluent – specifically a combination of the high pH (10.8) and high salt concentration (200 mM). We had previously seen, in initial experiments, that pH alone is not responsible for the high rate of depolymerization. At pH 11, sodium hydroxide alone, depolymerized lignin to only 20%, whereas a phosphate buffer at pH 11 depolymerized lignin over 80% in the span of 60 minutes. Even when the pH of sodium hydroxide is continuously adjusted, the depolymerization is only improved marginally. Therefore, in this section, we investigate salt and pH effects on product yields to determine if we can tune the products by

varying the type of salt, the concentration of the salt, and the pH. We measure the products: total soluble lignin, total phenolic content, total flavonoid content, and LNP concentration, as well as the properties: antioxidant capacity, LNP size, LNP polydispersity index, and LNP zeta potential.

5.2 Materials and Methods

5.2.1 Materials

Lignin was kindly donated by Archer Daniels Midland (ADM), Decatur IL. ADM extracts lignin from corn stover by the acetosolv (Organosolv using acetic acid) process. We used the following chemicals for depolymerization – sodium phosphate dibasic (Fischer), potassium phosphate monobasic (USP analytical test, JT Baker), sodium hydroxide (certified ACS, Fischer), phosphoric acid, sodium chloride (certified ACS, Fischer), sodium nitrate (certified ACS, Fischer), sodium carbonate (certified ACS, BDH), sodium bicarbonate (certified ACS, BDH). For flavonoid content we used: aluminum chloride hexahydrate (Alfa Aesar), sodium nitrite (98%, Alfa Aesar), Methanol (HPLC grade, Fisher). For phenolic content we used: Folin-Ciolcalteu reagent (Sigma Aldrich), sodium carbonate (ACS, VWR), gallic acid (97.5%, Sigma Aldrich). For antioxidant assay we used: rutin (>94%, TCI), Trolox (abcam), ABTS (TCI), potassium persulfate (certified ACS, Fischer). hexadecyltrimethylammonium bromide (CTAB) (>98%, Sigma Aldrich) was used in microscopy.

5.2.2 Lignin Solubilization

Lignin depolymerization was carried out as described in Obrzut et al. [18]. Synthetic MEC catholyte (depolymerization media) was used for the experiments and prepared with different salts to a total molarity of 227 mM. Four different salts were used for the depolymerization media:

sodium chloride (13 g·L^{-1}), sodium nitrate (19 g·L^{-1}), sodium carbonate/sodium bicarbonate (21 g·L^{-1} Na$_2$CO$_3$ and 2 g·L^{-1} NaHCO$_3$), and sodium phosphate dibasic/potassium phosphate monobasic (32 g·L^{-1} Na$_2$HPO$_4$ and 0.2 g·L^{-1} KH$_2$PO$_4$·H$_2$O). The four depolymerization medias were adjusted to pH 10.8 for initial depolymerization. Chloride, nitrate, and phosphate were adjusted with sodium hydroxide to increase the pH, carbonate was adjusted with phosphoric acid to decrease the pH. The amount of sodium hydroxide and phosphoric acid were negligible to the ionic strength.

Lignin depolymerization was conducted in a lab bench scale reactor (beaker) over 60 minutes. Lignin and depolymerization media were combined for a total concentration of 1 g/L. Over the course of 60 minutes the pH was monitored and adjusted to +/- 0.2 of pH 10.8 with sodium hydroxide, this amounted to 50-100 μL of sodium hydroxide for the chloride and nitrate based media. After the 60 minutes, basic experiments (b) were left as is, neutral samples (n) were neutralized with phosphoric acid to pH 7, and acidic samples (a) were acidified to pH 3.8.

The experiments were conducted at room temperature and observed for a total of one week. Measurements for solubilization, phenolic content, flavonoid content, antioxidant capacity, LNP concentration, size, PDI, and zeta potential were taken at day 0 and at day 7. The LNPs were observed under the SEM at day 7. **Table** 5.1 summarizes the type of salt used, concentration, pH and ionic strength.

Table 5.1. Summary of the experiments that were performed in this section. This includes the naming convention (label) which subsequent figures use, the salt type, the day of measurement, the concentration, the pH, and the ionic strength.

Label	Salt	Day	Conc (M)	pH	Ionic Strength (M)
Cl-B	Sodium Chloride	0	0.220	10.8	0.220
Cl-B-7	Sodium Chloride	7	0.220	10.8	0.220
Cl-N	Sodium Chloride	0	0.220	7	0.220
Cl-N-7	Sodium Chloride	7	0.220	7	0.220
NO3-B	Sodium Nitrate	0	0.220	10.8	0.220
NO3-B-7	Sodium Nitrate	7	0.220	10.8	0.220
NO3-N	Sodium Nitrate	0	0.220	7	0.220
NO3-N-7	Sodium Nitrate	7	0.220	7	0.220
NO3-A	Sodium Nitrate	0	0.220	3.8	0.220
NO3-A-7	Sodium Nitrate	7	0.220	3.8	0.220
CO3-B	Sodium Carbonate/ Sodium Bicarbonate	0	0.220	10.8	0.529
CO3-B-7	Sodium Carbonate/ Sodium Bicarbonate	7	0.220	10.8	0.529
CO3-N	Sodium Carbonate/ Sodium Bicarbonate	0	0.220	7	0.185
CO3-N-7	Sodium Carbonate/ Sodium Bicarbonate	7	0.220	7	0.185
PO4-B	Potassium Phosphate Monobasic/ Sodium Phosphate Dibasic	0	0.220	10.8	0.694
PO4-B-7	Potassium Phosphate Monobasic/ Sodium Phosphate Dibasic	7	0.220	10.8	0.694
PO4-N	Potassium Phosphate Monobasic/ Sodium Phosphate Dibasic	0	0.220	7	0.526
PO4-N-7	Potassium Phosphate Monobasic/ Sodium Phosphate Dibasic	7	0.220	7	0.526
PO4-A	Potassium Phosphate Monobasic/ Sodium Phosphate Dibasic	0	0.220	3.8	0.222
PO4-A-7	Potassium Phosphate Monobasic/ Sodium Phosphate Dibasic	7	0.220	3.8	0.222
PO4-B-110	Potassium Phosphate Monobasic/ Sodium Phosphate Dibasic	0	0.110	10.8	0.347
PO4-B-110-7	Potassium Phosphate Monobasic/ Sodium Phosphate Dibasic	7	0.110	10.8	0.347
PO4-N-110	Potassium Phosphate Monobasic/ Sodium Phosphate Dibasic	0	0.110	7	0.263
PO4-N-110-7	Potassium Phosphate Monobasic/ Sodium Phosphate Dibasic	7	0.110	7	0.263
PO4-B-440	Potassium Phosphate Monobasic/ Sodium Phosphate Dibasic	0	0.440	10.8	1.388
PO4-B-440-7	Potassium Phosphate Monobasic/ Sodium Phosphate Dibasic	7	0.440	10.8	1.388
PO4-N-440	Potassium Phosphate Monobasic/ Sodium Phosphate Dibasic	0	0.440	7	1.052
PO4-N-440-7	Potassium Phosphate Monobasic/ Sodium Phosphate Dibasic	7	0.440	7	1.052

5.2.3 Measurement of bulk properties – UV vis

The following properties were measured with UV vis spectroscopy (Eppendorf BioSpectrometer): soluble lignin, total phenolic content, total flavonoid content, antioxidant capacity. Total phenolic content and total flavonoid content were also measured after a series of filtrations for select experiments.

Solubilization or soluble lignin was determined through a calibration curve of lignin dissolved completely in pH 13 NaOH solution. The max peak occurred at 280 nm. Solubilization was measured on centrifuged samples in order to remove any residual solids or large LNPs that induce scattering in the UV readings. The total amount of phenolics was determined with the colorimetric Folin-Ciolcalteu method [81]. The Folin-Ciolcalteu method combines 100 μL of solubilized lignin with 2 mL of a 2% sodium carbonate solution. The mixture was incubated at room temperature for 5 minutes and then 100 μL of Folin-Ciolcalteu reagent was added and the mixture was incubated further for 30 minutes. The absorbance was measured at 750 nm. A calibration was performed with a solution of gallic acid (3, 4,5-trihydroxybenzoic acid) every time the experiment was performed [180]. The total amount of flavonoids was determined via the method by Zhishen et al [82]. For this method, 300 μL of solubilized lignin was combined with 3.4 mL of a 30% methanol solution, 150 μL of a 0.5 mmol L^{-1} sodium nitrate solution and 150 μL of a 0.3 mmol L^{-1} aluminum chloride hexahydrate solution at room temperature. 1 mL of 1 mol L^{-1} sodium hydroxide was added after 5 minutes and the absorbance was immediately measured at 510 nm. The calibration curve was made using the flavonoid rutin, (3′,4′,5,7-Tetrahydroxy-3-[α-L-rhamnopyranosyl-(1→6)-β-D-glucopyranosyloxy]flavone). A 100 mg/L sample of rutin was made with each set of experiments to test the accuracy of the calibration curve.

The antioxidant capacity was also determined by measuring the UV absorbance. We followed a modified version of the ABTS method first described by Cano et al. [221]. The $ABTS^+$ radical solution was prepared from 10 mL of 7mM $ABTS^+$ [2,2'-Azino-bis(3-ethyl-benzothiazoline-6-sulfonic acid)] solution in water and 10 mL of 2 mM potassium persulfate solution in water. The mixture was incubated in the dark at room temperature overnight. The $ABTS^+$ solution was diluted with water to an absorbance of 0.70 +/- 0.1 at 734 nm. Then 1 mL of

different concentrations of lignin (0, 2, 6, 10, 14, 16, 18, 20, 40, 60, 80, 100, 140, 160, 200, 300, 400, 600, 800 mg/L) were added to 2.0 mL of ABTS$^+$ diluted solution. The mixture was incubated in the dark for 6 minutes and were measured at 734 nm. The scavenging was calculated with the following equation:

$$Scavenging\ effect\ (\%) = \frac{A_c - A_t - CF}{A_c - CF}\ x\ 100$$

where A_C is the absorbance of the ABTS$^+$ diluted solution without any antioxidants added, A_t is the absorbance of the test, and CF is the correction factor due to pH. The correction factor for neutral samples of all salts, and basic samples of nitrate and chloride based depolymerization media is 0, the correction factor for pH 10.8 for phosphate and carbonate based depolymerization media varies as a function of concentration, these values are shown in **Table** 5.2 below. The concentration required to inhibit the ABST$^+$ by 50% (IC50) was determined by linear regression analysis. Trolox (6-hydroxy-2,5,7,8-tetramethylchroman-2-carboxylic acid) was used as a standard to verify the method. The IC50 of Trolox was found to be 21.5 mg/L, consistent with literature [222].

Table 5.2. The correction values for the absorbances due to the effect of phosphate and carbonate at basic pH.

Phosphate (Basic)		Carbonate (Basic)	
Concentration	Absorbance Correction	Concentration	Absorbance Correction
Between 0-20 mg/L	0	2 mg/L	0.041
40 mg/L	0.054	6 mg/L	0.076
60 mg/L	0.115	10 mg/L	0.137
80 mg/L	0.141	14 mg/L	0.186
100 mg/L	0.223	16 mg/L	0.204
140 mg/L	0.278	18 mg/L	0.225

160 mg/L	0.31	20 mg/L	0.227
Over 200 mg/L	0.405	40 mg/L	0.326
		Over 60 mg/L	0.441

5.2.4 Measurement of nanoparticles

LNP concentration, size, PDI, and zeta potential were determined with Nanoparticle Tracking Analysis (NTA) and Zetasizer. The NTA (Malvern Panalytical NanoSight NS300) was used according to Obrzut et al. to estimate both the concentration and size distribution [18]. The lignin solutions were diluted 50 times in water to be measured via NTA. The zetasizer (Malvern Panalytical Zetasizer Nano ZS) also has dynamic light scattering (DLS) capabilities to measure size and polydispersity index. The lignin solutions were diluted 10x for size and PDI and 50x for zeta potential measurements. Then, 1 mL of sample was placed in a DTS1070 disposable zeta potential cuvette or a plastic cuvette for DLS. Three measurements were taken for each sample with up to 100 zeta runs per sample. For these runs the refractive index of lignin was set at 1.61 [186].

5.3 Results

5.3.1 Effect of salt type

We evaluated the effects of four different salts inspired by their positions on the Hofmeister series. The Hofmeister series ranks salts based on their interactions with proteins, specifically salts to the right of the scale disrupt protein folding (chaotropes), causing proteins to denature and dissolve, whereas salts on the left of the scale stabilize proteins (kosmotropes). Due to potential similarities between proteins and lignins (large biopolymers with hydrophilic and hydrophobic

regions), we hypothesized that salts may produce LNPs or phenolics/flavonoids based on their position on the Hofmeister scale. We chose either sodium or potassium salts of phosphate (kosmotrope), carbonate (kosmotrope), nitrate (chaotrope), and chloride (middle of the scale) . We predict that LNPs will form in the order of the kosmotropes (carbonate > phosphate > chloride > nitrate) and that phenolics/flavonoids will form based on the order of the chaotropes (nitrate > chloride> phosphate > carbonate). **Figure** 5.1 shows the solubilization, phenolic content, flavonoid content, and antioxidant capacity of the four salts, in basic and neutral conditions, at days t=0 d and t= 7 d.
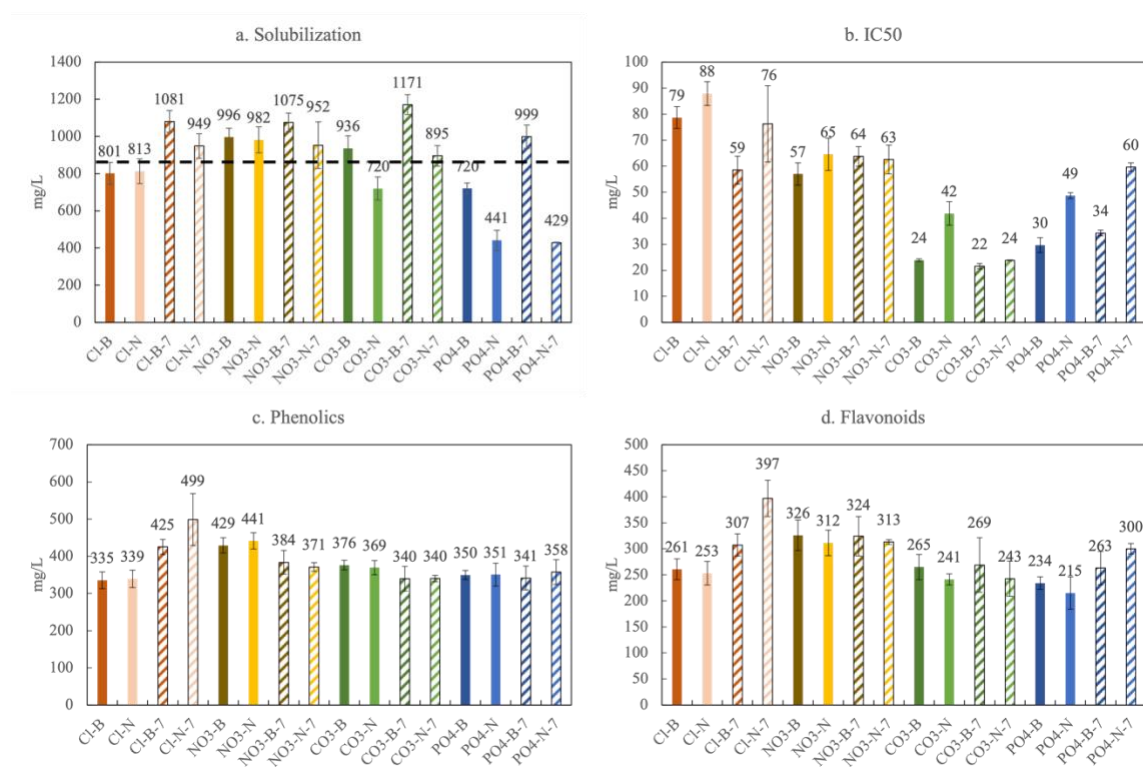
Figure 5.1 The a. solubilization, b. IC50, c. phenolic content, and d. flavonoid content for all salt types at neutral and basic pH at day 0 and 7.

Before discussing differences between salts, we provide a quick summary on the effect of pH and time within salt type. In order to determine whether the observed trends were significant, ANOVA was conducted. **Figure 5.2** shows the significant differences across time and **Figure 5.3** shows the significant differences across pH. For chloride (orange), we do not see a significant pH effect with solubilization, phenolic content, flavonoid content, or antioxidant capacity (except IC50 at $t = 0$ d). We do, however, see a slight time effect. At $t = 7$ d, the solubilization and flavonoid content increase significantly ($p < 0.05$) for the basic and neutral samples respectively. The antioxidant capacity and the phenolic content do not significantly change. For nitrate (yellow), we observe only negligible pH and time effects. Carbonate (green) and phosphate (blue) samples show similar patterns as a function of pH and time. Soluble lignin concentrations are strongly influenced by pH, with amounts decreasing 20 – 60% at neutral pH. The antioxidant capacity decreases ($\approx$ 2x the IC50) at neutral pH for carbonate samples at $t = 0$ and for both time points for phosphate samples. The IC50 values do not change with pH for carbonate samples at t=7d and these samples show the greatest antioxidant capacity among all the samples. There are not significant changes to phenolics and flavonoids, although these values are more variable, over pH or time.

		Solubilization	Phenolic Content	Flavonoid Content	IC50	LNP Concentration	LNP size	PDI	zeta
Cl⁻	Neutral			< 0.05		< 0.05		< 0.05	
	Basic	< 0.05				< 0.05	< 0.05	< 0.05	
NO₃⁻	Neutral								
	Basic								
CO₃²⁻	Neutral	< 0.05				< 0.05	< 0.05	< 0.05	
	Basic	< 0.05				< 0.05			
PO₄³⁻	Neutral			< 0.05	< 0.05	< 0.05	< 0.05	< 0.05	< 0.05
	Basic	< 0.05				< 0.05			

Figure 5.2. ANOVA for the significant differences across time (t=0d; t=7d). Data is shown for all four salts, in neutral and basic conditions. The green boxes indicate that the difference in product or property value is significant (i.e. p<0.05).

		Solubilization	Phenolic Content	Flavonoid Content	IC50	LNP Concentration	LNP size	PDI	zeta
Cl⁻	t = 0 d				< 0.05				
	t = 7 d								
NO₃⁻	t = 0 d								
	t = 7 d								
CO₃²⁻	t = 0 d	< 0.05			< 0.05	< 0.05	< 0.05	< 0.05	
	t = 7 d					< 0.05			
PO₄³⁻	t = 0 d	< 0.05							< 0.05
	t = 7 d	< 0.05							

Figure 5.3 ANOVA for the significant differences across pH (neutral; basic). Data is shown for all four salts, at t =0d and 7d. The green boxes indicate that the difference in product or property value is significant (i.e. p<0.05).

Across all conditions, high solubilization was achieved, showing an average close to 90% (895 mg/L soluble lignin), as indicated by a black dotted line in **Figure** 5.1. Below average soluble lignin yields occurred with the carbonate (t = 0d; pH 7) and phosphate (t =0d, pH 10.8 & 7; t =7d, pH 7) matrices. **Figure 5.4** summarizes any significant differences between salts. There are no differences in the phenolic content across salt type, pH, or time (average concentration – about 380 mg/L), with the most variability occurring with Cl⁻ (335 mg/L at t=0d, basic pH – minimum; 499 mg/L at t =7d, pH 7 – maximum). Bulk flavonoid yields are more variable, ranging from 215 mg/L (phosphate, t=0d, pH7) to 397 mg/L (Cl⁻, t=7d; pH7). Nitrate and carbonate values were relatively constant, whereas Cl⁻ and phosphate increased over time. For antioxidant capacity, there are significant differences between the buffers and the salts (i.e. $p < 0.05$ for carbonate and chloride, carbonate and nitrate, phosphate and chloride, phosphate and nitrate). In general, the simple salt mixtures displayed lower antioxidant capacity than the buffered salts and carbonate based depolymerization (t=0, basic pH; t=7d, pH 7 & 10.8) showed antioxidant values consistent with the industrial antioxidant Trolox (21 mg/L).

		Solubilization		Phenolic Content		Flavonoid Content		IC50		LNP Conc.		LNP size		PDI		zeta	
		t=0 d	t=7 d	t=0 d	t=7 d	t=0 d	t=7 d	t=0 d	t=7 d	t=0 d	t=7 d	t=0 d	t=7 d	t=0 d	t=7 d	t=0 d	t=7 d
CO_3^{2-}	Basic							<0.05						<0.05			
Cl^-	Neutral						<0.05	<0.05	<0.05			<0.05					
CO_3^{2-}	Basic	<0.05				<0.05		<0.05		<0.05							
NO_3^-	Neutral	<0.05				<0.05		<0.05									
CO_3^{2-}	Basic							<0.05					<0.05	<0.05			
PO_4^{3-}	Neutral	<0.05														<0.05	
Cl^-	Basic	<0.05				<0.05		<0.05						<0.05			
NO_3^-	Neutral	<0.05				<0.05		<0.05									
Cl^-	Basic							<0.05				<0.05					
PO_4^{3-}	Neutral	<0.05						<0.05				<0.05				<0.05	
NO_3^-	Basic	<0.05				<0.05		<0.05	<0.05			<0.05		<0.05			
PO_4^{3-}	Neutral	<0.05				<0.05						<0.05				<0.05	

Figure 5.4 ANOVA for the significant differences across different salts. Data is shown for all four salts, at t = 0 and 7 d, and a neutral and basic pH. The green boxes indicate that the difference in product or property value is significant (i.e. p<0.05).
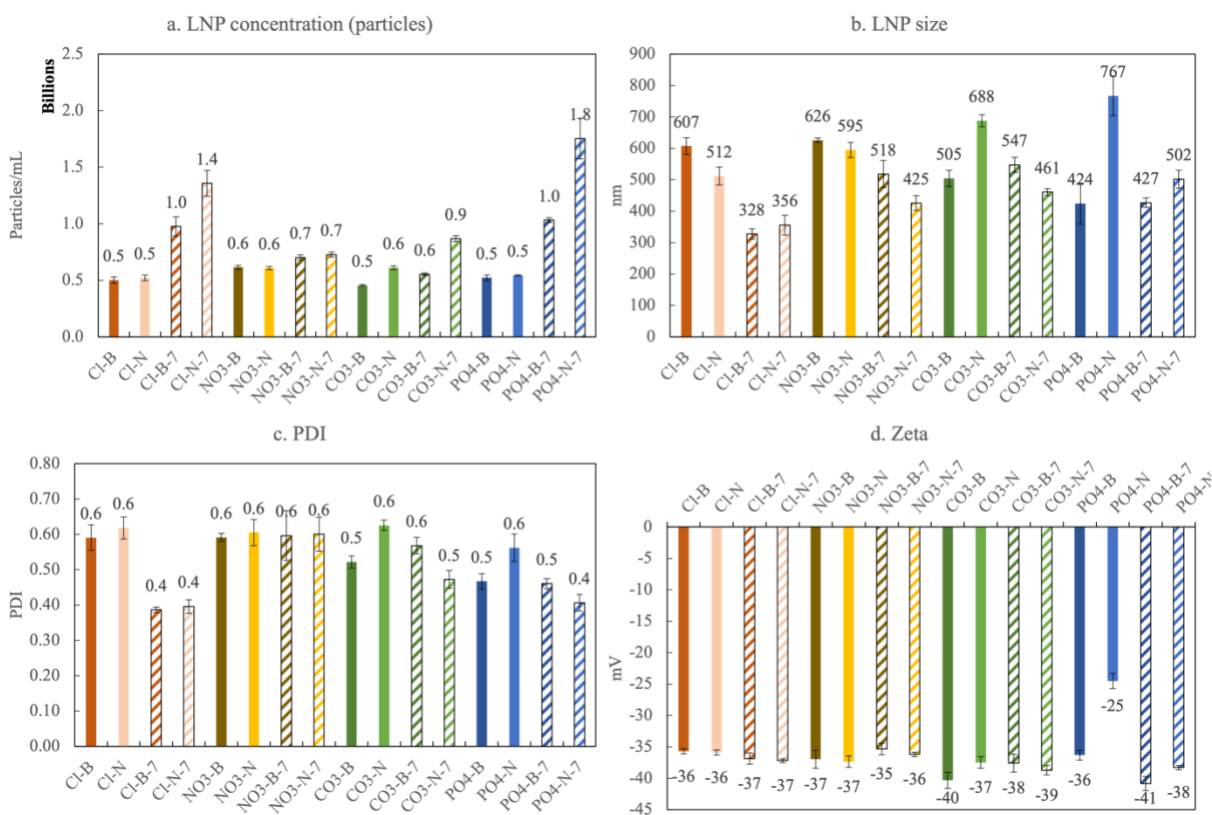
Figure 5.5 The a. LNP concentration, b. LNP size, c. PDI and d. Zeta for different salts at basic and neutral pH at day 0 and 7.

In **Figure** 5.5 the properties of the LNPs are presented. For chloride there is not a significant difference between LNP concentration, size, PDI, or zeta potential when comparing values at basic and neutral pH (**Figure 5.3**). With time, LNP concentration increases (2-3 fold), size decreases by roughly 30 – 45%, PDI also decreases (30%), and the zeta potential remains relatively constant (-36.5mV). LNPs having the smallest size and PDI are formed in a Cl^- matrix at either pH and t=7d. For nitrate conditions, LNP concentration, PDI and zeta potential are all essentially constant across pH and time, but LNP size diminishes slightly with time as pH is reduced from basic to neutral conditions. Carbonate and phosphate mixtures display similar trends with LNPs concentration increasing with time, and at t=7d large increases are observed with decreasing pH. The highest LNP concentration occurs in neutral phosphate mixtures at t = 7d. At t = 0 and pH 7, large LNP sizes are formed in carbonate and phosphate mixtures, but the LNPs grow significantly smaller with time at pH 7 with little change in size at basic pH. Largest LNP sizes are observed for carbonate and phosphate salts at t=0 and pH 7. PDI follows similar trends over a much smaller range in carbonate and phosphate mixtures. Overall, the zeta potentials are relatively similar and indicate stability, with the exception of LNPs in phosphate, pH 7 at t=0 which had lower stability at -25 mV, but became more stable (-38 mV) with time.
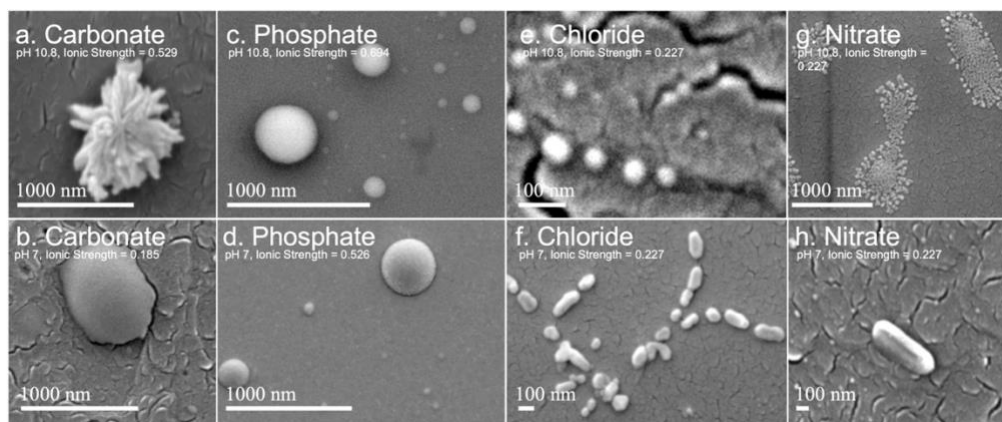
Figure 5.6. SEM images of LNPs formed by the different salts.

The biggest impact of salt type on LNP formation is revealed in the SEM images (Error! Reference source not found.) showing four different LNP shapes (flower-like, spheres, rods, amorphous aggregation of small spheres). The simple salt mixtures (Cl^- & NO_3^-) generate small spheres under basic conditions that become larger and rod-shaped at pH 7. LNP mixtures in phosphate buffer at both pHs but higher ionic strength than the simple salt mixtures, are large spheres. In a carbonate buffered mixture (basic pH, I≈0.5 M), LNPs form a distinct, flower-like structure large in size, which collapse to oblong spheres at pH 7 and I≈0.2 M. For a particular salt type, the shape of the LNP typically depends on pH, except in the case of phosphate, where both in neutral and basic conditions spherical LNPs are observed. In **Table** 5.3 possible hydrophilic/hydrophobic block structures are proposed to explain the LNP shapes observed in the SEM images. Briefly, a spherical micelle is typically formed when the polymer has a long hydrophilic head and a short hydrophobic tail, the opposite is true for rod-like micelles. Flower-like micelles are characterized by three blocks, a long hydrophilic block and two short hydrophobic blocks. **Table** 5.4 shows that the spherical and flower-like micelles have a greater oxygen content than the rod-like micelles, indicating that the hydrophilic blocks may in fact be longer. We also show that the salts do not react with the LNPs. LNP shape, then, is determined by a complex set of interactions between size/structure of soluble lignin oligomeric subunits, specific chemical interactions between salt ions and lignin subunits, attractive/repulsive electrostatic interactions, hydrophobic/hydrophilic interactions, pH, ionic strength, etc.

Table 5.3. The different micelle shapes assumed by lignin LNPs [122, 236].

Diagram	Shape	Description
	Flower-like	Long hydrophilic section, Two short hydrophobic sections
	Spherical	Long hydrophilic head, short hydrophobic tail
	Rod-like	Short hydrophilic head, long hydrophobic tail
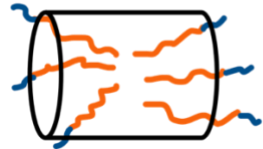
Table 5.4. EDS for select LNP samples. All samples indicate that the LNPs are made almost exclusively (~>90%) of carbon and oxygen.

Salt / Element	C	O	N	Cl	P	Na	K	Br
Cl - n	82.72	6.44	0	1.92	0	4.23	0	4.68
NO_3 - n	86.72	10.90	0	0	0	2.39	0	0
CO_3 - b	77.68	16.40	0	0.012	0	0.52	0.02	5.25
PO_4 - n	77.54	16.23	0	0.19	1.11	0.19	0	4.74

5.3.2 Effect of pH

We ran all the experiments at basic (10.8) and neutral (7) pH. We chose one of the buffer salts, phosphate, and one of the simple salts, nitrate, to run at an additional acidic (3.8) pH. **Figure** 5.7 shows the solubilization, phenolic content, flavonoid content, and antioxidant capacity (IC50) for nitrate and phosphate at basic, neutral, and acidic at day 0 and at day 7. **Figure** 5.8 and **Figure** **5.9** show the statistical significance (ANOVA) of all of these relationships.
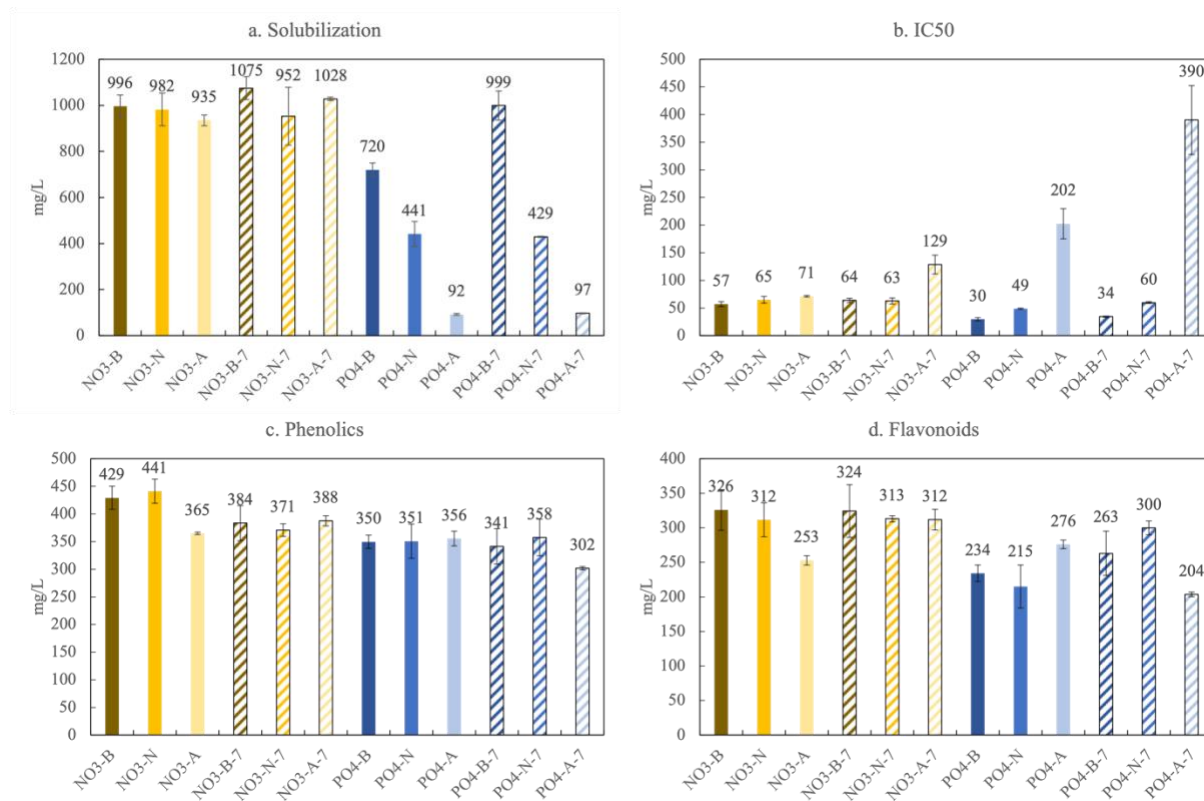
Figure 5.7. The a. solubilization, b. IC50, c. phenolic content, and d. flavonoid content for phosphate and nitrate at different pH (basic, neutral, and acidic) at day 0 and 7.

In **Figure** 5.7**a**, we observe that lignin is well solubilized in the nitrate based depolymerization media (yellow) and shows little variation with pH (dark to light indicates basic to acidic) and time (solid = day 0, striped = day 7). Further considering the NO_3^- results, there is some variation in phenolic content (**Figure** 5.7**c**), however it is not statistically significant. The flavonoid content (**Figure** 5.7**d**) is similar across NO_3^- experimental conditions, except for acidic pH at t=0. The IC50 (**Figure** 5.7**b**) results also remain constant across NO_3^- experimental conditions, with the exception of NO_3^--A at day 7 which shows a lower antioxidant capacity.

		Solubilization		Phenolic Content		Flavonoid Content		IC50		LNP conc.		LNP size		PDI		zeta	
		t = 0 d	t = 7 d	t = 0 d	t = 7 d	t = 0 d	t = 7 d	t = 0 d	t = 7 d	t = 0 d	t = 7 d	t = 0 d	t = 7 d	t = 0 d	t = 7 d	t = 0 d	t = 7 d
NO_3^-	A-B					<0.05				<0.05	<0.05	<0.05	<0.05		<0.05		
	A-N					<0.05				<0.05		<0.05	<0.05		<0.05		
	B-N																
PO_4^{3-}	A-B	<0.05	<0.05					<0.05	<0.05	<0.05		<0.05	<0.05	<0.05	<0.05	<0.05	<0.05
	A-N	<0.05	<0.05			<0.05	<0.05	<0.05	<0.05	<0.05	<0.05	<0.05	<0.05	<0.05	<0.05		<0.05
	B-N	<0.05	<0.05													<0.05	

Figure 5.8 ANOVA for the significant differences across pH (acidic; neutral; basic). Data is shown for nitrate and phosphate salts, at t =0d and 7d. The green boxes indicate that the difference in product or property value is significant (i.e. p<0.05).

		Solubilization	Phenolic Content	Flavonoid Content	IC50	LNP conc.	LNP size	PDI	zeta
NO_3^-	Acidic	<0.05		<0.05	<0.05	<0.05	<0.05	<0.05	
	Neutral								
	Basic								
PO_4^{3-}	Acidic		<0.05	<0.05			<0.05		
	Neutral			<0.05	<0.05	<0.05	<0.05	<0.05	<0.05
	Basic	<0.05				<0.05			

Figure 5.9 ANOVA for the significant differences across time (t=0d; t=7d). Data is shown for all nitrate and phosphate salts, in acidic, neutral, and basic conditions. The green boxes indicate that the difference in product or property value is significant (i.e. p<0.05).

In contrast to the NO_3^- results, the solubilized lignin for the phosphate based depolymerization is strongly influenced by pH. We see a high solubilization at the basic pH (72% at day 0 and 100% at day 7), however the solubilization drops to less than half (40%) at neutral pH , and less than 10% at acidic pH. The phenolic content is slightly less than that in the presence of NO_3^-, and relatively constant under the experimental conditions, except at low pH and t=7d where the bulk phenolic content is about 14% less than the average of the other values. The total flavonoid content is both more variable and about overall about 20% less than the NO_3^- values. In comparison to the NO_3^- conditions, the depolymerization mixtures produced in the presence of phosphate show greater antioxidant capacities (low IC50 values) except under acidic conditions at both times, which is consistent with the low soluble lignin measurements, but inconsistent with the total phenolic and flavonoid values. The lack of agreement among the characteristics of the phosphate depolymerization mixtures may be explained by the properties of LNPs, specifically

the amount of phenolics/flavonoids that are incorporated into the LNPs, which will be further discussed in section 5.3.4.

Figure 5.10 shows the properties related to LNPs, including concentration, size, PDI, and zeta potential. The initial LNP concentrations (average, 0.55 mg/L) and particle size are relatively similar across basic and neutral pH and salt. LNP concentration (**Figure** 5.10**a**) shows a small increase in the presence of NO_3^- at t=7d and a larger (2-3 fold) increase in concentration with phosphate at t=7d. LNP sizes (**Figure** 5.10**b**), too, decrease (no change to 20-30% decrease) over time . The PDI (**Figure** 5.10**c**) under NO_3^- (0.6) remains constant with time at basic and neutral pH, whereas is it slightly more variable in the presence of phosphate (0.5 on average). The zeta potential (**Figure** 5.10**d**) indicates moderate stability for the nitrate-based LNPs (-36 mV), unchanged by pH or time. Phosphate LNPs show similar zeta potentials, with the exception of neutral and acidic pH at t=0 at which much lower and less stable zeta potentials (-25 mV) were measured.

In both the case of the nitrate salt and the phosphate salt, at acidic pH there is immediate formation of LNPs, although the LNP concentration decreases over time. The low pH LNPs are initially large in size (7000 and 5000 nm for nitrate and phosphate, respectively) but display a dramatic decrease in size with time, although the acidic LNPs are still larger (about 1900 nm) than those under other conditions (< 500 nm on average). In addition, the PDI values of acidic LNPs are much less (30 – 50% lower) than the values under basic or neutral conditions and decreases substantially over time. and incipient stability for phosphate based LNPs (-25 mV).
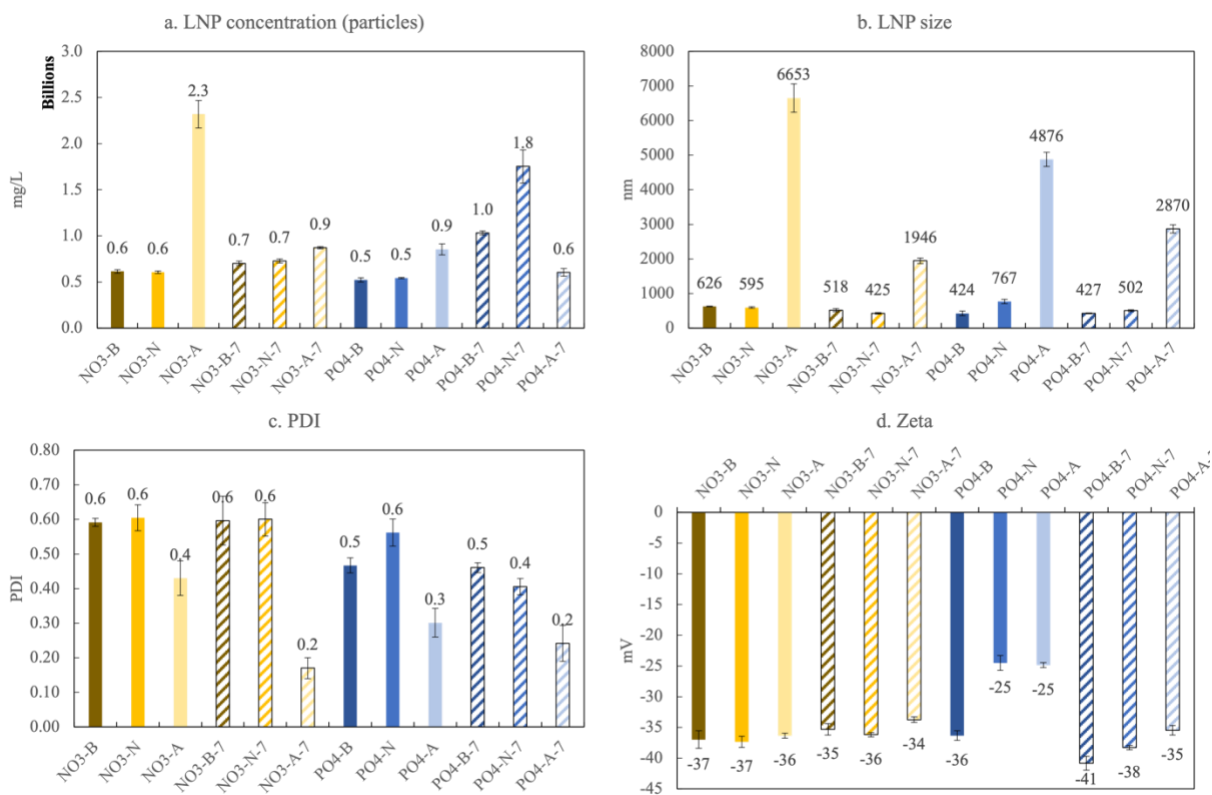
Figure 5.10 The a. LNP concentration, b. LNP size, c. PDI and d. Zeta potential for phosphate and nitrate at different pH (basic, neutral, and acidic) at day 0 and 7.

5.3.3 Effect of salt concentration

To test the effects of salt concentration and ionic strength, we considered different concentrations of phosphate: 110, 220, and 440 mM, at pH 7 and 10.8 and at day 0 and day 7. The corresponding ionic strengths are listed in **Table** 5.1 and depending on concentration and pH, vary from 0.26 – 1.4 M. In **Figure** 5.11 we compare the solubilization, phenolic content, flavonoid content and antioxidant capacity for all of the phosphate samples.
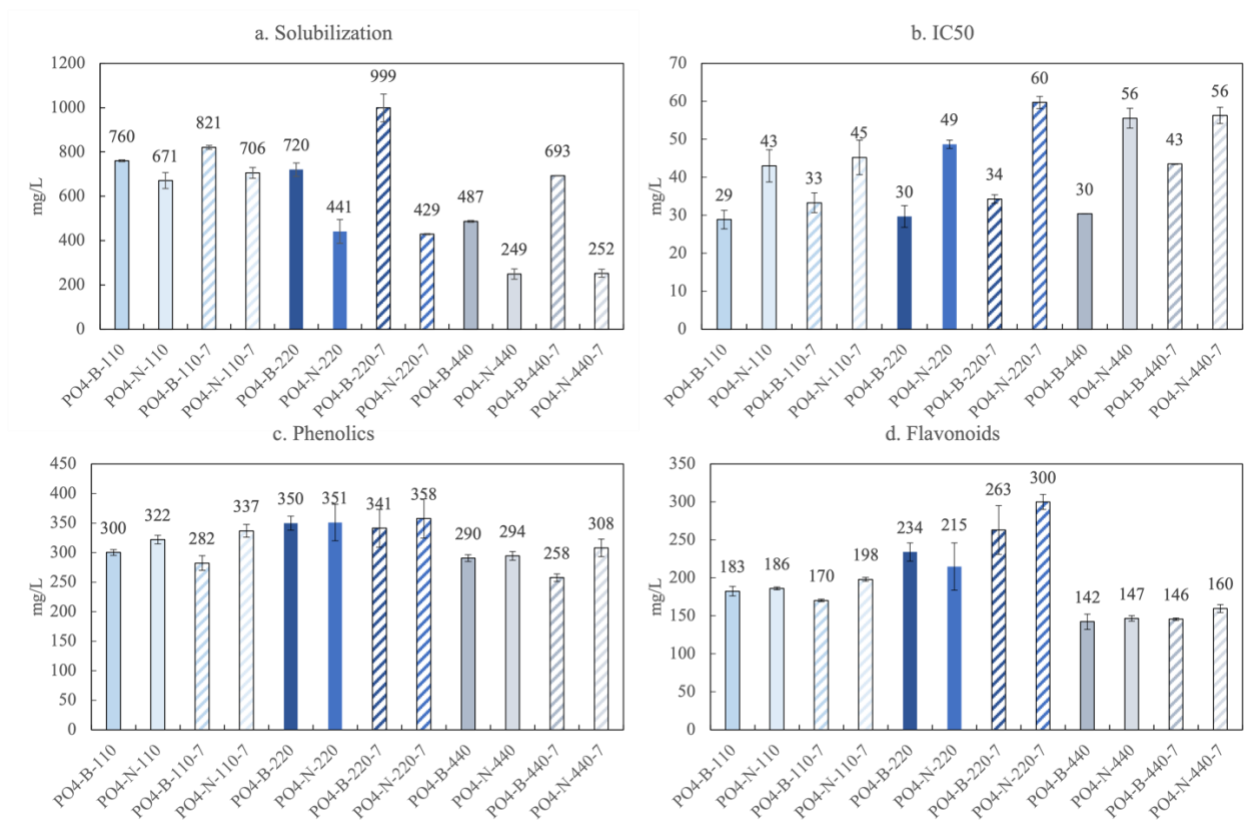
Figure 5.11. The a. solubilization, b, IC50, c. phenolic content, and d. flavonoid content for phosphate at 110, 220, and 440 mM at neutral and basic pH at day 0 and 7.

In **Figure** 5.11 we see that there are changes to solubilization based on phosphate concentration. Notably, in neutral conditions at t=0, solubilization decreases as the concentration of phosphate increases, roughly decreasing by 20% with each doubling of the concentration (67% to 44% to 24% soluble lignin corresponding to 110 to 220 to 440 mM phosphate). This trend is also present at t = 7 d. Neutralization of pH has a larger impact at higher concentrations. For example, for 110 mM at t = 0 d, we observe a 76% solubilization in basic conditions and 67% in neutral, less than a 10% decrease. For both 220 and 440 mM, solubilization upon neutralization decreases by nearly 30% incrementally. Maximum solubilization (≈100%) occurs under basic conditions, 220 mM phosphate, pH 10.8. Despite these trends in the solubilization, there are not many differences in the phenolic content, although slightly higher yields occur at 220 mM

phosphate. For the flavonoids, the 220 mM solution also produces significantly more flavonoids. There are no significant differences between salt concentration for the antioxidant capacity, only significant differences with respect to pH. Higher antioxidant activity is observed at basic pH, t=0 for all phosphate concentrations and is slightly diminished at t=7d.
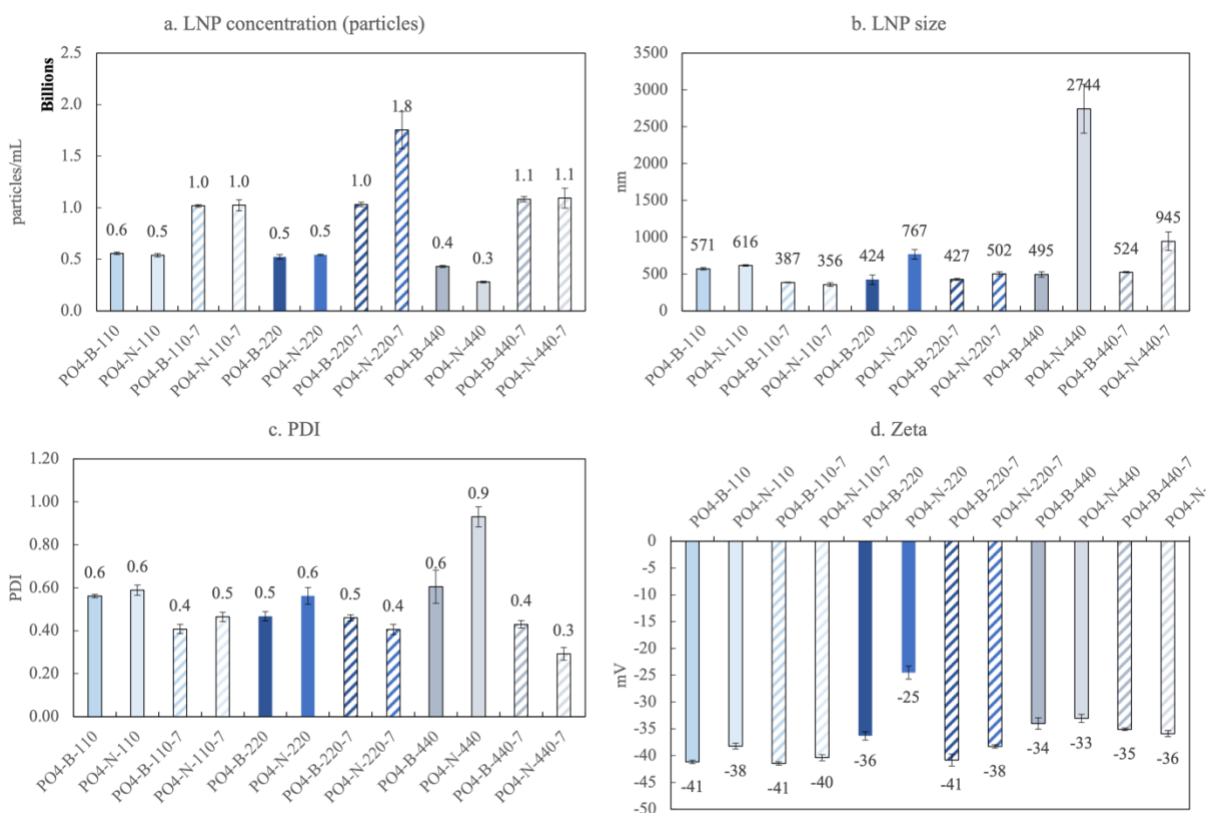
Figure 5.12. The a. LNP concentration, b. LNP size, c. PDI, and d. Zeta potential for phosphate at 110, 220, and 440 mM at neutral and basic pH at day 0 and 7.

Figure 5.12 reports LNP data for the different concentrations of phosphate and generally, salt concentration seems to have a smaller effect on LNP characteristics except in a few cases. For LNP concentration, the same pattern of increase in concentration with time is observed at each phosphate concentration, although 220 mM produces significantly more LNPs than 110 mM or 440 mM at day 7. For LNP size, 440 mM at t = 7 d, is the only condition that produces LNPs that are significantly larger (2744 nm) than the LNPs (average size ≈ 550 nm) formed in the other

conditions. The same is true for the PDI (average 0.5 vs. 0.9 for 440 mM at pH7, t=0). The zeta potential for 220 mM at t = 0 d, is significantly lower (-25 mV, less stable) than the other conditions (range -33 – 41 mV, average -38). In general, LNPs in higher phosphate concentration (440 mM) bear slightly lower zeta potentials (average -34.5 mV). Significant differences across different across different phosphate concentrations are summarized in **Figure 5.13**.

		Solubilization		Phenolic Content		Flavonoid Content		IC50		LNP conc.		LNP size		PDI		zeta	
		t=0d	t=7d	t=0d	t=7d	t=0d	t=7d	t=0d	t=7d	t=0d	t=7d	t=0d	t=7d	t=0d	t=7d	t=0d	t=7d
Neutral	110-220	<0.05	<0.05				<0.05									<0.05	
	110-440	<0.05	<0.05							<0.05		<0.05		<0.05			
	220-440	<0.05	<0.05	<0.05		<0.05	<0.05			<0.05		<0.05		<0.05		<0.05	
Basic	110-220			<0.05													
	110-440	<0.05							<0.05	<0.05				<0.05			
	220-440	<0.05	<0.05	<0.05		<0.05	<0.05			<0.05							

Figure 5.13 ANOVA for the significant differences across phosphate concentrations (110; 220; 440). Data is shown for t=0d and t=7d, as well as for neutral and basic pH. The green boxes indicate that the difference in product or property value is significant (i.e. p<0.05).

5.3.4 Effect of filtration on phenolic and flavonoids content

Figure 5.14 illustrates the effects of centrifugation and differential filtration on the phenolic and flavonoid content at t=0 for the different salts and different pH values. We typically conduct all our measurements, except solubilization, on uncentrifuged samples. Our aim is to characterize the mixture as a whole and demonstrate its potential in industrial applications without separation. Yet, given differences in LNP characteristics and antioxidant capacity among conditions, it is likely that some fraction of bulk phenolic and flavonoid content is associated with the colloidal fraction of lignin depolymerization mixtures.

Here we characterize product yields and properties in the lignin depolymerization mixtures of various salts as a function of colloidal size based on differential filtration and compare centrifugation to filtration through 400 nm, 200 nm, 100 nm pore size membranes. Although the bulk phenolic and flavonoid content typically does not change with different salts, the other

characteristics such as solubilization, LNPs size and shape, and antioxidant capacity do change. We hypothesize, then, that the proportion of solution phase phenolics and flavonoids relative to colloidal bound phenolics and flavonoids changes across salt types. In **Figure** 5.14 at basic pH the phenolic and flavonoid yields show negligible changes with centrifugation for all salts. In carbonate and phosphate mixtures, phenolic concentration is relatively constant among filtered samples, but there is a 10-20% decline when comparing centrifuged and filtered samples, meaning that a small amount of phenolic content (10 -20%) is associated with the colloidal fraction >400 nm. In Cl^- and NO_3^- mixtures a steady decline in bulk phenolic content occurs as filtration pore size decreases (50 – 60% decline in 100 nm filtrate relative to centrifuged samples). The bulk flavonoid concentration in carbonate and phosphate mixtures is relatively stable among various centrifuged/filtered samples (largest difference, 17 – 25% decline in 100 nm samples). In the Cl^- and NO_3^- mixtures at basic pH, the flavonoid content also tends to be associated with the solution phase, although the results are a little more variable and the Cl^- conditions show a slightly greater (30%) decrease in the 100 nm filtrate.

In neutral pH conditions, however, the amount of phenolics and flavonoids decreases significantly with filtration under all salt conditions, indicating that these chemical fractions become strongly associated with the colloidal fraction of the mixtures. In all salt cases, phenolics decrease from 35-48% to around 10% when going from uncentrifuged samples to samples filtered through 100 nm membranes. Flavonoids decrease similarly, from 24-28% to 5-7% in all cases besides nitrate, in which flavonoids remain at about 16% at the lowest filtration (100 nm). These results indicate that in neutral conditions that a greater fraction of phenolic and flavonoid content is associated with LNPs. This also aligns with **Figure** 5.1**b** which illustrates that the antioxidant

capacity decrease with neutralization (less so in the case of nitrate) suggesting that free phenolics

and flavonoids may be better antioxidants than those attached to the LNPs.
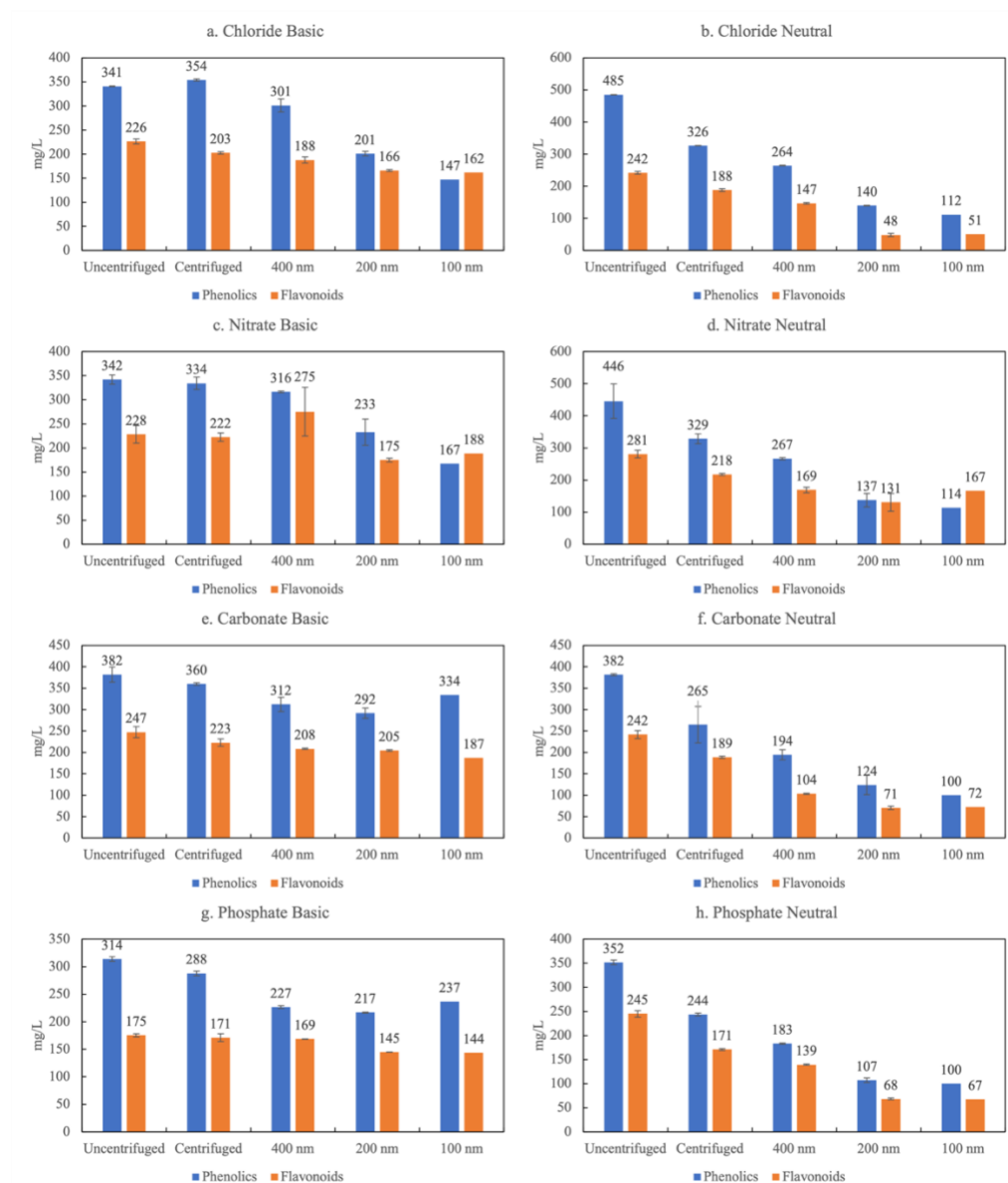
Figure 5.14. Phenolic and Flavonoid content for different filtrations including: uncentrifuged, centrifuged, 400 nm, 200 nm, and 100 nm for A. Chloride Basic, B. Chloride Neutral, C. Nitrate Basic, D. Nitrate Neutral, E. Carbonate Basic, F. Carbonate Neutral, G. Phosphate Basic, and H. Phosphate Neutral

We also see in **Figure** 5.14 some differences between the salts. For example, in basic conditions we see that phosphate and carbonate have a higher phenolic content than chloride and nitrate in the 100 nm filtrations. This is consistent with phosphate and carbonate having a lower IC50 in basic conditions (higher antioxidant capacity). Even so, the major trends emerge when considering pH, not salt. Upon running an ANOVA on the data, there are not many other significant differences between salt type (**Figure** 5.15).

		Phenolics				Flavonids			
		Uncentrifuged.	Centrifuged	400 nm	200 nm	Uncentrifuged.	Centrifuged	400 nm	200 nm
CO_3^{2-}	Basic				< 0.05				
Cl^-	Neutral			< 0.05					
CO_3^{2-}	Basic								< 0.05
NO_3^-	Neutral			< 0.05					
CO_3^{2-}	Basic					< 0.05	< 0.05		< 0.05
PO_4^{3-}	Neutral								
Cl^-	Basic								
NO_3^-	Neutral								< 0.05
Cl^-	Basic			< 0.05			< 0.05		
PO_4^{3-}	Neutral	< 0.05		< 0.05					
NO_3^-	Basic			< 0.05			< 0.05	< 0.05	
PO_4^{3-}	Neutral			< 0.05			< 0.05		< 0.05

Figure 5.15 ANOVA for the significant differences between salt types across different filtrations (uncentrifuged; centrifuged; 400 nm, 200 nm). Data is shown for neutral and basic pH. The green boxes indicate that the difference in product or property value is significant (i.e. p<0.05).

5.4 Discussion

In the previous section, we observed many different relationships and trends. This section will focus on the major relationships to highlight four major observations: 1) the effect of acidic pH conditions on LNPs, 2) the relationship between LNP shape and antioxidant capacity, 3) the Hofmeister series, and 4) the differences between buffer and simple salt effects.

With reference to **Figure** 5.10, the major effect of pH is that there is an instantaneous production of high LNP yield, having large size and low PDI. Typically, LNP concentration increases over the course of a week, closing mass balance on depolymerized lignin. Decreasing the pH to 3.8 in both phosphate and nitrate salts allows LNP production to close mass balance

immediately. **Figure** 5.16 shows the SEM image of a LNP formed in phosphate buffer at pH 3.8 at day 7. The LNP is large and amorphous and looks very similar to the LNPs discovered by Frangville et al [104]. The reason that we observe such different properties at pH 3.8, likely because the mechanism of formation shifts from micellization (**Figure** 2.11) to acid precipitation (**Figure** 2.10).
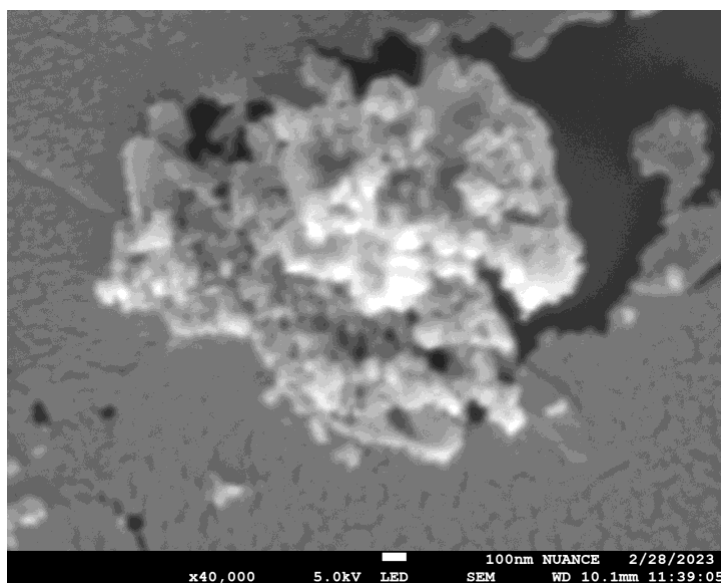
Figure 5.16. SEM image of LNP formed by phosphate salt at pH 3.8

The different LNP shapes shown in **Figure 5.6** may have an influence on the antioxidant capacity in **Figure** 5.1 **b** due to differences in the surface area to volume ratio (SA:V). We observe that a higher SA:V ratio has a lower IC50, i.e a higher antioxidant capacity. Hydrophilic phenolic groups on the external surface of the LNP micelle are responsible for the free radical scavenging. Hence, the greater the LNP surface area, the greater the amount of exposed phenolic groups and the greater the antioxidant capacity. Looking at the various shapes, we estimate that the flower-like micelle (carbonate) has higher surface area and should have the highest antioxidant capacity, which is what we observe. The spherical LNPs formed by phosphate salts have the second highest

antioxidant capacity. The rod-like have the lowest SA:V ratio and the lowest antioxidant capacity. Shape is not the only factor that informs SA:V ratio, the size (i.e. the radius) also has an effect. Typically, the smaller the radius, the larger the SA:V ratio, and specifically, we observe that when the LNPs are smaller in basic conditions, the higher the antioxidant capacity.
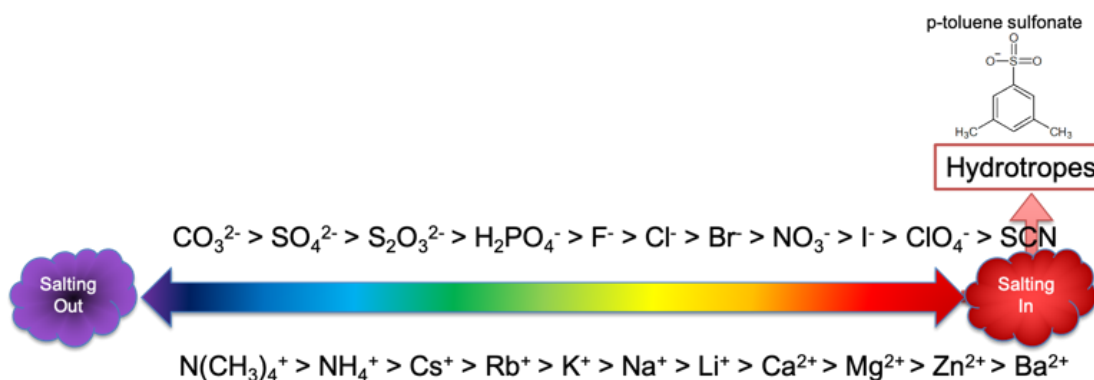
Figure 5.17 Reprinted from Figure 2.14: Reactivity of salt in accordance to the Hoffmeister scale [128]

Our inspiration for this investigation of salt effects was based on the Hofmeister series (**Figure** 2.14), which has been reprinted as **Figure** 5.17 . The Hofmeister series was experimentally discovered to explain the stability of proteins. On one end, we have kosmotropic ions, these are responsible for decreasing the solubility of the protein (i.e. salting out), these salts are often used to induce protein aggregation in pharmaceutical preparation and at various stages of protein extraction and purification. On the other end of the scale we have chaotropic, which denature and dissolve proteins (i.e. salting in). We hypothesized that as move from one end of the Hofmeister scale to the other, from the more kosmotropic salts (carbonate & phosphate) to the more chaotropic salts (nitrate & chloride), we would be able to tune the concentration and properties of LNP. However, the Hofmeister series is not absolute. In fact, the Hofmeister series is based on negatively charged hydrophobic surfaces, so by introducing hydrophilic surfaces, increasing the salt concentration, or by changing the pH, the Hofmeister series may no longer hold [237]. Despite

the knowledge about specific ion effects, including the Hofmeister series, that exists across various industries, a general predictive theory has yet to be developed that explains these effects, which is likely due to the complexity of interactions influenced by the properties of salts including size, charge density and distribution, polarizability, hydrophobicity and charge shielding, ion-pairing, solvation, permeability, complexation, stickiness, and interfacial disruption [238]. Despite measuring LNP properties, we do not see the formation of LNPs following the order of the Hofmeister Series. This may be explained by the complexity of LNP mechanisms, which involve two parts: 1) dissolution/depolymerization, and 2) reducing/modifying solubility - either by introducing an acid for precipitation or by adding an antisolvent to induce micellization. We would have expected that nitrate solubilizes lignin to the greatest extent (step 1 of the mechanism), producing the most flavonoids and phenolics, whereas phosphate and carbonate stabilize the most LNPs (step 2 of the mechanism). Due to the mechanism having two distinct steps, it is difficult to use the Hofmeister series as a predictive tool.

Interestingly, the phosphate mixture supports the best LNP formation. Multivalent salts have the benefit of functioning as having both chaotropic and kosmotropic properties, depending on the pH [239]. For example, using **Table** 5.5, in basic conditions, phosphate exists primarily in its -2/-3 charge state, which may better serve to dissolve lignin, when the solution is neutralized, either by intentional pH adjustment or by time, there is a shift to phosphate in its -2/-1 charge state, which seemingly may stabilize LNPs.

Table 5.5 The speciation and ionic strength for each of the salts at different pH values

pH	Basic (~10.8)		Neutral (~7.0)		Acidic (~3.8)	
	Speciation Charge:(mM)	Ionic strength (mM)	Speciation Charge:(mM)	Ionic strength	Speciation Charge:(mM)	Ionic strength
NO_3^{-1}	**-1 : (227)**	227	**-1 : (227)**	227	**-1 : (227)**	227
Cl^{-1}	**-1 : (227)**	227	**-1 : (227)**	227	**-1 : (227)**	227
PO_4^{-3}	**-3: (4.5)** **-2: (215.5)** -1: (0) 0: (0)	694	-3: (0) **-2: (152.1)** **-1: (74.9)** 0: (0)	526	-3: (0) -2: (0) **-1: (215.5)** **0: (4.5)**	222
CO_3^{-2}	**-2: (179.3)** **-1: (47.7)** 0: (0)	529	-2: (0) **-1: (186.1)** **0: (40.9)**	185	-2: (0) **-1: (0.6)** **0: (226.4)**	0.6

There are cases in which neutralization affects buffers (phosphate, carbonate) more than it affects salts (chloride, nitrate). This is seen in **Figure** 5.1 **a and b**, with regards to solubilization and antioxidant capacity decreasing when the phosphate and carbonate solutions are neutralized, but the there is no effect with the neutralization of chloride and nitrate. This is also observed in **Figure** 5.5 **b and c** when neutralizing increases the size of the LNPs and PDI for carbonate and phosphate but not for chloride and nitrate. We initially thought that these phenomena could be attributed to differences in ionic strength for the buffers at different pH but remain unchanged for simple salts, as see in **Table** 5.5**.** Ionic strength can be manipulated either by concentration or by the charge on the ion (pH). However, in section 5.3.3 Effect of salt concentration, changes to the

salt concentration, which change the ionic strength, did not have the same effects that we saw previously when we changed the pH. This makes it difficult to separate out the specific chemical effects from the electrostatic effects and ionic strength effects.

5.5 Conclusions

Our aim was to evaluate whether the LNPs produced in our biorefinery could be tuned by varying factors in our depolymerization media, specifically, the salt concentration, salt type, and the pH. We hypothesized that salt type would stabilize LNP formation in a similar order in which they stabilize proteins (Hofmeister series). While, we found that not to be true, we did find that the salt type influences the shape of the LNP. We can vary the shape from spherical (phosphate), to rod-like (chloride and nitrate), and to flower-like (carbonate). These changes to the shape also influence the surface area to volume ratio of the LNPs which subsequently change the antioxidant capacity of the LNPs. The high surface area of the flower-like LNPs produced in the carbonate media promote the highest antioxidant capacity, making LNPs formed in this method competitive with industrial sources of antioxidants.

We also found that pH can be used to tune properties of LNPs. We specifically evaluated changes to solubilization, phenolic content, flavonoid content, antioxidant capacity, LNP concentration, size, shape, stability, and polydispersity. The pH can be used to tune the size and the antioxidant capacity of LNPs produced by phosphate and carbonate, as well as the association of phenolics/flavonoids with the LNPs. This could be due to various properties including ionic strength, buffering capacity, charge, as well as specific chemical properties of the different salts at different pHs. Additionally, an acidic pH can be used to produce a high concentration of large LNPs instantaneously, rather than over a one-week period.

Chapter 6 : Conclusions

6.1 Summary

The work presented in this thesis aimed to show that lignin can be refined through a biorefinery under mild conditions to preserve aromaticity and create high-yielding and high-value products. Despite, lignin being the only source of renewable aromatic carbon, most of it is burned for low value energy. Research that aims to extract more value from lignin still employs harsh conditions (i.e. high temperature, high pressure, extreme pH, dangerous reagents, expensive catalysts) that either remove aromaticity or valuable functional groups or produce very low yields of products which limit the commercially viability of the process. Our biorefinery operates under ambient temperature and pressure and uses a renewable "green" depolymerization media – the MEC catholyte. Under these conditions, lignin is depolymerized to preserve aromaticity as well as the oxygen containing functional groups that give our products antioxidant properties. Our biorefinery integrates a microbial electrolysis cell coupled with lignin depolymerization to produce four product streams. Two of the product streams come from the MEC: 1) clean water, by removing 60% of the acetate from a high volatile fatty acid waste stream (common from food waste – like brewery waste) and 2) a caustic and high ionic strength effluent. The effluent is a renewable source of caustic that can be produced on a small, distributed scale. From the lignin we produce 1) discrete aromatics in the form of phenolics and flavonoids and 2) lignin nanoparticles. Both product streams close mass balance and have properties that make them good antioxidants,

and offering a range of potential applications in the pharmaceutical, nutraceutical, and cosmetic industry among others.

6.2 Key Outcomes and Findings

6.2.1 MEC Mediated Biorefinery – High Value Products from Lignin

In Chapter 3, it was demonstrated that lignin depolymerization could be coupled to a microbial electrolysis cell to create a biorefinery recovering energy and materials from waste materials. A key finding in this section was the discovery that lignin undergoes depolymerization/solubilization with a combination of caustic pH and high salt concentration, eliminating the need to operate the MEC to produce hydrogen peroxide. We also characterized the bulk properties of the depolymerized lignin, including solubilization, phenolic content and flavonoid content. We found high solubilization (>80%) with almost 50% bulk phenolics and 20% bulk flavonoids. Furthermore, we characterized discrete aromatics through high resolution and tandem LCMS and found 14 distinct compounds, making up to 11% of the solubilized lignin. Most of the compounds are in the form of flavonoids or oligomers, which are compounds that are not typically the target of base catalyzed depolymerization although they have immense potential applications due to their antioxidant capabilities. The conditions of our biorefinery are favorable for rearrangement and repolymerization which result in these stable larger products. Finally, we were able to close mass balance, which is rarely demonstrated in base catalyzed depolymerization, through the production of lignin nanoparticles. The LNPs are dispersed ranging from under 100 nm to 500 nm. They are spherical in shape and have good stability. They form under basic and neutral conditions over the course of two weeks, although it is in neutral conditions where most of the mass is in the form of LNPs.

6.2.2 Effect of Lignin Source and Extraction on Products and Properties

In the biorefinery described in Chapter 3, our lignin input is from the Organosolv extraction of a herbaceous source (corn stover). In Chapter 4, we explored the robustness of our biorefinery when it comes to changing the source and extraction of lignin. The biomass source informs us of the amount of lignin available, as well as the number of β-O-4 linkages (breakable linkages) and the ratio of monolignols – specifically the ratio of the Syringyl unit to the Guiacyl Unit (S/G). It is reported in the literature, and we confirmed for our materials, that softwood has the greatest lignin content, but the lowest β-O-4 content, as well as it is made up of exclusively G units. Herbaceous sources have the lowest amount of lignin but the highest number of β-O-4 linkages. It is also the only source to contain a significant (up to 5%) portion of the p-hydroxyphenyl unit (H). This unit is responsible for some of the discrete aromatic we measured in Chapter 3, specifically p-coumaric acid. Hardwood has an intermediate amount of lignin and β-O-4 linkages. The extraction method further modifies the structure of lignin, specifically the β-O-4 linkages. Although most industrial lignins are extracted via the hard Klason and lignosulfonate extraction (paper and pulp industry), we used the Klason extraction in our experiments because it does not result in the incorporation of sulfur into the lignin. This extraction preserves aromaticity but removed most of the β-O-4 linkages, making depolymerization difficult. However, it was the only extraction that worked on all three of the biomass sources. The Organosolv extraction is medium harshness, it modifies the structure of lignin by removing some but not most of the β-O-4 linkages. The Organosolv extraction is used in the bioethanol industry. The Milled Wood extraction is the mildest and preserves the structure of lignin well. However, it is low yielding and low purity. This type of extraction is never used industrially. We found that our biorefinery produces the most products –

phenolics, flavonoids, and LNPs – with the Organosolv extraction of herbaceous lignin. The conditions of our biorefinery have moderate success depolymerizing the Klason extraction of herbaceous and hardwood lignin (35-62% solubilization, up to 30% phenolics, up to 23% flavonoids, and up to 28% LNPs). We did not have success depolymerizing lignin from the Klason extraction of softwood. We also found relationships between the number of β-O-4 linkages and solubilization, phenolic content, flavonoid content, LNP concentration, size and PDI. There were also relationships between the products and properties such as between the flavonoid content and antioxidant capacity, as well as between the LNP size and antioxidant capacity. The relationships are stronger when comparing values within the same source.

6.2.3 Effect of Salt and pH on the Properties of Lignin Nanoparticles

Finally, in Chapter 5, we sought to tune the properties of the LNPs by making changes to the depolymerization media (MEC catholyte effluent). We examined how changes to the pH, salt type, and salt concentration affected the properties of LNPs, including, size, PDI, stability, shape, and antioxidant capacity. We found three major conclusions in this section. The first conclusion is that salt behavior predicted by the Hofmeister series did not apply to lignin solubilization and LNP formation. The second conclusion is that changing the salt type (i.e. phosphate, carbonate, chloride, nitrate) changes the shape and size of the LNPs, as well as the antioxidant capacity. We found that LNPs formed via the phosphate media were spherical, via the carbonate media were flower-like, and via the nitrate or chloride media were rod-like. The antioxidant capacity followed the trend of being highest for LNPs with the highest surface are to volume ratio (carbonate > phosphate > chloride = nitrate). The third conclusion from this section is that pH, specifically acidic pH, can be used to produce large and narrowly dispersed LNPs rapidly. However, these

LNPs are amorphous and are not stable over 7 days. pH can also be used to tune the properties of LNPs formed via the phosphate or carbonate media. This is because changes to the pH, change the ionic strength of the solutions in the case of multivalent salts or buffers or change the properties of the reactive salts. In basic conditions, LNPs are smaller and have a stronger antioxidant capacity. In fact, in basic carbonate conditions, we have a product mixture with an antioxidant capacity comparable to the industrial standard, Trolox. The implications here are that lignin, a resource that is often regarded as just a waste, could be used as a natural source of antioxidant in the cosmetic, nutraceutical, or pharmaceutical industry. LNPs also have potential uses as drug delivery systems, fertilizer/pesticide delivery systems, UV protectants, food preservatives, and many other uses.

6.3 Future Work

There's several additional questions that future research should seek to answer, specifically in regard to scaling this biorefinery up from a lab scale. There can also be more done in terms of the analytical chemistry for determining the discrete compounds present, along with separation costs and product worth.

1) In our research, the microbial electrolysis cell ran on acetate which a modeled high volatile fatty acid wastewater. It would be useful to run the MEC with a real wastewater to test both the performance metrics of the MEC (i.e. VFA removal) as well as the effects, if any, on the volume and properties (i.e. salt concentration, pH) on the catholyte effluent upon which our biorefinery depends on. Additionally, the MEC was initially operated to produce hydrogen peroxide. We found that hydrogen peroxide is not necessary for our depolymerization; in fact, oxidizing lignin with hydrogen peroxide in caustic removes the aromaticity of depolymerized products (see Chapter 3). Operating the MEC for hydrogen peroxide is difficult but since it is not necessary, we may consider using a microbial fuel

cell (MFC) to produce electricity in addition to treating wastewater and producing caustic effluent. The MEC/MFC should be tested in scale models to determine the consistency and volume they can operate at.

2) In Chapter 4, we found that the herbaceous source of lignin was the best lignin to run depolymerization on in the conditions of our biorefinery. However, we only tested one type of herbaceous source – corn stover. This is a useful source of lignin for our biorefinery because Organosolv lignin is a byproduct from converting cellulose into bioethanol (a biofuel) – which is the second largest source of commercial lignin. Bioethanol is a clean source of energy, often being produced from corn stover which is a second-generation biofuel. If we were to bypass relying on the bioethanol industry for corn stover lignin, it is not as simple as collecting corn stover at the end of a corn harvest, as much of that stover needs to be left on the field as to not remove organic matter from the soil. Different types of grasses should be tested and their efficacy in our biorefinery. The different types of grasses may have different amounts of lignin, β-O-4 content, and growing time that may make certain species more ideal to use as a lignin stream in the conditions of our biorefinery. Grasses do not compete as a food supply [238]. We also may use grass from yard waste streams. In the case of yard waste, the efficiency of our biorefinery on mixed biomass streams (i.e different types of grasses, leaves, twigs) should be tested. This may help our biorefinery work in individual neighborhoods, with yard waste providing lignin streams, combined with MECs that are operating in local breweries and producing products that stimulate local economies.

3) We were also limited in identifying and quantifying all the discrete monomers, flavonoids, and oligomers present in our depolymerized lignin mixture. In Chapter 3, we saw the

discrepancy between identified compounds (11%) and total phenolics and flavonoids (50% and 20%, respectively). Although some of the bulk phenolics and flavonoids are thought to be incorporated into the LNPs, in the time before they incorporate it may be useful to identify and quantify the remaining compounds. We were limited mostly by the availability of standards. Even in the 11% that we identified, there is uncertainty because most of our identifications did not have standards to calibrate with. Our quantification may also be underestimated because every individual compound has a different calibration curve. It is possible that with all the right standards we may get closer to matching the bulk quantification. Additionally, matching with the appropriate standard may allow us to attach monetary value to each compound and the mixture, which may help inform decisions for the cost/benefit of separation. Obtaining standards will have to be done through chemical synthesis.

4) Finally, in assessing the feasibility of running this biorefinery to scale a Life Cycle Assessment (LCA) and Techno-economic Assessment (TEA) should be performed to measure sustainability metrics, as well, as cost/benefit analysis of running this biorefinery. In this case we could compare the cost and sustainability of obtaining caustic from MEC/MFC vs. traditional caustic sources vs. other technologies. We should also look at the sustainability of removing plants (i.e. corn stover or grasses) from the field in order to depolymerize them rather than allowing nutrients to return back into the soil. We also should look at the products, we know we close mass balance with products, but we should look at properties and value of the mixture versus the individual component and decide whether the cost of separation may be worth the increase in value.

References

1. Santos-Sanchez, N.F., et al., *Antioxidant Compounds and their antioxdiant mechanism.* Intech Open, 2019.
2. Rossiger, B., G. Unkelback, and D. Pufky-Heinrich, *Base-Catalyzed Depolymerization of Lignin: History, Challenges and Perspectives*, in *Lignin- Trends and Applications*, M. Poletto, Editor. 2018, IntechOpen. p. 1-308.
3. Erdocia, X., et al., *Base catalyzed depolymerization of lignin: Influence of Organosolv lignin nature.* Biomass and Bioenergy, 2014. **66**: p. 379-386.
4. Griffin, J., et al., *Hybrid Approach for Selective Sulfoxidation via Bioelectrochemically Derived Hydrogen Peroxide over a Niobium(V)–Silica Catalyst.* ACS Sustainable Chemistry & Engineering, 2018. **6**(6): p. 7880-7889.
5. Wang, J., et al., *Atomic Force Microscopy and Molecular Dynamics Simulations for Study of Lignin Solution Self-Assembly Mechanisms in Organic-Aqueous Solvent Mixtures.* ChemSusChem, 2020. **13**(17): p. 4420-4427.
6. V. Masson-Delmotte, P.Z., H. O. Pörtner, D. Roberts, J. Skea, P.R. Shukla, A. Pirani, W. Moufouma-Okia, C. Péan, R. Pidcock, S. Connors, J. B. R. Matthews, Y. Chen, X. Zhou, M. I. Gomis, E. Lonnoy, T. Maycock, M. Tignor, T. Waterfield, *Global warming of 1.5°C. An IPCC Special Report on the impacts of global warming of 1.5°C above pre-industrial levels and related global greenhouse gas emission pathways, in the context of strengthening the global response to the threat of climate change, sustainable development, and efforts to eradicate poverty*. 2018.
7. Glasser, W.G., *About Making Lignin Great Again—Some Lessons From the Past.* Frontiers in Chemistry, 2019. **7**(565).
8. Dresselhaus, M.S. and I.L. Thomas, *Alternative energy technologies.* Nature, 2001. **414**(6861): p. 332-337.
9. Sun, Z., et al., *Bright Side of Lignin Depolymerization: Toward New Platform Chemicals.* Chem Rev, 2018. **118**(2): p. 614-678.
10. Rinaldi, R., et al., *Paving the Way for Lignin Valorisation: Recent Advances in Bioengineering, Biorefining and Catalysis.* Angew Chem Int Ed Engl, 2016. **55**(29): p. 8164-215.
11. Bartolomei, E., et al., *Lignin Depolymerization: A Comparison of Methods to Analyze Monomers and Oligomers.* ChemSusChem, 2020. **13**(17): p. 4633-4648.
12. Zhang, T., et al., *Short-Time Hydrothermal Treatment of Poplar Wood for the Production of a Lignin-Derived Polyphenol Antioxidant.* ChemSusChem, 2020. **13**(17): p. 4478-4486.
13. Tan, E.C.D. and P. Lamers, *Circular Bioeconomy Concepts—A Perspective.* Frontiers in Sustainability, 2021. **2**.
14. Tuck, C.O., et al., *Valorization of Biomass: Deriving More Value from Waste.* Science, 2012. **337**(6095): p. 695.
15. Kang, S., et al., *Hydrothermal conversion of lignin: A review.* Renewable and Sustainable Energy Reviews, 2013. **27**: p. 546-558.
16. Speight, J.G., *Chapter 6 - Catalytic Cracking*, in *The Refinery of the Future*, J.G. Speight, Editor. 2011, William Andrew Publishing: Boston. p. 181-208.
17. Ubando, A.T., C.B. Felix, and W.H. Chen, *Biorefineries in circular bioeconomy: A comprehensive review.* Bioresour Technol, 2020. **299**: p. 122585.
18. Obrzut, N., et al., *Valorization of Lignin under Mild Conditions: Biorefining Flavonoids and Lignin Nanoparticles.* ACS Sustainable Chemistry & Engineering, 2022. **11**(2): p. 491-501.

19.   Pauly, M. and K. Keegstra, *Cell-wall carbohydrates and their modification as a resource for biofuels.* Plant J, 2008. **54**(4): p. 559-68.

20.   Liu, Q., L. Luo, and L. Zheng, *Lignins: Biosynthesis and Biological Functions in Plants.* Int J Mol Sci, 2018. **19**(2).

21.   Li, T. and S. Takkellapati, *The current and emerging sources of technical lignins and their applications.* Biofuel Bioprod Biorefin, 2018. **0**: p. 1-32.

22.   Ganewatta, M.S., H.N. Lokupitiya, and C. Tang, *Lignin Biopolymers in the Age of Controlled Polymerization.* Polymers, 2019. **11**(7): p. 1176.

23.   Schutyser, W., et al., *Chemicals from lignin: an interplay of lignocellulose fractionation, depolymerisation, and upgrading.* Chem Soc Rev, 2018. **47**(3): p. 852-908.

24.   Feghali, E., et al., *Convergent reductive depolymerization of wood lignin to isolated phenol derivatives by metal-free catalytic hydrosilylation.* Energy & Environmental Science, 2015. **8**(9): p. 2734-2743.

25.   Anderson, E.M., et al., *Differences in S/G ratio in natural poplar variants do not predict catalytic depolymerization monomer yields.* Nat Commun, 2019. **10**(1): p. 2033.

26.   Bose, S.K., et al., *Lignin content versus syringyl to guaiacyl ratio amongst poplars.* Bioresour Technol, 2009. **100**(4): p. 1628-33.

27.   Normark, M., et al., *Analysis, pretreatment and enzymatic saccharification of different fractions of Scots pine.* BMC Biotechnol, 2014. **14**: p. 20.

28.   Mann, D.G.J., et al., *Rapid Assessment of Lignin Content and Structure in Switchgrass (Panicum virgatum L.) Grown Under Different Environmental Conditions.* BioEnergy Research, 2009. **2**(4): p. 246-256.

29.   Roberts, V.M., et al., *Towards quantitative catalytic lignin depolymerization.* Chemistry, 2011. **17**(21): p. 5939-48.

30.   Taherzadeh, M., et al., *Sustainable Resource Recovery and Zero Waste Approaches*. 2019: Elsevier Science.

31.   Bajpai, P., *Chapter 12 - Pulping Fundamentals*, in *Biermann's Handbook of Pulp and Paper* 2018, Elsevier. p. 295-351.

32.   Chen, H., *3 - Lignocellulose biorefinery feedstock engineering*, in *Lignocellulose Biorefinery Engineering*, H. Chen, Editor. 2015, Woodhead Publishing. p. 37-86.

33.   Karlsson, M., et al., *Toward a Consolidated Lignin Biorefinery: Preserving the Lignin Structure through Additive-Free Protection Strategies.* ChemSusChem, 2020. **13**(17): p. 4666-4677.

34.   Thornburg, N.E., et al., *Mesoscale Reaction-Diffusion Phenomena Governing Lignin-First Biomass Fractionation.* ChemSusChem, 2020. **13**(17): p. 4495-4509.

35.   Yamamoto, M., et al., *Importance of Lignin Coniferaldehyde Residues for Plant Properties and Sustainable Uses.* ChemSusChem, 2020. **13**(17): p. 4400-4408.

36.   Subbotina, E., et al., *Zeolite-Assisted Lignin-First Fractionation of Lignocellulose: Overcoming Lignin Recondensation through Shape-Selective Catalysis.* ChemSusChem, 2020. **13**(17): p. 4528-4536.

37.   Cai, C., et al., *Comparison of Two Acid Hydrotropes for Sustainable Fractionation of Birch Wood.* ChemSusChem, 2020. **13**(17): p. 4649-4659.

38.   Cronin, D.J., et al., *Deep Eutectic Solvent Extraction of High-Purity Lignin from a Corn Stover Hydrolysate.* ChemSusChem, 2020. **13**(17): p. 4678-4690.

39.   De Santi, A., et al., *Lignin-First Fractionation of Softwood Lignocellulose Using a Mild Dimethyl Carbonate and Ethylene Glycol Organosolv Process.* ChemSusChem, 2020. **13**(17): p. 4468-4477.

40.   Liu, X., et al., *Recent Advances in the Catalytic Depolymerization of Lignin towards Phenolic Chemicals: A Review.* ChemSusChem, 2020. **13**(17): p. 4296-4317.

41.   Majdar, R.E., C. Crestini, and H. Lange, *Lignin Fractionation in Segmented Continuous Flow.* ChemSusChem, 2020. **13**(17): p. 4735-4742.

42.   Tindall, G.W., et al., *Fractionating and Purifying Softwood Kraft Lignin with Aqueous Renewable Solvents: Liquid-Liquid Equilibrium for the Lignin-Ethanol-Water System.* ChemSusChem, 2020. **13**(17): p. 4587-4594.

43.   Tricker, A.W., et al., *Similarities in Recalcitrant Structures of Industrial Non-Kraft and Kraft Lignin.* ChemSusChem, 2020. **13**(17): p. 4624-4632.

44.   Xu, J., et al., *Biomass Fractionation and Lignin Fractionation towards Lignin Valorization.* ChemSusChem, 2020. **13**(17): p. 4284-4295.

45.   Wang, S., et al., *Pyrolysis behaviors of four lignin polymers isolated from the same pine wood.* Bioresour Technol, 2015. **182**: p. 120-127.

46.   Cao, Y., et al., *Advances in lignin valorization towards bio-based chemicals and fuels: Lignin biorefinery.* Bioresour Technol, 2019. **291**: p. 121878.

47.   Morais, A.R. and R. Bogel-Lukasik, *Green chemistry and the biorefinery concept.* Sustainable Chem. Processes, 2013. **1**(1).

48.   Moncada B, J., V. Aristizábal M, and C.A. Cardona A, *Design strategies for sustainable biorefineries.* Biochemical Engineering Journal, 2016. **116**: p. 122-134.

49.   Abdelaziz, O.Y. and C.P. Hulteberg, *Lignin Depolymerization under Continuous-Flow Conditions: Highlights of Recent Developments.* ChemSusChem, 2020. **13**(17): p. 4382-4384.

50.   Jiang, X., et al., *Tracing Sweetgum Lignin's Molecular Properties through Biorefinery Processing.* ChemSusChem, 2020. **13**(17): p. 4613-4623.

51.   Poveda-Giraldo, J.A., J.C. Solarte-Toro, and C.A. Cardona Alzate, *The potential use of lignin as a platform product in biorefineries: A review.* Renewable and Sustainable Energy Reviews, 2021. **138**.

52.   *Alpena Biorefinery*. Available from: https://www.energy.gov/eere/bioenergy/alpena-biorefinery.

53.   Lu, L. and Z.J. Ren, *Microbial electrolysis cells for waste biorefinery: A state of the art review.* Bioresour Technol, 2016. **215**: p. 254-264.

54.   Rozendal, R.A., et al., *Towards practical implementation of bioelectrochemical wastewater treatment.* Trends Biotechnol, 2008. **26**(8): p. 450-9.

55.   Logan, B.E. and K. Rabaey, *Conversion of wastes into bioelectricity and chemicals by using microbial electrochemical technologies.* Science, 2012. **337**(6095): p. 686-90.

56.   Lewis, A.J., et al., *Hydrogen production from switchgrass via an integrated pyrolysis-microbial electrolysis process.* Bioresour Technol, 2015. **195**: p. 231-41.

57.   Thygesen, A., et al., *Upgrading of straw hydrolysate for production of hydrogen and phenols in a microbial electrolysis cell (MEC).* Appl Microbiol Biotechnol, 2011. **89**(3): p. 855-65.

58.   Li, X., et al., *One-Pot Conversion of Lignin into Naphthenes Catalyzed by a Heterogeneous Rhenium Oxide-Modified Iridium Compound.* ChemSusChem, 2020. **13**(17): p. 4409-4419.

59.   Li, Y., et al., *Mechanistic Study of Diaryl Ether Bond Cleavage during Palladium-Catalyzed Lignin Hydrogenolysis.* ChemSusChem, 2020. **13**(17): p. 4487-4494.

60.   Shen, X., et al., *Product-oriented Direct Cleavage of Chemical Linkages in Lignin.* ChemSusChem, 2020. **13**(17): p. 4367-4381.

61.   Xue, Z., et al., *Highly Efficient Cleavage of Ether Bonds in Lignin Models by Transfer Hydrogenolysis over Dual-Functional Ruthenium/Montmorillonite.* ChemSusChem, 2020. **13**(17): p. 4579-4586.

62.   Jing, Y., et al., *Chemicals from Lignin: A Review of Catalytic Conversion Involving Hydrogen.* ChemSusChem, 2020. **13**(17): p. 4181-4198.

63. Klinger, G.E., et al., *Nucleophilic Thiols Reductively Cleave Ether Linkages in Lignin Model Polymers and Lignin.* ChemSusChem, 2020. **13**(17): p. 4394-4399.
64. Li, H., et al., *Amine-Mediated Bond Cleavage in Oxidized Lignin Models.* ChemSusChem, 2020. **13**(17): p. 4660-4665.
65. Qu, C., et al., *Directly Microwave-Accelerated Cleavage of C-C and C-O Bonds of Lignin by Copper Oxide and H2 O2.* ChemSusChem, 2020. **13**(17): p. 4510-4518.
66. Xiang, Z., et al., *Photocatalytic Conversion of Lignin into Chemicals and Fuels.* ChemSusChem, 2020. **13**(17): p. 4199-4213.
67. Du, X., et al., *Electrochemical Lignin Conversion.* ChemSusChem, 2020. **13**(17): p. 4318-4343.
68. Garedew, M., et al., *Greener Routes to Biomass Waste Valorization: Lignin Transformation Through Electrocatalysis for Renewable Chemicals and Fuels Production.* ChemSusChem, 2020. **13**(17): p. 4214-4237.
69. Li, C., et al., *Catalytic Transformation of Lignin for the Production of Chemicals and Fuels.* Chem Rev, 2015. **115**(21): p. 11559-624.
70. Park, M.R., et al., *Response of Pseudomonas putida to Complex, Aromatic-Rich Fractions from Biomass.* ChemSusChem, 2020. **13**(17): p. 4455-4467.
71. Stevens, J.C. and J. Shi, *Biocatalysis in ionic liquids for lignin valorization: Opportunities and recent developments.* Biotechnol Adv, 2019. **37**(8): p. 107418.
72. Toledano, A., L. Serrano, and J. Labidi, *Organosolv lignin depolymerization with different base catalysts.* Journal of Chemical Technology & Biotechnology, 2012. **87**(11): p. 1593-1599.
73. Wang, H., M. Tucker, and Y. Ji, *Recent Development in Chemical Depolymerization of Lignin: A Review.* Journal of Applied Chemistry, 2013. **2013**: p. 1-9.
74. Mathieu, Y., et al., *Molecular Oxygen Lignin Depolymerization: An Insight into the Stability of Phenolic Monomers.* ChemSusChem, 2020. **13**(17): p. 4743-4758.
75. Prothmann, J., et al., *Nontargeted Analysis Strategy for the Identification of Phenolic Compounds in Complex Technical Lignin Samples.* ChemSusChem, 2020. **13**(17): p. 4605-4612.
76. Terrell, E., et al., *Contributions to Lignomics: Stochastic Generation of Oligomeric Lignin Structures for Interpretation of MALDI-FT-ICR-MS Results.* ChemSusChem, 2020. **13**(17): p. 4428-4445.
77. Wang, S., et al., *Unlocking Structure-Reactivity Relationships for Catalytic Hydrogenolysis of Lignin into Phenolic Monomers.* ChemSusChem, 2020. **13**(17): p. 4548-4556.
78. Carnelli, P.F., et al., *Valorization of Lignin Under Mild Conditions: A Biorefinery Approach Incorporating A Microbial Electrolysis Cell.* In prep.
79. Cogulet, A., P. Blanchet, and V. Landry, *Wood degradation under UV irradiation: A lignin characterization.* Journal of Photochemistry and Photobiology B: Biology, 2016. **158**: p. 184-191.
80. An, L., et al., *Enhancing the solubility and antioxidant activity of high-molecular-weight lignin by moderate depolymerization via in situ ethanol/acid catalysis.* Industrial Crops and Products, 2019. **128**: p. 177-185.
81. Khorasani Esmaeili, A., et al., *Antioxidant Activity and Total Phenolic and Flavonoid Content of Various Solvent Extracts fromIn VivoandIn VitroGrownTrifolium pratenseL. (Red Clover).* BioMed Research International, 2015. **2015**: p. 1-11.
82. Zhishen, J., T. Mengcheng, and W. Jianming, *The determination of flavonoid contents in mulberry and their scavenging effects on superoxide radicals.* Food Chemistry, 1999. **64**(4): p. 555-559.
83. Haupert, L.J., et al., *Characterization of model compounds of processed lignin and the lignome by using atmospheric pressure ionization tandem mass spectrometry.* Fuel, 2012. **95**: p. 634-641.

84.   Henriksen, T., et al., *The relative influences of acidity and polarity on responsiveness of small organic molecules to analysis with negative ion electrospray ionization mass spectrometry (ESI-MS).* J Am Soc Mass Spectrom, 2005. **16**(4): p. 446-55.

85.   Jarrell, T.M., et al., *Characterization of Organosolv switchgrass lignin by using high performance liquid chromatography/high resolution tandem mass spectrometry using hydroxide-doped negative-ion mode electrospray ionization.* Green Chem., 2014. **16**(5): p. 2713-2727.

86.   Marcum, C.L., et al., *A Fundamental Tandem Mass Spectrometry Study of the Collision-Activated Dissociation of Small Deprotonated Molecules Related to Lignin.* ChemSusChem, 2016. **9**(24): p. 3513-3526.

87.   Owen, B.C., et al., *High-performance liquid chromatography/high-resolution multiple stage tandem mass spectrometry using negative-ion-mode hydroxide-doped electrospray ionization for the characterization of lignin degradation products.* Anal Chem, 2012. **84**(14): p. 6000-7.

88.   Sheng, H., et al., *(-)ESI/CAD MS(n) Procedure for Sequencing Lignin Oligomers Based on a Study of Synthetic Model Compounds with beta-O-4 and 5-5 Linkages.* Anal Chem, 2017. **89**(24): p. 13089-13096.

89.   Kim, H., et al., *Characterization and Elimination of Undesirable Protein Residues in Plant Cell Wall Materials for Enhancing Lignin Analysis by Solution-State Nuclear Magnetic Resonance Spectroscopy.* Biomacromolecules, 2017. **18**(12): p. 4184-4195.

90.   Kim, H. and J. Ralph, *Solution-state 2D NMR of ball-milled plant cell wall gels in DMSO-d(6)/pyridine-d(5).* Org Biomol Chem, 2010. **8**(3): p. 576-91.

91.   Mansfield, S.D., et al., *Whole plant cell wall characterization using solution-state 2D NMR.* Nat Protoc, 2012. **7**(9): p. 1579-89.

92.   Meng, X., et al., *Determination of hydroxyl groups in biorefinery resources via quantitative (31)P NMR spectroscopy.* Nat Protoc, 2019. **14**(9): p. 2627-2647.

93.   Singh, S.K. and P.L. Dhepe, *Ionic liquids catalyzed lignin liquefaction: mechanistic studies using TPO-MS, FT-IR, RAMAN and 1D, 2D-HSQC/NOSEY NMR.* Green Chemistry, 2016. **18**(14): p. 4098-4108.

94.   Talebi Amiri, M., et al., *Establishing lignin structure-upgradeability relationships using quantitative (1)H-(13)C heteronuclear single quantum coherence nuclear magnetic resonance (HSQC-NMR) spectroscopy.* Chem Sci, 2019. **10**(35): p. 8135-8142.

95.   Meng, Q., et al., *Sustainable production of benzene from lignin.* Nat Commun, 2021. **12**(1): p. 4534.

96.   Bomgardner, M.M., *The Problem with Vanilla*, in *C&EN*. 2016.

97.   Zirbes, M., et al., *High-Temperature Electrolysis of Kraft Lignin for Selective Vanillin Formation.* ACS Sustainable Chemistry & Engineering, 2020. **8**(19): p. 7300-7307.

98.   Luo, J., et al., *Selective Lignin Oxidation towards Vanillin in Phenol Media.* ChemistrySelect, 2016. **1**(15): p. 4596-4601.

99.   del Río, J.C., et al., *Lignin Monomers from beyond the Canonical Monolignol Biosynthetic Pathway: Another Brick in the Wall.* ACS Sustainable Chemistry & Engineering, 2020. **8**(13): p. 4997-5012.

100. Khan, I., K. Saeed, and I. Khan, *Nanoparticles: Properties, applications and toxicities.* Arabian Journal of Chemistry, 2019. **12**(7): p. 908-931.

101. Salata, O., *Applications od nanoparticles in biology and medicine.* Journal of Nanobiotechnology, 2004. **2**(3).

102. Xia, T., et al., *Toxic Potential of Materials at the Nanolevel.* Science, 2006. **311**(5761): p. 622-627.

103. Duval, A. and M. Lawoko, *A review on lignin-based polymeric, micro- and nano-structured materials.* Reactive and Functional Polymers, 2014. **85**: p. 78-96.

104. Frangville, C., et al., *Fabrication of environmentally biodegradable lignin nanoparticles.* Chemphyschem, 2012. **13**(18): p. 4235-43.

105. Roopan, S.M., *An overview of natural renewable bio-polymer lignin towards nano and biotechnological applications.* Int J Biol Macromol, 2017. **103**: p. 508-514.

106. Sipponen, M.H., et al., *Lignin for Nano- and Microscaled Carrier Systems: Applications, Trends, and Challenges.* ChemSusChem, 2019. **12**(10): p. 2039-2054.

107. Guo, Y., et al., *Self-assembly and paclitaxel loading capacity of α-tocopherol succinate-conjugated hydroxyethyl cellulose nanomicelle.* Colloid and Polymer Science, 2015. **294**(1): p. 135-143.

108. Iravani, S. and R.S. Varma, *Greener synthesis of lignin nanoparticles and their applications.* Green Chemistry, 2020. **22**(3): p. 612-636.

109. Lievonen, M., et al., *A simple process for lignin nanoparticle preparation.* Green Chemistry, 2016. **18**(5): p. 1416-1422.

110. Qian, Y., et al., *Fabrication of uniform lignin colloidal spheres for developing natural broad-spectrum sunscreens with high sun protection factor.* Industrial Crops and Products, 2017. **101**: p. 54-60.

111. Richter, A.P., et al., *Synthesis and Characterization of Biodegradable Lignin Nanoparticles with Tunable Surface Properties.* Langmuir, 2016. **32**(25): p. 6468-77.

112. Tian, D., et al., *Lignin valorization: lignin nanoparticles as high-value bio-additive for multifunctional nanocomposites.* Biotechnol Biofuels, 2017. **10**: p. 192.

113. Rahman, O.u., et al., *Lignin nanoparticles: synthesis, characterization and corrosion protection performance.* New Journal of Chemistry, 2018. **42**(5): p. 3415-3425.

114. Si, M., et al., *Synchronous and rapid preparation of lignin nanoparticles and carbon quantum dots from natural lignocellulose.* Green Chemistry, 2018. **20**(15): p. 3414-3419.

115. Sipponen, M.H., et al., *Understanding Lignin Aggregation Processes. A Case Study: Budesonide Entrapment and Stimuli Controlled Release from Lignin Nanoparticles.* ACS Sustain Chem Eng, 2018. **6**(7): p. 9342-9351.

116. Qian, Y., et al., *Formation of uniform colloidal spheres from lignin, a renewable resource recovered from pulping spent liquor.* Green Chemistry, 2014. **16**(4).

117. Sipponen, M.H., et al., *All-lignin approach to prepare cationic colloidal lignin particles: stabilization of durable Pickering emulsions.* Green Chemistry, 2017. **19**(24): p. 5831-5840.

118. Li, H., et al., *Preparation of Nanocapsules via the Self-Assembly of Kraft Lignin: A Totally Green Process with Renewable Resources.* ACS Sustainable Chemistry & Engineering, 2016. **4**(4): p. 1946-1953.

119. Xiong, F., et al., *Preparation and formation mechanism of size-controlled lignin nanospheres by self-assembly.* Industrial Crops and Products, 2017. **100**: p. 146-152.

120. Li, N., X. Pan, and J. Alexander, *A facile and fast method for quantitating lignin in lignocellulosic biomass using acidic lithium bromide trihydrate (ALBTH).* Green Chemistry, 2016. **18**(19): p. 5367-5376.

121. Mishra, P.K. and A. Ekielski, *The Self-Assembly of Lignin and Its Application in Nanoparticle Synthesis: A Short Review.* Nanomaterials (Basel), 2019. **9**(2).

122. Gaucher, G., et al., *Block copolymer micelles: preparation, characterization and application in drug delivery.* J Control Release, 2005. **109**(1-3): p. 169-88.

123. Guerlain, C., et al., *Self-assembly of a triblock terpolymer mediated by hydrogen-bonded complexes.* Journal of Polymer Science Part A: Polymer Chemistry, 2015. **53**(3): p. 459-467.

124. Simoes, S.M., et al., *Polymeric micelles for oral drug administration enabling locoregional and systemic treatments.* Expert Opin Drug Deliv, 2015. **12**(2): p. 297-318.

125.   Wu, Z., et al., *Self-Assembly of Nanoclusters into Mono-, Few-, and Multilayered Sheets via Dipole-Induced Asymmetric van der Waals Attraction.* ACS Nano, 2015. **9**(6): p. 6315-6323.

126.   Zheng, Y., et al., *Asymmetric gold nanodimer arrays: electrostatic self-assembly and SERS activity.* Journal of Materials Chemistry A, 2015. **3**(1): p. 240-249.

127.   Cailotto, S., et al., *Sustainable Strategies in the Synthesis of Lignin Nanoparticles for the Release of Active Compounds: A Comparison.* ChemSusChem, 2020. **13**(17): p. 4759-4767.

128.   Hyde, A.M., et al., *General Principles and Strategies for Salting-Out Informed by the Hofmeister Series.* Organic Process Research & Development, 2017. **21**(9): p. 1355-1370.

129.   Xu, H.N., Y. Liu, and L. Zhang, *Salting-out and salting-in: competitive effects of salt on the aggregation behavior of soy protein particles and their emulsifying properties.* Soft Matter, 2015. **11**(29): p. 5926-32.

130.   Smith, A.M., A.A. Lee, and S. Perkin, *The Electrostatic Screening Length in Concentrated Electrolytes Increases with Concentration.* J Phys Chem Lett, 2016. **7**(12): p. 2157-63.

131.   Jeremiasse, A.W., et al., *Use of Biocompatible Buffers to Reduce the Concentration Overpotential for Hydrogen Evolution.* Environmental Science & Technology, 2009. **43**(17): p. 6882-6887.

132.   Yossan, S., et al., *Hydrogen production in microbial electrolysis cells: Choice of catholyte.* International Journal of Hydrogen Energy, 2013. **38**(23): p. 9619-9624.

133.   Wang, Y., et al., *Production of vanillin from lignin: The relationship between β-O-4 linkages and vanillin yield.* Industrial Crops and Products, 2018. **116**: p. 116-121.

134.   Rodrigues Pinto, P.C., E.A. Borges da Silva, and A.E. Rodrigues, *Lignin as Source of Fine Chemicals: Vanillin and Syringaldehyde*, in *Biomass Conversion: The Interface of Biotechnology, Chemistry and Materials Science*, C. Baskar, S. Baskar, and R.S. Dhillon, Editors. 2012, Springer Berlin Heidelberg: Berlin, Heidelberg. p. 381-420.

135.   Henn, A. and M.L. Mattinen, *Chemo-enzymatically prepared lignin nanoparticles for value-added applications.* World J Microbiol Biotechnol, 2019. **35**(8): p. 125.

136.   Chen, L., et al., *Green synthesis of lignin nanoparticle in aqueous hydrotropic solution toward broadening the window for its processing and application.* Chemical Engineering Journal, 2018. **346**: p. 217-225.

137.   Figueiredo, P., et al., *In vitro evaluation of biodegradable lignin-based nanoparticles for drug delivery and enhanced antiproliferation effect in cancer cells.* Biomaterials, 2017. **121**: p. 97-108.

138.   Ahmed, E.M., *Hydrogel: Preparation, characterization, and applications: A review.* Journal of Advanced Research, 2015. **6**(2): p. 105-121.

139.   Mattinen, M.L., et al., *Colloidal Lignin Particles as Adhesives for Soft Materials.* Nanomaterials (Basel), 2018. **8**(12).

140.   Wang, B., et al., *Green and Facile Preparation of Regular Lignin Nanoparticles with High Yield and Their Natural Broad-Spectrum Sunscreens.* ACS Sustainable Chemistry & Engineering, 2019. **7**(2): p. 2658-2666.

141.   Pizzino, G., et al., *Oxidative Stress: Harms and Benefits for Human Health.* Oxidative medicine and cellular longevity, 2017. **2017**: p. 8416763-8416763.

142.   Nimse, S.B. and D. Pal, *Free radicals, natural antioxidants, and their reaction mechanisms.* RSC Advances, 2015. **5**(35): p. 27986-28006.

143.   Eunok Choe and D.D. Min, *Mechanisms of Antioxidants in the Oxidation of Food.* Comprehensive Reviews in Food Science and Food Safety, 2009. **8**(4): p. 345-358.

144.   Lu, J.M., et al., *Chemical and molecular mechanisms of antioxidants: experimental approaches and model systems.* J Cell Mol Med, 2010. **14**(4): p. 840-60.

145. Blainski, A., G.C. Lopes, and J.C. de Mello, *Application and analysis of the folin ciocalteu method for the determination of the total phenolic content from Limonium brasiliense L.* Molecules, 2013. **18**(6): p. 6852-65.

146. Brand-Williams, W., M.E. Cuvelier, and C. Berset, *Use of a free radical method to evaluate antioxidant activity.* LWT - Food Science and Technology, 1995. **28**(1): p. 25-30.

147. Dewanto, V., et al., *Thermal Processing Enhances the Nutritional Value of Tomatoes by Increasing Total Antioxidant Activity.* Journal of Agricultural and Food Chemistry, 2002. **50**(10): p. 3010-3014.

148. Guo, Z., et al., *New Lignin Streams Derived from Heteropoly Acids Enhanced Neutral Deep Eutectic Solvent Fractionation: Toward Structural Elucidation and Antioxidant Performance.* ACS Sustainable Chemistry & Engineering, 2020. **8**(32): p. 12110-12119.

149. Trevisan, H. and C.A. Rezende, *Pure, stable and highly antioxidant lignin nanoparticles from elephant grass.* Industrial Crops and Products, 2020. **145**.

150. Xu, J., et al., *Lignin-Incorporated Nanogel Serving As an Antioxidant Biomaterial for Wound Healing.* ACS Applied Bio Materials, 2020.

151. Yang, W., et al., *Valorization of Acid Isolated High Yield Lignin Nanoparticles as Innovative Antioxidant/Antimicrobial Organic Materials.* ACS Sustainable Chemistry & Engineering, 2018. **6**(3): p. 3502-3514.

152. Zhang, X., et al., *Controlled Preparation of Corncob Lignin Nanoparticles and their Size-Dependent Antioxidant Properties: Toward High Value Utilization of Lignin.* ACS Sustainable Chemistry & Engineering, 2019. **7**(20): p. 17166-17174.

153. Zhao, L., et al., *Improving antioxidant activity of lignin by hydrogenolysis.* Industrial Crops and Products, 2018. **125**: p. 228-235.

154. Shang, Y., et al., *Applications of Nanotechnology in Plant Growth and Crop Protection: A Review.* Molecules, 2019. **24**(14).

155. Pandorf, M., et al., *Graphite nanoparticle addition to fertilizers reduces nitrate leaching in growth of lettuce (Lactuca sativa).* Environmental Science: Nano, 2020. **7**(1): p. 127-138.

156. Alba-Lois, L. and C. Segal-Kischinevzky, *Yeast Fermentation and the Making of Beer and Wine.* Nature Education, 2010. **3**(9): p. 17.

157. Ragauskas, A.J., et al., *Lignin valorization: improving lignin processing in the biorefinery.* Science, 2014. **344**(6185): p. 1246843.

158. Takkellapati, S., T. Li, and M.A. Gonzalez, *An Overview of Biorefinery Derived Platform Chemicals from a Cellulose and Hemicellulose Biorefinery.* Clean Technol Environ Policy, 2018. **20**(7): p. 1615-1630.

159. Holladay, J.E., et al., *Top Value-Added Chemicals from Biomass - Volume II—Results of Screening for Potential Candidates from Biorefinery Lignin*. 2007. p. PNNL-16983, 921839.

160. Perlack, R.D., et al., *Biomass as Feedstock for a Bioenergy and Bioproducts Industry: The Technical Feasibility of a Billion-Ton Annual Supply.* 2005: p. 78.

161. Gosselink, R.J.A., et al., *Co-ordination network for lignin—standardisation, production and applications adapted to market requirements (EUROLIGNIN).* Industrial Crops and Products, 2004. **20**(2): p. 121-129.

162. Strassberger, Z., S. Tanase, and G. Rothenberg, *The pros and cons of lignin valorisation in an integrated biorefinery.* RSC Advances, 2014. **4**(48): p. 25310-25318.

163. Sarkanen, K.V. and C.H. Ludwig, *Lignins: occurrence, formation, structure and reactions*. 1971: Wiley-Interscience. p. 1-952.

164. Amen-Chen, C., H. Pakdel, and C. Roy, *Production of monomeric phenols by thermochemical conversion of biomass: a review.* Bioresource Technology, 2001. **79**(3): p. 277-299.

175

165. Zakzeski, J., et al., *The Catalytic Valorization of Lignin for the Production of Renewable Chemicals.* Chemical Reviews, 2010. **110**(6): p. 3552-3599.
166. Chen, Z. and C. Wan, *Biological valorization strategies for converting lignin into fuels and chemicals.* Renewable and Sustainable Energy Reviews, 2017. **73**: p. 610-621.
167. Zhang, Z., J. Song, and B. Han, *Catalytic Transformation of Lignocellulose into Chemicals and Fuel Products in Ionic Liquids.* Chemical Reviews, 2017. **117**(10): p. 6834-6880.
168. Fiorentino, G., M. Ripa, and S. Ulgiati, *Chemicals from biomass: technological versus environmental feasibility. A review.* Biofuels, Bioproducts and Biorefining, 2017. **11**(1): p. 195-214.
169. Gall, D.L., et al., *Biochemical transformation of lignin for deriving valued commodities from lignocellulose.* Current Opinion in Biotechnology, 2017. **45**: p. 120-126.
170. Li, C., et al., *Catalytic Transformation of Lignin for the Production of Chemicals and Fuels.* Chemical Reviews, 2015. **115**(21): p. 11559-11624.
171. Rinaldi, R., et al., *Paving the Way for Lignin Valorisation: Recent Advances in Bioengineering, Biorefining and Catalysis.* Angewandte Chemie International Edition, 2016. **55**(29): p. 8164-8215.
172. Sun, Z., et al., *Bright Side of Lignin Depolymerization: Toward New Platform Chemicals.* Chemical Reviews, 2018. **118**(2): p. 614-678.
173. Behling, R., S. Valange, and G. Chatel, *Heterogeneous catalytic oxidation for lignin valorization into valuable chemicals: what results? What limitations? What trends?* Green Chemistry, 2016. **18**(7): p. 1839-1854.
174. Gallezot, P., *Catalytic routes from renewables to fine chemicals.* Catalysis Today, 2007. **121**(1): p. 76-91.
175. Rößiger, B., G. Unkelbach, and D. Pufky-Heinrich, *Base-Catalyzed Depolymerization of Lignin: History, Challenges and Perspectives*, in *Lignin - Trends and Applications*. 2018. p. 1-308.
176. Escapa, A., et al., *Microbial electrolysis cells: An emerging technology for wastewater treatment and energy recovery. From laboratory to pilot plant and beyond.* Renewable and Sustainable Energy Reviews, 2016. **55**: p. 942-956.
177. Smolders, G.J.F., et al., *Model of the anaerobic metabolism of the biological phosphorus removal process: Stoichiometry and pH influence.* Biotechnology and Bioengineering, 1994. **43**(6): p. 461-470.
178. Nogueira, R.F.P., M.C. Oliveira, and W.C. Paterlini, *Simple and fast spectrophotometric determination of H2O2 in photo-Fenton reactions using metavanadate.* Talanta, 2005. **66**(1): p. 86-91.
179. Blainski, A., G.C. Lopes, and J.C.P. De Mello, *Application and Analysis of the Folin Ciocalteu Method for the Determination of the Total Phenolic Content from Limonium Brasiliense L.* Molecules, 2013. **18**(6): p. 6852-6865.
180. Khorasani Esmaeili, A., et al., *Antioxidant Activity and Total Phenolic and Flavonoid Content of Various Solvent Extracts from In Vivo and In Vitro Grown Trifolium pratense L. (Red Clover).* BioMed Research International, 2015. **2015**: p. e643285.
181. Barnaba, C., et al., *Identification and quantification of 56 targeted phenols in wines, spirits, and vinegars by online solid-phase extraction – ultrahigh-performance liquid chromatography – quadrupole-orbitrap mass spectrometry.* Journal of Chromatography A, 2015. **1423**: p. 124-135.
182. Bhat, G., *HPLC-DAD-ESI-MS/MS Identification and Characterization of Major Constituents of Iris crocea, Iris germanica and Iris spuria Growing in Kashmir Himalayas, India.* Journal of Analytical & Bioanalytical Techniques, 2014. **5**(6): p. 1-10.
183. Tian, C., et al., *HPLC Quantification of Nine Chemical Constituents from the Five Parts of Abutilon theophrasti Medic.* Journal of Chromatographic Science, 2014. **52**(3): p. 258-263.

184. Owen, B.C., et al., *High-Performance Liquid Chromatography/High-Resolution Multiple Stage Tandem Mass Spectrometry Using Negative-Ion-Mode Hydroxide-Doped Electrospray Ionization for the Characterization of Lignin Degradation Products.* Analytical Chemistry, 2012. **84**(14): p. 6000-6007.

185. Parsons, M.E.M., et al., *A Protocol for Improved Precision and Increased Confidence in Nanoparticle Tracking Analysis Concentration Measurements between 50 and 120 nm in Biological Fluids.* Frontiers in Cardiovascular Medicine, 2017. **4**: p. 68.

186. Li, Y., et al., *Optically Transparent Wood from a Nanoporous Cellulosic Template: Combining Functional and Structural Performance.* Biomacromolecules, 2016. **17**(4): p. 1358-64.

187. Bajpai, P., *Chemicals Used in Deinking and Their Function*, in *Recycling and Deinking of Recovered Paper*, P. Bajpai, Editor. 2014, Elsevier: Oxford. p. 121-137.

188. Brooks, R.E. and S.B. Moore, *Alkaline hydrogen peroxide bleaching of cellulose.* Cellulose, 2000. **7**(3): p. 263-286.

189. Litter, M.I., *Introduction to Photochemical Advanced Oxidation Processes for Water Treatment*, in *Environmental Photochemistry Part II*, P. Boule, D.W. Bahnemann, and P.K.J. Robertson, Editors. 2005, Springer: Berlin, Heidelberg. p. 325-366.

190. Paulsson, M. and J. Parkås, *Review: light-induced yellowing of lignocellulosic pulps – mechanisms and preventive methods.* BioResources, 2012. **7**(4): p. 5995-6040.

191. Torres, C.R.G., et al., *Influence of pH on the Effectiveness of Hydrogen Peroxide Whitening.* Operative Dentistry, 2014. **39**(6): p. E261-E268.

192. Jang, D., S. Kwon, and S. Jo, *Effect of Phosphate Stabilizers in Hydrogen Peroxide Decomposition on Manganese-Based Catalysts.* Journal of Propulsion and Power, 2015. **31**(3): p. 904-911.

193. Watts, R.J., et al., *Hydrogen peroxide decomposition in model subsurface systems.* Journal of Hazardous Materials, 1999. **69**(2): p. 229-243.

194. Yang, X., et al., *Effect of phosphate on heterogeneous Fenton oxidation of catechol by nano-Fe 3 O 4 : Inhibitor or stabilizer?* Journal of Environmental Sciences, 2016. **39**: p. 69-76.

195. Ma, R., Y. Xu, and X. Zhang, *Catalytic Oxidation of Biorefinery Lignin to Value-added Chemicals to Support Sustainable Biofuel Production.* ChemSusChem, 2015. **8**(1): p. 24-51.

196. Roberts, V.M., et al., *Towards Quantitative Catalytic Lignin Depolymerization.* Chemistry - A European Journal, 2011. **17**(21): p. 5939-5948.

197. Toledano, A., L. Serrano, and J. Labidi, *Improving base catalyzed lignin depolymerization by avoiding lignin repolymerization.* Fuel, 2014. **116**: p. 617-624.

198. Qian, Y., et al., *Formation of uniform colloidal spheres from lignin, a renewable resource recovered from pulping spent liquor.* Green Chemistry, 2014. **16**(4): p. 2156.

199. Frangville, C., et al., *Fabrication of Environmentally Biodegradable Lignin Nanoparticles.* ChemPhysChem, 2012. **13**(18): p. 4235-4243.

200. Sipponen, M.H., et al., *Understanding Lignin Aggregation Processes. A Case Study: Budesonide Entrapment and Stimuli Controlled Release from Lignin Nanoparticles.* ACS Sustainable Chemistry & Engineering, 2018. **6**(7): p. 9342-9351.

201. Adamcyk, J., et al., *Influence of Temperature and Lignin Concentration on Formation of Colloidal Lignin Particles in Solvent-Shifting Precipitation.* Sustainability, 2022. **14**(3): p. 1219.

202. Nakama, Y., *Chapter 15 - Surfactants*, in *Cosmetic Science and Technology*, K. Sakamoto, et al., Editors. 2017, Elsevier: Amsterdam. p. 231-244.

203. Cdm, *Waste Characterization Study*. 2010, Chicago Department of Environment.

204. Prasad, S., A. Singh, and H.C. Joshi, *Ethanol as an alternative fuel from agricultural, industrial and urban residues.* Resources, Conservation and Recycling, 2007. **50**(1): p. 1-39.

205. IlinoisDepartmentofAgriculture. *Facts About Illinois Agriculture*. 2022 [Accessed September 16th, 2022]; Available from: https://www2.illinois.gov/sites/agr/About/Pages/Facts-About-Illinois-Agriculture.aspx.

206. Ragauskas, A.J., et al., *Lignin Valorization: Improving Lignin Processing in the Biorefinery.* Science, 2014. **344**(6185): p. 1246843-1246843.

207. Kien, C.L., et al., *Stable Isotope Model for Assessing Production of Short Chain Fatty Acids from Colon-Derived Sugar: Application in Pigs.* The Journal of Nutrition, 1996. **126**(12): p. 3069-3076.

208. Lordan, R., et al., *Total, Neutral, and Polar Lipids of Brewing Ingredients, By-Products and Beer: Evaluation of Antithrombotic Activities.* Foods, 2019. **8**(5): p. 171.

209. Sun, R.-C., *Lignin Source and Structural Characterization.* ChemSusChem, 2020. **13**(17): p. 4385-4393.

210. Katahira, R., et al., *Base-Catalyzed Depolymerization of Biorefinery Lignins.* ACS Sustainable Chemistry & Engineering, 2016. **4**(3): p. 1474-1486.

211. Anastas, P. and N. Eghbali, *Green chemistry: principles and practice.* Chem Soc Rev, 2010. **39**(1): p. 301-12.

212. Tungmunnithum, D., et al., *Flavonoids and Other Phenolic Compounds from Medicinal Plants for Pharmaceutical and Medical Aspects: An Overview.* Medicines, 2018. **5**(3): p. 93.

213. Lahive, C.W., et al., *An Introduction to Model Compounds of Lignin Linking Motifs; Synthesis and Selection Considerations for Reactivity Studies.* ChemSusChem, 2020. **13**(17): p. 4238-4265.

214. Meyer, J.R., et al., *Kinetics of Secondary Reactions Affecting the Organosolv Lignin Structure.* ChemSusChem, 2020. **13**(17): p. 4557-4566.

215. Musl, O., et al., *Hydrophobic Interaction Chromatography in 2 D Liquid Chromatography Characterization of Lignosulfonates.* ChemSusChem, 2020. **13**(17): p. 4595-4604.

216. Neiva, D.M., et al., *Lignin from Tree Barks: Chemical Structure and Valorization.* ChemSusChem, 2020. **13**(17): p. 4537-4547.

217. Sun, R.C., *Lignin Source and Structural Characterization.* ChemSusChem, 2020. **13**(17): p. 4385-4393.

218. Sun, R.C., J.S.M. Samec, and A.J. Ragauskas, *Preface to Special Issue of ChemSusChem on Lignin Valorization: From Theory to Practice.* ChemSusChem, 2020. **13**(17): p. 4175-4180.

219. BjÖRkman, A., *Isolation of Lignin from Finely Divided Wood with Neutral Solvents.* Nature, 1954. **174**(4440): p. 1057-1058.

220. Obst, J.R. and T.K. Kirk, *Isolation of lignin*, in *Methods in Enzymology*. 1988, Academic Press. p. 3-12.

221. Cano, A., M. Acosta, and M.B. Arnao, *A method to measure antioxidant activity in organic media: application to lipophilic vitamins.* Redox Rep, 2000. **5**(6): p. 365-70.

222. Noreen, H., et al., *Measurement of total phenolic content and antioxidant activity of aerial parts of medicinal plant Coronopus didymus.* Asian Pac J Trop Med, 2017. **10**(8): p. 792-801.

223. Van den Bosch, S., et al., *Reductive lignocellulose fractionation into soluble lignin-derived phenolic monomers and dimers and processable carbohydrate pulps.* Energy & Environmental Science, 2015. **8**(6): p. 1748-1763.

224. Eswaran, S.C.D., et al., *Molecular structural dataset of lignin macromolecule elucidating experimental structural compositions.* Sci Data, 2022. **9**(1): p. 647.

225. Li, M., Y. Pu, and A.J. Ragauskas, *Current Understanding of the Correlation of Lignin Structure with Biomass Recalcitrance.* Front Chem, 2016. **4**: p. 45.

226. Ratnaweera, D.R., et al., *The impact of lignin source on its self-assembly in solution.* RSC Advances, 2015. **5**(82): p. 67258-67266.

227. Smit, A. and W. Huijgen, *Effective fractionation of lignocellulose in herbaceous biomass and hardwood using a mild acetone Organosolv process.* Green Chemistry, 2017. **19**(22): p. 5505-5514.

228. Pandey, K.K., *A study of chemical structure of soft and hardwood and wood polymers by FTIR spectroscopy.* Journal of Applied Polymer Science, 1999. **71**(12): p. 1969-1975.

229. Shahidi, F. and Y. Zhong, *Measurement of antioxidant activity.* Journal of Functional Foods, 2015. **18**: p. 757-781.

230. Cano, A., et al., *ABTS/TAC Methodology: Main Milestones and Recent Applications.* Processes, 2023. **11**(1).

231. Pylypchuk, I.V., et al., *Structural and molecular-weight-dependency in the formation of lignin nanoparticles from fractionated soft- and hardwood lignins.* Green Chemistry, 2021. **23**(8): p. 3061-3072.

232. Danaei, M., et al., *Impact of Particle Size and Polydispersity Index on the Clinical Applications of Lipidic Nanocarrier Systems.* Pharmaceutics, 2018. **10**(2).

233. Jackson, J.C., et al., *Sustainable Cellulose Nanocrystals for Improved Antimicrobial Properties of Thin Film Composite Membranes.* ACS Sustainable Chemistry & Engineering, 2021. **9**(19): p. 6534-6540.

234. Noronha, V.T., et al., *Physical Membrane-Stress-Mediated Antimicrobial Properties of Cellulose Nanocrystals.* ACS Sustainable Chemistry & Engineering, 2021. **9**(8): p. 3203-3212.

235. Schneider, W.D.H., A.J.P. Dillon, and M. Camassola, *Lignin nanoparticles enter the scene: A promising versatile green tool for multiple applications.* Biotechnol Adv, 2021. **47**: p. 107685.

236. Hameed, N., et al., *Flower like micellar assemblies in poly(styrene)-block-poly(4-vinyl pyridine)/poly(acrylic acid) complexes.* Materials Letters, 2015. **147**: p. 92-96.

237. Schwierz, N., et al., *Reversed Hofmeister series—The rule rather than the exception.* Current Opinion in Colloid & Interface Science, 2016. **23**: p. 10-18.

238. Gregory, K.P., et al., *Understanding specific ion effects and the Hofmeister series.* Phys Chem Chem Phys, 2022. **24**(21): p. 12682-12718.

239. Zongo, L., H. Lange, and C. Crestini, *A Study of the Effect of Kosmotropic and Chaotropic Ions on the Release Characteristics of Lignin Microcapsules under Stimuli-Responsive Conditions.* ACS Omega, 2019. **4**(4): p. 6979-6993.

240. Hu, Y.-B., et al., *Effect of pH and Phosphate on Calcium Carbonate Polymorphs Precipitated at near-Freezing Temperature.* Crystal Growth & Design, 2015. **15**(4): p. 1596-1601.

241. Mahapatra, S., et al., *Biofuels and their sources of production: A review on cleaner sustainable alternative against conventional fuel, in the framework of the food and energy nexus.* Energy Nexus, 2021. **4**.